Formation & Evolution of early-types galaxies

Maxime Bois

UNIVERSITE CLAUDE BERNARD LYON 1

Thèse de Doctorat

Specialité : Astrophysique

pour obtenir le titre de

Docteur ès sciences

de l'Université Claude Bernard Lyon 1

Présentée par

Maxime Bois

Formation & Evolution of early-types galaxies: Numerical simulations of galaxy mergers

Thèse soutenue le 23 février 2011
Numéro d'ordre : 36 - 2011

Jury:

President :	Bruno Guiderdoni	-	Observatoire de Lyon
Reviewers :	Pascale Jablonka	-	EPF (Lausanne)
	Romain Teyssier	-	Université de Zürich
Examiners :	Thierry Contini	-	Observatoire Midi-Pyrenées
	Jean-Francois Gonzalez	-	Observatoire de Lyon
	Frédéric Bournaud	-	CEA (Saclay)
Advisor :	Eric Emsellem	-	Obs. de Lyon & ESO (Munich)

Many evil things still lingered there, and others were dispersed and fled into the dark
and roamed in the waste places of the world, awaiting a more evil hour;
and Sauron they did not find.
J.R.R Tolkien, The Silmarillion

Un grand merci à tous ceux qui m'ont aidé de près ou de loin
à l'accomplissement de cette thèse.

Une pensée spéciale à ma famille, à mes amis et à Laurence.

Résumé

Une simple classification morphologique des galaxies de l'Univers local montre deux grandes familles: (1) les galaxies disques, avec des bras spiraux et dans deux-tiers des cas une barre stellaire; et (2) les galaxies elliptiques et lenticulaires, dites galaxies de type précoce ou early-type galaxies (ETGs), qui sont dominées par une composante stellaire sphéroidale. Les galaxies les plus massives de l'Univers local sont les ETGs. Ces galaxies présentent aussi une large variété de dynamique stellaire: elles peuvent avoir un champ de vitesse régulier et aligné avec la photométrie ou perpendiculaire à la photométrie; ne présenter aucune rotation globale; ou alors être composées de deux disques en contre-rotation l'un par rapport à l'autre (Kinematically Distinct Core ou KDC). Ces signatures dans la dynamique stellaire des ETGs et leur importante masse sont des signes d'interactions passées, en particulier des signes de fusions de galaxies.

Le but principal de ma thèse est d'analyser un large échantillon de simulations numériques à haute résolution de fusions binaires de galaxies. Ces fusions sont dites "idéalisées" car elles ne prennent pas en compte le contexte cosmologique de formation des galaxies : deux galaxies en isolation sont lancées sur une orbite permettant la fusion de ces galaxies, le résultat final attendu de la fusion étant une ETG. L'analyse statistique de ce large échantillon de simulations nous permet de relier les conditions initiales de la fusion à la galaxie finale. J'ai démontré que le rapport de masse entre les spirales initiales et que l'orientation de leurs moments angulaires sont des points essentiels à la formation des ETGs avec peu ou beaucoup de rotation et des KDCs. La morphologie de la spirale (rapport Bulbe/Disque) est aussi un point important pour la formation des KDC mais son impact n'est pas clair et de nouvelles simulations sont nécessaires pour conclure.

Durant ma thèse, j'ai aussi étudié l'importance de la résolution dans les simulations numériques de fusion de galaxies. J'ai montré que le nombre de particules et la taille des cellules utilisées ont une importance prépondérante dans les résultats finaux. Une trop faible résolution (*i.e.* peu de particules et une grille grossière) ne permet pas de suivre l'évolution rapide du potentiel gravitationnel lors de la fusion. Dans ce cas, certaines particules n'évacuent pas leur moment angulaire vers l'extérieur de la galaxie: la galaxie résultante de la fusion garde ainsi une plus forte rotation. A haute résolution, la dispersion de ces orbites est résolue, la galaxie résultante possède donc une faible rotation et peut former, sous certaines conditions initiales, un KDC.

Abstract

A simple morphological classification of the galaxies in the local Universe shows two main families: (1) the disc galaxies, with spiral arms and in two-thirds of these galaxies a stellar bar; and (2) the elliptical and lenticular galaxies, labelled early-type galaxies (ETGs), which are dominated by a spheroidal stellar component. ETGs are among the most massive galaxies of the local Universe and present a red color, meaning that their stars are old. These galaxies also present a large diversity of stellar dynamics: they may have a regular rotation pattern aligned with the photometry or perpendicular to it; they can present no global rotation at all; or may hold a central stellar component with a rotation axis distinct from the outer stellar body called a Kinematically Distinct Core (KDC). These features observed in the dynamics of the ETGs and their large mass are clearly signs of past interactions, especially signs of galaxy mergers.

The main goal of my thesis is to analyse a large sample of high-resolution numerical simulations of binary galaxy mergers. These binary mergers are called "idealized" because they do not take into account the full cosmological context of galaxy formation: two isolated spiral galaxies are launched in an orbit resulting in a merger of the galaxies, the final remnant is an ETG. The statistical analysis of this large sample of simulations enables us to link the initial conditions of the merger to the final merger remnant. I demonstrated that the mass ratio between the spiral progenitors and the orientation of their spins of angular momentum are the main drivers for the formation of fast and slow rotating ETGs and the KDCs. The morphology of the initial spiral (Bulge/Disc ratio) seems also to play a major role for the formation of the different types of ETGs but its impact is not completelly clear, and other simulations are planned to clarify this problem.

During my thesis, I also studied the importance of the resolution in the numerical simulations of galaxy mergers. I showed that the number of particles and the size of the computational grid have a predominant role in the final product of the merger. A too low resolution (*i.e.* too few particles and a coarse grid) can not follow the rapid evolution of the gravitational potential during the merger. In this case, the angular momentum is not as efficiently transfered to the outer parts of the galaxy: the merger remnant keeps thus a strong and regular rotation. At higher resolution, the scattering of the orbit is resolved and the merger remnant may end-up with, under some special initial conditions, a slow rotation and may form a KDC.

Contents

List of Figures

Chapter 1

Review on local galaxies

Contents

A simple classification of galaxies in the local Universe based on their morphology reveals two different classes: the disc-dominated galaxies and the spheroid-dominated galaxies. The morphology of these two classes of galaxies is not the only difference: their intrinsic properties are also distinct. This must imply a different process of formation. The first section of this chapter is dedicated to the study of the properties of the observed local galaxies. The second section will review the numerical simulations used to recover the formation history and the properties of local galaxies. These sections will mainly focus on spheroid-dominated early-type galaxies.

1.1 Observed galaxies in the local Universe

From a sample of 400 observed local galaxies, [Hubble 1926] proposed a classification based on their morphology: "*About 3 per cent are irregular, but the remaining nebulae fall into a sequence of type forms characterized by rotational symmetry about dominating nuclei*". This study served as a basis for the well-known Hubble's tuning fork (see Fig. 1.1, [Hubble 1936]), where the right side is composed of disc-dominated galaxies, with spiral arms and/or stellar bar, called spiral galaxies; and the left side is composed of spheroid-dominated galaxies called elliptical

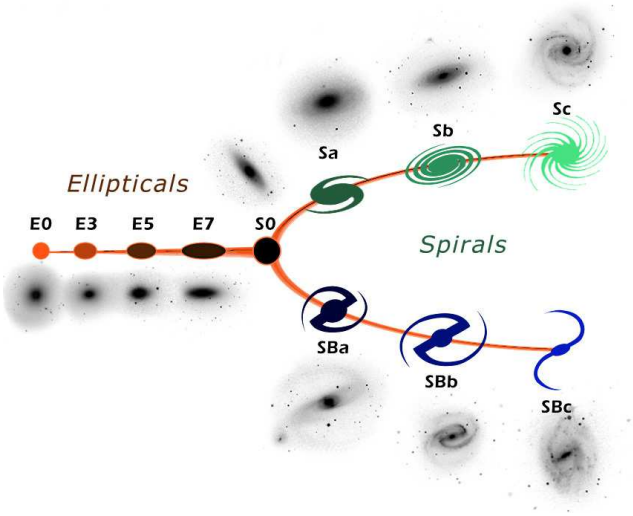

Figure 1.1: Hubble's classification of galaxies

galaxies. At the meeting point of these two categories, one can find the S0 lenticular galaxies which present both disc – but without spiral structures – and spheroid structures. Elliptical and lenticular galaxies are included in a larger group called early-type galaxies or ETGs. Spiral galaxies are also known as late-type galaxies.

1.1.1 Spiral galaxies

In the Hubble's classification of galaxies, spiral galaxies are divided in two branches: spirals with (called SB) or without (called S) a central stellar bar. In the local Universe, bars are found in about two-thirds of spiral galaxies, either in the optical or the infrared [Eskridge *et al.* 2000, Menéndez-Delmestre *et al.* 2007]. Regardless of the bar, these galaxies form a continuous sequence from those having a small bulge and loosely bound arms, called S(B)c at the extreme right of the tuning fork, to those having a prominent bulge and tightly bound arms, called S(B)a close to the S0 lenticular galaxies. The theory of formation of spiral structures is not the aim of this thesis, and we therefore guide the interested reader to reviews by [Toomre 1977] or [Marochnik & Suchkov 1996] on that subject.

Spiral galaxies are composed of a bulge and a disc of stars, a disc of gas and a dark matter halo. The radial surface brightness profile of the stellar bulge can be fit with a Sérsic profile of the form $e^{-r^{1/n}}$ [Sérsic 1968] and the stellar disc with a exponential function [Freeman 1970], *i.e.* a Sérsic profile with $n = 1$. Looking at the colour-magnitude diagram and colour-mass diagram of 151 642 galaxies at

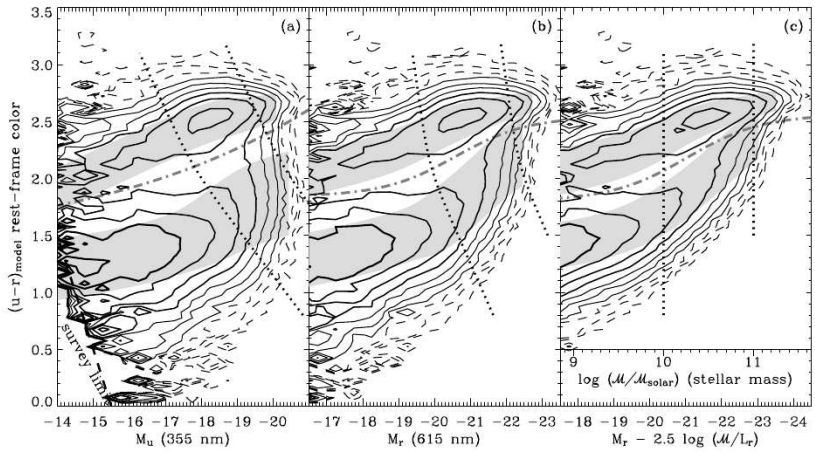

Figure 1.2: (Extracted from [Baldry *et al.* 2006]) Comparison between galaxy colour-magnitude and colour-mass relations. The (u-r) colour is plotted versus (a) M_u , (b) M_r and (c) log M. The dotted lines represent galaxies with stellar masses of 10^{10} and $10^{11}M_\odot$. The grey regions represent the colour means and $\pm 1\sigma$ ranges of the red and blue sequences. The dash-dotted lines represent the best-fitting dividers between the sequences based on the criteria of [Baldry *et al.* 2004].

$z < 0.1$ in Fig. 1.2, the vast majority of the spiral galaxies (below the dash-dotted line) are the less massive galaxies and belong to a region called the "blue cloud" [Strateva *et al.* 2001, Baldry *et al.* 2006]. These galaxies are populated by recently formed young stars and are thus blue. They contain gas and present ongoing star formation activity – at all redshifts – which is correlated with the total gas surface density: see *e.g.* [Kennicutt 1998, Bigiel *et al.* 2008, Daddi *et al.* 2010b] in observations and [Teyssier *et al.* 2010] in simulations of galaxy mergers.

1.1.2 Early-type galaxies

In the colour-magnitude diagram and colour-mass diagram of Fig. 1.2, we see that local early-type galaxies span a large range in mass: from masses typical for spiral galaxies to very massive galaxies. At all mass ranges, the ETGs are clearly recognizable by their reddish colour and form a group called "the red sequence" (above the dash-dotted line of Fig. 1.2). ETGs are dominated by old stellar populations, they may have a gaseous component but in a non significant quantity and then show very little star formation activity [Roberts & Haynes 1994, Shapiro *et al.* 2010]. [de Vaucouleurs 1948] first thought

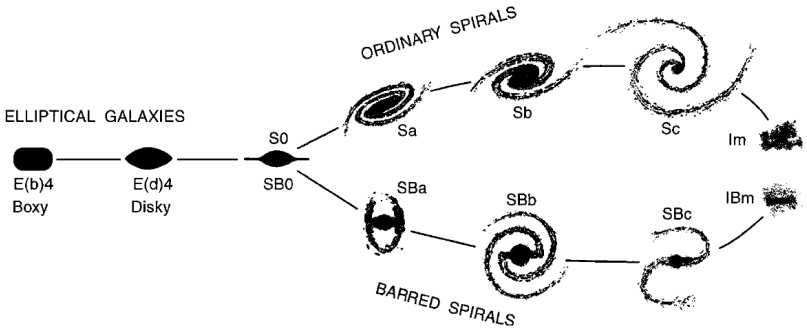

Figure 1.3: (Extracted from [Kormendy & Bender 1996]) Revision of the Hubble's classification of galaxies.

that the luminosity profiles of ETGs followed the $e^{-r^{1/4}}$ function, which is the Sérsic profile with $n = 4$. But Sérsic profiles with different values of n better reproduce the large variety of ETGs, see *e.g.* [Ferrarese *et al.* 2006].

Elliptical galaxies are classified, in the Hubble's tuning-fork, as a function of their apparent flattening: ellipticals with high flattening are located near the lenticular S0 galaxies while the round elliptical are at the extreme left of the classification. However, the distinction between flat and round shapes is dependent of the viewing angle of the galaxy and does not characterise its intrinsic morphology. [Kormendy & Bender 1996] proposed a revision of the Hubble's classification, see Fig. 1.3. They ordered ellipticals as a function of the discyness or boxyness of their isophote shapes, claiming that discy ellipticals tend to rotate rapidly while boxy ellipticals have less rotation. This classification has the same drawback than the Hubble's one: a galaxy can be either discy or boxy depending on the viewing angle (see Fig. A1 in Section 2.2).

Observational techniques have been improved to obtain the kinematical informations of local early-type galaxies, and have revealed a wealth of different structures. Long-slit spectroscopy surveys have shown the presence of Kinematically Distinct Cores (KDC) or misalignments between the photometric and kinematic axis [Franx & Illingworth 1988, Jedrzejewski & Schechter 1988, Bender 1988, de Zeeuw & Franx 1991, Rix & White 1992]. KDCs, usually defined as a central stellar component with a rotation axis distinct from the outer stellar body (see *e.g.* [Krajnović *et al.* 2008]), have been claimed to be a signature of a past interaction.

More recently, the emergence of integral field spectrographs, such as the SAURON spectrograph [Bacon *et al.* 2001], allowed the mapping of local ETGs up

to about one effective radius. The SAURON survey [de Zeeuw *et al.* 2002] has introduced a new view of ETGs, classifying them in two families – the fast and the slow rotators – according not only to their morphology, but also to their kinematics [Emsellem *et al.* 2007, Cappellari *et al.* 2007]. These two classes are intrinsically different and seem to correspond to different populations of galaxies: while the fast rotators present regular rotation patterns aligned with the photometry, the slow rotators have low angular momentum, show misalignments between the photometry and the velocity axes and often contain a KDC.

1.1.3 Cosmological context of galaxy formation

Spiral and ETGs are surrounded by an extended halo of dark matter (DM) [Zwicky 1933]. These DM haloes could themselves be embedded in deeper potential well of DM, forming a cluster of galaxies.

In the ΛCDM models, based on the Big Bang theory, DM haloes arose from the initial fluctuations of the Cosmic Microwave Background [Spergel *et al.* 2003]. These initial fluctuations have grown through gravitational instabilities [Searle & Zinn 1978]. Following the denser regions, the primordial gas falls in the central part of the DM haloes and settles in a rotational disc [Fall & Efstathiou 1980]: spiral galaxies are thus thought to form first. These first haloes could have grown by mergers with surrounding haloes to form bigger and bigger structures. The galaxies in the centre of the DM haloes may have thus also merged: this scenario is called "the hierarchical growth of galaxies". This scenario seems to be supported by high-redshift observations: ETGs – which are thought to form via mergers of galaxies [Schweizer 1982, Struve *et al.* 2010] – do not dominate the mass distribution of galaxies at high-z [Trujillo *et al.* 2007, Ferreras *et al.* 2009].

Observations of local galaxies should not be the only tool to be used to understand the cosmological evolution of galaxies as we only probe a specific instant of the Universe. And observing distant galaxies is a very challenging task due to the small amount of residual light and the size of the sources. Numerical simulations of galaxy formation are thus promising and complementary in that sense.

1.2 Numerical simulations of galaxy formation

Since the last massive extinction of the dinosaurs on Earth 65 Myr ago (its cause is still prone to debates, see e.g. [Schulte *et al.* 2010, Archibald *et al.* 2010]), the Sun

has made just more than a quarter of its orbit around the Galactic centre. Galactic and extra-galactic timescales are not appropriate for our human observations and we thus can not follow the time evolution of galaxies: we have only access to a specific snapshot. Numerical simulations have thus been implemented to study the evolution and interactions of galaxies.

1.2.1 Past simulations

The first simulation of galaxy interaction has been realised by [Holmberg 1941]. He did not used a computer, but a mechanical system of 37 light-bulbs per galaxy: each mass element is replaced by light. The gravitational forces are therefore correlated to the amount of light received by each light-bulb and then, the lamps are moved step by step. The simulation took place on a plane which obviously bring some constraints: the galaxies have to be disc galaxies and need to be edge-on when they interact. With such a system, [Holmberg 1941] was able to capture the development of spiral arms due to the tidal forces during the interaction (see also [Oh *et al.* 2008] for a recent study on this subject). However, its central lamps had not been disturbed during the interaction and the effect of the tidal forces on the creation of a stellar bar has not been captured (see [Barnes & Hernquist 1996]).

The first "numerical" simulations has been made by [von Hoerner 1960] which has integrated the equations of motion of a random cluster with 16 stars (see also [von Hoerner 1963] with 25 stars – both articles in German). With increasing computer resources, simulations have increased the number of particles: [Aarseth 1963] with 100 and [Aarseth & Saslaw 1972] with 500 particles. [Toomre & Toomre 1972] studied the formation of spirals and galactic bridges during galaxy interactions, but using only restricted three-body interactions.

The first noticeable "N-body" simulations of galaxy merger has been made by [Gerhard 1981]. He used 250 particles to reproduce a disc galaxy (with an exponential disc, a core and a halo) and simulated galaxy mergers with different initial conditions. He finds that if the spins of the discs and the orbit are aligned, it gives a remnant with a fast rotation while if the spins of the discs are anti-parallel to the one of the orbit, the remnant has the slowest final rotation (with some counter-rotating particles). The shape and kinematics of its remnants resemble elliptical galaxies and can match some properties of observed elliptical galaxies, like *e.g.* the $\epsilon - V/\sigma$ diagram (the projected ellipticity versus the mean velocity divided by the velocity dispersion values). From simulations of mergers of disc galaxies, [Farouki & Shapiro 1982] also find that the merger remnants resemble elliptical

galaxies in their morphology, luminosity profile, velocity and velocity dispersion values. [Barnes 1988] was the first to include a dark matter halo around his disc progenitors. These extensive haloes are efficient to soak up the orbital angular momentum which affect the dynamics of the final remnant.

During that period, two different methods have been developed to include a treatment of the gas component in the simulations: the SPH technique ([Gingold & Monaghan 1977, Lucy 1977]) for which the gas particles are not placed on a grid and the resolution of the gas can thus be adjusted within the simulation; and the sticky-particle method ([Negroponte & White 1983]) for which the gas particles evolve on the same grid as the stellar particles and can have inelastic collisions between themselves and thus dissipate energy.

Since the 90's, numerical simulations have included stars+gas+DM for a steady increase of the number of particles and decrease of the spatial resolution (*i.e.* the size of the computational grid). Such increase in the resolution obviously tends to lower the particle noise but may also have drastic effects on the results of the simulations: [Naab *et al.* 2007, Navarro *et al.* 2010] have pointed out some discrepancies in cosmological simulations made at different resolutions and [Cox *et al.* 2006b, Hopkins *et al.* 2008, Di Matteo *et al.* 2008a] in star formation activity in ongoing mergers. In this thesis, I will show in Chapter 2 that the resolution may particularly affect the dynamics of some merger remnants.

In the next section, I will describe the major recent studies which helped our comprehension of the formation and evolution of galaxies via numerical simulations of "idealized" mergers and large scale cosmological simulations.

1.2.2 Recent studies on "idealized" galaxy mergers

The term "idealized" simulations of galaxy mergers encompasses all the simulations made without a specific inclusion of the cosmological context. It can be either binary or multiple mergers with realistic (or not) initial conditions in order to study the role of a specific parameter on the properties of the merger remnants. I will here describe some recent studies of "idealized" simulations and their results.

Effect of the mass ratio on the morphology: Before 1998, simulations of binary mergers were made using two equal-mass galaxy progenitors and the difference between boxy and discy ETGs was thought to be due to the initial gas fraction. [Barnes 1998] showed that discy ETGs can result from a merger of a large disc

galaxy and a smaller companion without a gaseous component. [Naab *et al.* 1999] confirmed this result: simulating equal-mass and unequal-mass (with the lower companion has a third of the main progenitor mass) mergers, they found that the unequal-mass remnant presents discy isophotes while the equal-mass remnant presents boxy isophotes. From these studies, the importance of the mass ratio on the morphology of the remnant has emerged and is now considered as a key parameter in the formation of ETGs. One can distinguish three main ranges of mass ratios with different impacts on the remnants: (1) the "major" mergers with mass ratios comprised between 1:1 and 3:1 (in this notation the mass of the lighter progenitor is equal to the mass of the main progenitor divided by the first number); (2) the "intermediate" mergers with a mass ratio between 4:1 and 10:1; and (3) the "minor" mergers with a mass ratios $>$ 10:1.

Major mergers between spiral galaxies are known to severely impact the morphology of the galaxies and to produce elliptical-like galaxies ([Naab & Burkert 2003, Bournaud *et al.* 2005, Naab & Trujillo 2006, Naab *et al.* 2006a, Cox *et al.* 2006a]). Intermediate merger remnants present a disc-like morphology but with elliptical-like kinematics, they may be associated to S0 lenticular galaxies or very flattened ellipticals ([Bournaud *et al.* 2004, Bournaud *et al.* 2005]). A minor merger between a spiral galaxy and a small companion just slightly disturbs the spiral and may heat its disc but does not lead to an S0/elliptical galaxy ([Villalobos & Helmi 2008, Moster *et al.* 2010]). However, the effect of several minor mergers may be dramatic for the survival of the disc if the total mass accreted via the smaller companions is at least half of the initial mass of the spiral galaxy: such scenario can produce an elliptical galaxy [Weil & Hernquist 1994, Weil & Hernquist 1996, Bournaud *et al.* 2007].

Some studies have shown that major mergers of disc galaxies could produce disc dominated remnants if the initial amount of gas is high (*e.g.* at high redshift) [Springel & Hernquist 2005, Robertson *et al.* 2006, Hopkins *et al.* 2009b]. However, I will show in Chapters 2 and 3 of this thesis that this scenario is unlikely, and this has also been confirmed by [Bournaud *et al.* 2010a].

Effect of the gas on the morphology: In the local Universe, spiral galaxies contain a gaseous component, and much more is present at high redshift [Daddi *et al.* 2010a, Tacconi *et al.* 2010]. Spiral galaxies as progenitors for a merger should be simulated with gas dissipation. The presence of the gas greatly affect the shape of the remnants [Bekki & Shioya 1997]. More recent studies share

the same conclusions [Naab *et al.* 2006a, Hopkins *et al.* 2008, Hopkins *et al.* 2009a, Hopkins *et al.* 2009c, Hoffman *et al.* 2010].

However, cares must be taken when dealing with the gas in the simulations. In a galaxy, the gas is present in the interstellar medium at different temperatures, different densities and different phases: from a temperature of 20K and very high densities for molecular gas to $\sim 10^6$K and a very low density for hot ionized gas (see [Ferrière 2001] for a review on the interstellar environment of the Milky Way, see also [Lequeux 2005] for a general review). However, the simulated gas particles can not reach these extreme conditions and thus can not reproduce the full behaviour of the gas in galaxy mergers. Recent simulation techniques are promising as the gas can reach very low temperatures and thus well describe the star-forming regions of molecular clouds [Powell *et al.* 2010, Teyssier *et al.* 2010, Bournaud *et al.* 2010b].

Large scale signatures of interactions: Observations of local galaxies have revealed that galaxy mergers severely affect not only the central part of the galaxies, but also their large scale structures. Galaxy mergers produce shells, tidal tails and streams, tidal dwarf galaxies or giant globular clusters. This can provide us with a lot of information on the formation history of a galaxy. The most famous observed large scale structures are the long tails in NGC 4038/39 (the Antennae) or the tails and shells of NGC 5557 (see Fig. 4.8).

In the 90's, some studies have tried to constrain the mass and shape of the dark matter haloes around galaxies using the morphology of the tidal tails as indicators [Dubinski *et al.* 1996, Mihos *et al.* 1998, Springel & White 1999]. More recently, it has been showed by [Feldmann *et al.* 2008] that a dissipation component is required to reproduce the morphologies of the observed tidal debris observed in nearby ETGs. This result is also found by [Bournaud *et al.* 2008]: using a very high resolution for a simulation of a gas-rich merger, the formation of massive young stellar clusters (potentially globular clusters) could be resolved.

Using the morphological and kinematical informations of the central part of an observed galaxy and its large scale environment, it is then possible to recover the initial state of the galaxies before the interaction, see [Teyssier *et al.* 2010] for a study on the Antennae and [Michel-Dansac *et al.* 2010] for the Leo ring. However, our knowledge on the formation of shells, streams,... is limited: improved simulations made at high-resolution would be an asset to study the link between the initial conditions and the formation of such large scale structures.

Impact on the remnants' kinematics: As seen previously, the morphology both at small and large scales is severely impacted during a major merger of spiral galaxies: the initial disc shape is destroyed and the galaxy becomes spheroid-dominated. There is, indeed, a counter-part in the kinematics of the remnant. The first simulations showed that the boxy remnants were rotating slowly while the discy ones were fastly rotating: the addition of a gaseous component transformed the boxy and slowly rotating remnants into the discy and fastly rotating ones. This trend has been confirmed recently in [Hoffman *et al.* 2010].

The mass ratio of the progenitors is also known to be a key parameter on the formation of slowly and fastly rotating ETGs: slowly rotating remnants can only be produced by equal-mass mergers [Naab & Burkert 2003, Bournaud *et al.* 2004, Bournaud *et al.* 2005]. Using the λ_R parameter (a proxy for the stellar angular momentum, see Section 2.2) instead of the traditional V/σ value, [Jesseit *et al.* 2009] found the same results.

However, using two ellipticals E0 without apparent rotation as progenitors, [Di Matteo *et al.* 2009] show that part of the orbital angular momentum is transferred to the internal angular momentum of the galaxies during the merger. The merger remnant is then fastly rotating and flattened by rotation. This effect is also seen by [Qu *et al.* 2010]: collisionless minor mergers can either increase or decrease the internal angular momentum of the initial spiral galaxy via the transfer of the orbital angular momentum. The picture of formation of the slowly or fastly rotating remnants could thus be more complex than previously thought.

The kinematics of ETGs can reveal complex sub-structures such as KDCs (see Section 1.1.2). Via simulations of gas-rich spiral galaxy mergers, [Hernquist & Barnes 1991, Jesseit *et al.* 2007, Hoffman *et al.* 2010] have demonstrated that a KDC could be formed in the remnant due to the presence of gas: the gas may fall in the centre of the remnant in counter-rotation and continued star formation in this gaseous disc may produce a central component with decoupled kinematics. In the remnants of [Di Matteo *et al.* 2008b], a counter-rotating component can be formed both in dissipational and dissipationless mergers of an elliptical and a spiral galaxy. If the spin of the spiral is anti-parallel to the spin of the orbit, the external part of the remnant acquires the angular momentum of the orbit while its central part is dominated by the initial internal spin of the spiral: these two contributions are thus in counter-rotation. [Balcells & Quinn 1990] also probed this effect in a 5:1 merger of two oblate ETGs with a retrograde spin (with respect to the orbital spin): the companion adopts the sign of the orbital angular

momentum during the merger while the most massive progenitor is not influenced: this forms a central decoupled component. [Crocker *et al.* 2009] showed that the KDC in the observed galaxy NGC 4550 was not due to infalling gas with counter-rotation but was very probably due to the merger of two disc galaxies with opposite spins.

These different results tend to prove that the mechanisms of formation of KDCs are either multiple or not understood. We have then decided in this thesis to study a large sample of simulations, made at an unmatched resolution, of spiral and ETG mergers with different initial conditions to understand the mechanisms of formation of the slowly and fastly rotating ETGs and their associated sub-structures. The results of this study can be found in Chapter 3, the comparison with observations of local galaxies can be found in Chapter 5.

1.2.3 Large scale cosmological simulations

Cosmological simulations has been developed to understand the process of formation of galaxies in a realistic (and not idealized) way. These simulations mean to represent a large volume of the Universe from its initial state (at the recombination) to the present days. The initial conditions are based on the observed small variations of temperature (*i.e.* density) of the cosmic microwave background (see *e.g.* [Spergel *et al.* 2003]) and the associated cosmological parameters. The dark matter particles are placed on the simulation box to match the properties of the early Universe, gaseous and stellar particles are placed to follow the dark matter contribution. At the start of the simulation, the particles evolve through gravitational instabilities. As a consequence, [Aarseth & Fall 1980] have confirmed that merging occurs hierarchically and that the massive galaxies are formed via mergers of smaller galaxies. They also pointed out that the number of merger remnants was more frequent in groups of galaxies than in the field.

[Meza *et al.* 2003] have studied the formation of an elliptical galaxy in a cosmological simulation. Two modes of mass accretion are observed alternatively: smooth accretion of cold gas which produce a rotational disc and galaxy mergers which disperse the stellar disc into spheroid. In their simulation, the last interaction is a major merger: it transforms all the gas into stars and redistributes all the stars into a spheroid shape with a clear rotation pattern and no sub-structures. This final remnant may resemble some present-day ETGs.

Large scale simulations are clearly an asset to understand the formation of galaxies. However, to simulate a large volume of the Universe, it usually means

a relatively low resolution. This low resolution can properly follow the evolution of the large haloes of dark matter but can not properly resolve the small-scale interactions within a galaxy during a merger. To combine both large and small scales, techniques of re-simulation have been recently developed. It consists of recording the history of the interactions on a specific galaxy and re-simulate these interactions at higher resolution (see Section 4.4.1). This technique has been applied to simulate field or central galaxies. The galaxies in the centre of a group are massive and have experienced many interactions including major mergers. The field galaxies resemble more the intermediate mass ETGs and some are found to not have merged with an equal mass companion but only with minor galaxies. In all cases, the effect of minor mergers, which are much more frequent than major mergers, is determinant in shaping the galaxies [Naab *et al.* 2007, Naab *et al.* 2009, Martig *et al.* 2009, Feldmann *et al.* 2010]

In this thesis (in Section 4.4.1), I will analyse the time evolution of a field ETG which has been simulated using a new technique of re-simulation (see [Martig *et al.* 2009]). This first simulation is only the beginning of a new collaboration which should result in a larger sample of simulations. The aim of this project is to study the morphological and kinematical transformations due to the different interactions which occur during the life-time of a galaxy.

Chapter 2

The effects of numerical resolution in simulations of galaxy mergers

Contents

2.1 Introduction to the article

During my thesis, I first worked on the effects of the numerical resolution in simulations of galaxy mergers. An increase of the numerical resolution was known to change the results of the dark matter profiles in cosmological simulations or to change the star formation activity in galaxy mergers [Cox *et al.* 2006b, Naab *et al.* 2007, Hopkins *et al.* 2008, Di Matteo *et al.* 2008a, Navarro *et al.* 2010]. My thesis aims to study the morphology and the kinematics of merger remnants, but the role of the resolution for such purpose has not been explored thoroughly. We have thus simulated galaxy mergers at three different resolutions and the results associated to this study have been published in MNRAS in August 2010 in [Bois *et al.* 2010]. This article is now a part of my thesis and the reader can find it just below as it has been published.

2.2 Paper I: "Formation of slowly rotating early-type galaxies via major mergers: a resolution study"

Monthly Notices
of the
ROYAL ASTRONOMICAL SOCIETY

Mon. Not. R. Astron. Soc. **406,** 2405–2420 (2010) doi:10.1111/j.1365-2966.2010.16885.x

Formation of slowly rotating early-type galaxies via major mergers: a resolution study

M. Bois,[1,2⋆] F. Bournaud,[3] E. Emsellem,[1,2] K. Alatalo,[4] L. Blitz,[4] M. Bureau,[5] M. Cappellari,[5] R. L. Davies,[5] T. A. Davis,[5] P. T. de Zeeuw,[2,6] P.-A. Duc,[3] S. Khochfar,[7] D. Krajnović,[2] H. Kuntschner,[8] P.-Y. Lablanche,[1] R. M. McDermid,[9] R. Morganti,[10] T. Naab,[11,12] T. Oosterloo,[10] M. Sarzi,[13] N. Scott,[5] P. Serra,[10] A. Weijmans[14] and L. M. Young[15]

[1]*Université Lyon 1, Observatoire de Lyon, Centre de Recherche Astrophysique de Lyon and Ecole Nationale Supérieure de Lyon, 9 avenue Charles André, F-69230 Saint-Genis Laval, France*
[2]*European Southern Observatory, Karl-Schwarzschild Strasse 2, 85748 Garching, Germany*
[3]*CEA, IRFU, SAp et Laboratoire AIM, CEA Saclay – CNRS – Université Paris Diderot, 91191 Gif-sur-Yvette, France*
[4]*Department of Astronomy and Radio Astronomy Laboratory, University of California, Berkeley, CA 94720, USA*
[5]*Denys Wilkinson Building, University of Oxford, Keble Road, Oxford OX1 3RH*
[6]*Sterrewacht Leiden, Leiden University, Postbus 9513, 2300 RA Leiden, the Netherlands*
[7]*Max-Planck Institute for Extraterrestrial Physics, Giessenbachstrae, 85748 Garching, Germany*
[8]*Space Telescope European Coordinating Facility, European Southern Observatory, Karl-Schwarzschild Strasse 2, 85748 Garching, Germany*
[9]*Gemini Observatory, Northern Operations Centre, 670 N. A'ohoku Place, Hilo, HI 96720, USA*
[10]*Netherlands Foundation for Research in Astronomy (ASTRON), Postbus 2, 7990 AA Dwingeloo, the Netherlands*
[11]*Universitäts-Sternwarte München, Scheinerstr. 1, D-81679 München, Germany*
[12]*Max-Planck Institute for Astrophysics, Karl-Schwarzschild Strasse 1, 85741 Garching, Germany*
[13]*Centre for Astrophysics Research, University of Hertfordshire, Hatfield, Herts AL1 09AB*
[14]*Dunlap Institute for Astronomy & Astrophysics, University of Toronto, 50 St. George Street, Toronto, ON M5S 3H4, Canada*
[15]*Department of Physics, New Mexico Institute of Mining and Technology, Socorro, NM 87801, USA*

Accepted 2010 April 20. Received 2010 February 5; in original form 2009 July 23

ABSTRACT

We study resolution effects in numerical simulations of gas-rich and gas-poor major mergers, and show that the formation of slowly rotating elliptical galaxies often requires a resolution that is beyond the present-day standards to be properly modelled. Our sample of equal-mass merger models encompasses various masses and spatial resolutions, ranging from about 200 pc and 10^5 particles per component (stars, gas and dark matter), i.e. a gas mass resolution of $\sim 10^5\,M_\odot$, typical of some recently published major merger simulations, to up to 32 pc and $\sim 10^3\,M_\odot$ in simulations using 2.4×10^7 collisionless particles and 1.2×10^7 gas particles, among the highest resolutions reached so far for gas-rich major merger of massive disc galaxies. We find that the formation of fast-rotating early-type galaxies, that are flattened by a significant residual rotation, is overall correctly reproduced at all such resolutions. However, the formation of slow-rotating early-type galaxies, which have a low-residual angular momentum and are supported mostly by anisotropic velocity dispersions, is strongly resolution-dependent. The evacuation of angular momentum from the main stellar body is largely missed at standard resolution, and systems that should be slow rotators are then found to be fast rotators. The effect is most important for gas-rich mergers, but is also witnessed in mergers with an absent or modest gas component (0–10 per cent in mass). The effect is robust with respect to our initial conditions and interaction orbits, and originates in the physical treatment of the relaxation process during the coalescence of the galaxies. Our findings show that a high-enough resolution is required to

⋆E-mail: mbois@eso.org

accurately model the global properties of merger remnants and the evolution of their angular momentum. The role of gas-rich mergers of spiral galaxies in the formation of slow-rotating ellipticals may therefore have been underestimated. Moreover, the effect of gas in a galaxy merger is not limited to helping the survival/rebuilding of rotating disc components: at high resolution, gas actively participates in the relaxation process and the formation of slowly rotating stellar systems.

Key words: galaxies: elliptical and lenticulars, cD – galaxies: formation – galaxies: interactions – galaxies: kinematics and dynamics.

1 INTRODUCTION

Numerical simulations have been intensively used for more than two decades to study the properties of the remnants of galaxy mergers and the role of hierarchical merging in the formation of elliptical-like early-type galaxies (Hernquist & Barnes 1991; Barnes 1992; Mihos et al. 1995). With the increasing resolution and large statistical samples (e.g. Naab & Burkert 2003; Bournaud, Jog & Combes 2005; Di Matteo et al. 2007, 2008; Chilingarian et al. 2010), modern work tends to quantify in details the properties of major and minor merger remnants, and accurate comparisons with observed properties of early-type galaxies can now be envisioned (e.g. Burkert et al. 2008).

A general concern, though, is that the impact of the spatial and the mass resolutions on the detailed properties of the systems under scrutiny remains largely overlooked, and whether or not simulations of mergers have converged with today's typical resolution remains unexplored. Obviously, increasing resolution enables simulations to directly resolve cold gas clouds and clustered star formation (e.g. Bournaud, Duc & Emsellem 2008; Kim, Wise & Abel 2009), but whether these additional small-scale ingredients can significantly impact the global, large-scale morphology and kinematics of merger remnants has not been studied in detail. In cosmological simulations, an increase in resolution (i.e. an increase in the number of particles and/or decrease of the softening length) can affect the baryonic density and circular velocity profiles of individual galaxies in a halo (Naab et al. 2007). Navarro et al. (2010) also studied numerical convergence via a suite of Λ cold dark matter (ΛCDM) simulations and confirmed that the halo mass distributions were better described by Einasto profiles that are not, stricly speaking, universal.

While many resolution studies have been made in cosmological simulations, few have focused on galaxy merger simulations. Cox et al. (2006a), Hopkins et al. (2008) and e.g. Di Matteo et al. (2008) included some checks of the effect of resolution on the star formation activity of ongoing mergers. But a resolution study aimed at examining the detailed morphology and kinematics of relaxed merger remnants (i.e. galaxies which tend to be roughly S0 or elliptical-like) has not yet been conducted.

Models of galaxy mergers have reached particularly high resolution with the work of Wetzstein, Naab & Burkert (2007) (70 pc softening with 4×10^6 particles in total – but only 45 000 for the gas component), Li, Mac Low & Klessen (2004) (10 to 100 pc and 5×10^5 gas particles per galaxy), Naab et al. (2007) (8×10^6 particles with a 125 pc resolution in a cosmological resimulation of an individual galaxy halo). The highest resolution for gas-rich mergers have been achieved recently by Bournaud et al. (2008) for mergers of bright spiral galaxies, with a total of 3.6×10^7 particles including more than 10^7 gas particle, and a 32 pc softening size, and Kim et al. (2009) with a spatial resolution of 3.8 pc and a mass resolution of $2 \times 10^3\,\mathrm{M}_\odot$ (for dwarf or low-mass spirals, though). But such high-resolution studies have focused on small-scale gas physics and structure formation, without studying the impact of high resolution on the global properties of the elliptical-like galaxies formed in major mergers.

Large samples of simulations of idealized galaxy mergers remain typically limited to softening lengths of about 100–300 pc, and $\sim 10^5$ particles per galaxy (see samples in Naab & Burkert 2003; Bournaud, Combes & Jog 2004; Cox et al. 2006b; Naab, Jesseit & Burkert 2006; Bournaud, Jog & Combes 2007; Di Matteo et al. 2007; Cox et al. 2008). Whether or not the relatively limited numerical resolution used in such studies affects the global properties of merger remnants is still a largely open question: for instance, the detailed comparison of major merger remnants with the observed anisotropy-flattening relation by Burkert et al. (2008) relies on simulations with 2×10^4 gas particles per galaxy, a gas particle mass $\sim 3 \times 10^5\,\mathrm{M}_\odot$ and a spatial resolution (softening) of about 200 pc.

Within the context of the ATLAS^{3D} project (http://purl.org/atlas3d), an extensive set of numerical simulations is being conducted to support the multiwavelength survey of a complete sample of early-type galaxies within the local (40 Mpc) volume, in terms of various formation mechanisms of early-type galaxies: binary mergers, multiple mergers, disc instabilities, etc. An ambitious series of simulations of mergers are being specifically performed and analysed for this purpose (Bois et al. in preparation). To properly interpret the results from these simulation efforts, as well as to understand the robustness of the existing and the past studies of galaxy mergers, we first probe the effect of spatial and mass resolutions on the global structure of binary disc merger remnants.

In this paper, we study the effect of numerical resolution on the global morphology and the kinematics of the simulated remnants of binary, equal-mass major mergers. We wish to examine resolutions ranging from the typical resolutions used in recent, large simulations samples, to some of the highest merger simulations ever performed. We study both Wet (collisionless) and Wet (gas-rich) mergers of disc galaxies. The modelled interaction orbits lead to the formation of both fast rotators, i.e. early-type galaxies flattened by significant rotational support, and slow rotators, i.e. early-type galaxies with low-residual rotation, supported (and flattened) by (anisotropic) velocity dispersions, following the classification detailed in Emsellem et al. (2007, see also Section 2) (hereafter E07). We find that the formation of fast rotators is overall correctly reproduced with numerical simulations at modest resolutions. In contrast, the formation of slow-rotating systems is correctly reproduced only at high resolution (Section 3), above the resolution of most of the recently published merger simulations. The influence of gas on the structure of merger remnants, compared to Wet mergers, also differs at high resolution, and is not limited to easing the survival and/or

rebuilding of rotating disc components. In Section 4, we further examine the origin of this observed resolution effect in the formation of slow-rotating systems. We show that it is not an artefact from different initial conditions or interaction orbits, but that the physical treatment of the merging process is actually biased when the resolution is too low. The effect of the resolution has been tested on other simulations producing slow rotators and we find that it is a systematic one (Section 5). We summarize our results, discuss the required resolution for accurate studies and the general implications for the formation of elliptical galaxies in Section 6.

2 SIMULATIONS AND ANALYSIS

2.1 Method

2.1.1 Code

We use the particle-mesh code described in Bournaud et al. (2008), and references therein.

This code uses a Cartesian grid on which the particles are meshed with a 'Cloud-In-Cell' interpolation. The gravitational potential is computed with an FFT-based Poisson solver and particle motions are integrated with a leap-frog algorithm and a time-step of 0.5 Myr.

Interstellar gas dynamics is modelled with the sticky-particle scheme with elasticity parameters $\beta_t = \beta_r = 0.6$. This scheme neglects the temperature and thermal pressure of the gas, assuming it is dominated by its turbulent pressure, which is the case for the star-forming interstellar medium at the scales that are studied here (Elmegreen & Scalo 2004; Burkert 2006). The velocity dispersion of the particles model the turbulence and their mutual collisions are inelastic to ensure that the turbulence dissipates over about a vertical crossing time (Mac Low 1999).

The star formation rate is computed using a Schmidt–Kennicutt law: it is then proportional to the gas density in each cell to the exponent 1.5. Gas particles are converted to star particles with a corresponding rate in each cell. Energy feedback from supernovae is accounted for with the scheme proposed by Mihos & Hernquist (1994). Each stellar particle formed has a number of supernovae computed from the fraction of stars above 8 $M_\odot$ in a Miller–Scalo initial mass function. A fraction ϵ of the 10^{51} erg energy of each supernova is released in the form of radial velocity kicks applied to gas particles within the closest cells. We use $\epsilon = 2 \times 10^{-4}$, as Mihos & Hernquist (1994) suggest that realistic values lie around 10^{-4} and less than 10^{-3}.

2.1.2 Set-up for initial disc galaxies

The baryonic mass of our model galaxies is 10^{11} $M_\odot$. In Wet merger simulations, this mass is purely stellar. In Wet merger simulations, 80 per cent of this mass is stellar and 20 per cent is gaseous. The initial gas and stellar discs are Toomre discs, with a scalelength of 4 kpc and a truncation radius of 10 kpc for the stars, respectively, 8 and 20 kpc for the gas. 20 per cent of the stars are in a spherical bulge, modelled with a Hernquist (1990) profile with a 700 pc scalelength. The dark matter halo is modelled with a Burkert profile (Burkert 1995), a 7-kpc scalelength and a truncation radius of 70 kpc, inside which the dark matter mass is 3×10^{11} $M_\odot$.

The two 'progenitor' disc galaxies in each simulation are identical, the total mass of the remnant will be 2×10^{11} $M_\odot$ which is consistent with the *slow-rotator* mass range observed in the ATLAS^{3D} sample (E07).

2.1.3 Orbits

We have used two interacting orbits, for each kind of merger (Dry and Wet) and each resolution level. None corresponds to a very specific and unlikely configuration like coplanar discs, or polar orbits.

The first orbit is called *'fast'* because it forms fast-rotating early-type galaxies. The velocity at an infinite distance is 170 km s^{-1} and the pericentre distance is 30 kpc. This orbit is prograde with respect to the first progenitor disc, with an inclination of the orbital plane wrt the disc plane of 25°. The orbit is retrograde wrt the other progenitor disc, with an inclination of 45°.

The second orbit is called '*slow*' because it forms slow-rotating early-type galaxies (at least at high-enough resolution). The velocity at an infinite distance is 140 km s^{-1} and the pericentre distance is 25 kpc. This orbit is prograde with respect to the first progenitor disc, with an inclination of the orbital plane wrt the disc plane of 45°. The orbit is retrograde wrt the other progenitor disc, with an inclination of 25°.

These orbits as well as those used in additional tests (Section 5) have a total energy $E > 0$ or $E \simeq 0$, corresponding to initially unbound galaxy pairs. Such orbits are representative of the most common mergers in ΛCDM cosmology (Khochfar & Burkert 2006).

2.1.4 Standard, high and very high resolutions

Dry and Wet mergers have been simulated for each orbit at three resolution levels. The detail for these resolutions are indicated in Table 1. The *very high* resolution arguably corresponds to the highest resolution simulation of a Wet major merger performed so far (see Bournaud et al. 2008).

We will label each simulation with the following nomenclature:

(i) the first item indicates a *Wet* or *Dry* merger, i.e. gas-rich or gas-free progenitors;

(ii) the second item specifies the chosen orbit: the one producing *fast-rotators* or *slow-rotators* (at least at high-enough resolution);

(iii) the last item indicates the resolution level: *standard*, *high* or *very high*;

For instance, the *wet-fast-high* simulation refers to the high-resolution models of a Wet merger on the orbit producing a fast-rotating early-type galaxy.

2.2 Analysis of the relaxed merger remnants

We analyse the merger remnants after 1.2 Gyr in the simulation, which is 800–900 Myr after the first pericentre passage, and 600–700 Myr after the central coalescence. The remnants are thus relaxed when the analysis is performed. Tidal debris can still be orbiting around the merger remnant, but the bulk of the stellar mass in the central body does not show significant evolution. Analysis

Table 1. Label for the resolution, softening length, number of particles per component (stars, gas and dark matter) and total number of particles in the simulation for the three resolutions.

Label	Softening length	Particles/component	Total particles
standard	180 pc	10^5	6×10^5
high	80 pc	10^6	6×10^6
very high	32 pc	6×10^6	3.6×10^7

performed at earlier and later instants did not show significant variations, so spurious effects related to time evolution should not affect the comparison of the three different resolution levels.

2.2.1 *Projected maps*

Intrinsic and apparent properties of the merger remnant (e.g. the apparent ellipticity) are directly linked with its orbital structure (Jesseit, Naab & Burkert 2005). To probe the relaxed merger remnants, we have therefore built projected maps of the stellar mass density, line-of-sight velocity and velocity dispersion fields. Two-dimensional maps are useful to reveal the wealth of photometric or kinematic structures associated with a galaxy merger, e.g. globular clusters or kinematic misalignments (see Bendo & Barnes 2000; Jesseit et al. 2007).

The projected maps cover a 16×16 kpc^2 field of view around the density peak of each system: our analysis is conducted up to a limit of three effective radii R_e, which encloses most of the baryonic mass of early-type galaxies, and the typical effective radius of our merger remnants is 2.5 kpc. Each projection was computed on a 100×100 pixel grid. The pixel size is 160×160 pc^2, which approximately corresponds to the size of the softening length of our *standard-res* simulations, and is kept fixed for all resolutions.

To obtain statistically significant results, we have built such maps and performed the subsequent analysis with 200 isotropically distributed viewing angles (i.e. 200 different line of sights). In this way, we do not characterize and compare the merger remnant under a particular projection, but their global, statistical properties. As an example, Fig. 1 shows the effect of the projections on the radial λ_R profiles for one simulation. Among these 200 profiles, the lowest (near zero) and the highest values correspond, respectively, to the merger remnant seen nearly face-on (i.e. the lowest apparent ellipticity) or nearly edge-on (i.e. the highest apparent ellipticity). Our choice of 200 projections ensures that neighbouring projections are separated only by 10° in any direction, so that intermediate viewing angles would not show significant differences.

2.2.2 *Physical parameters*

Our analysis is based on a few simple morphological and kinematic parameters – a choice mainly motivated by the fact that these parameters are often being used as standards in studies of nearby elliptical galaxies.

The morphological parameters pertains to the photometry: we measure the ellipticity ϵ (defined as $1 - b/a$, where a and b are the semimajor and minor axes, respectively) and a_4/a which is the fourth (cosine) Fourier coefficient of the deviation of isophotes from a perfect ellipse ($a_4/a > 0$ and $a_4/a < 0$ correspond to discy and boxy isophotes, respectively). These two parameters are computed using the KINEMETRY software tool[1] which can be used to perform standard ellipse-fitting of galaxy images, as well as to study galaxy kinematics (Krajnović et al. 2006). For the kinematic analysis, apart from the first two velocity moments (velocity and velocity dispersion), we use the λ_R parameter, a robust proxy for the baryonic projected angular momentum, as defined in E07:

$$\lambda_R \equiv \frac{\langle R|V|\rangle}{\langle R\sqrt{V^2+\sigma^2}\rangle}.$$

[1] http://www-astro.physics.ox.ac.uk/dxk/idl/

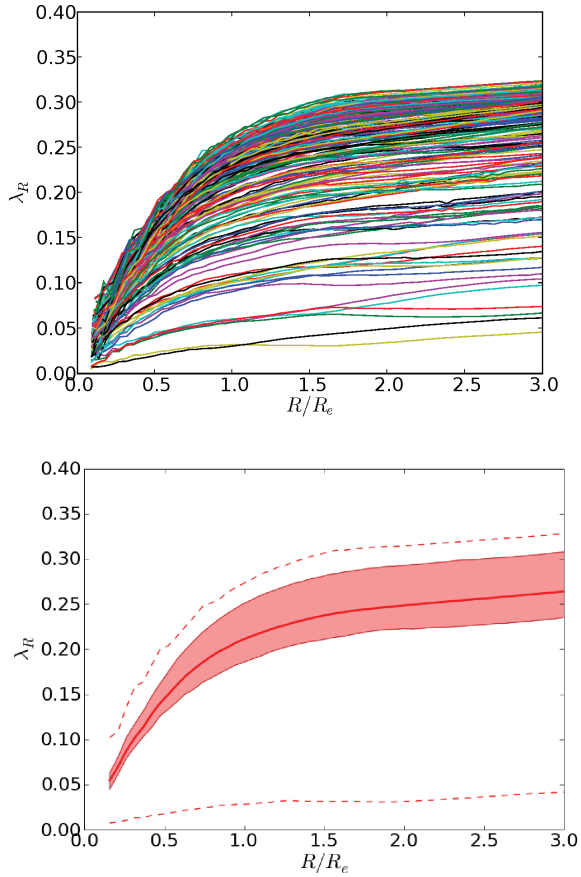

Figure 1. Top panel: λ_R profiles of all 200 projections for the *Dry-Fast-very high* simulation. The profiles are plotted as a function of R/R_e (radius normalized by the effective radius for each projection). Each line here corresponds to a given projection. Bottom panel: corresponding median (thick solid line), quartiles (thin solid line) and maximal and minimal values (dashed lines) at each radius. This representation of the results illustrates the fact that all values are between the dashed lines, and 50 per cent of the projections are in the filled area. Each line plotted in this panel does not correspond to one specific projection: the median or quartiles are derived for different projections at each radius.

In E07, λ_R was used to reveal two families of early-type galaxies, the *slow-rotators* with $\lambda_R \leq 0.1$ and the *fast-rotators* with $\lambda_R > 0.1$ at one effective radius R_e. In a recent study, Jesseit et al. (2009) have simulated binary disc mergers to investigate the λ_R parameter: tests on their merger remnants reveal that λ_R is a good indicator of the true angular momentum content in early-type galaxies. As emphasized in E07, Cappellari et al. (2007) and Krajnović et al. (2008), fast and slow rotators exhibit qualitatively and quantitatively different stellar kinematics. λ_R is thus an interesting parameter to probe, and should indicate whether or not the kinematics of the merger remnants are equally resolved at different resolutions.

For each above-mentioned parameter, we have computed the minimum, maximum, mean values, as well as the 1st and 3rd quartiles over all the projections at individual radii, to quantify the statistical distribution of these parameters in a simple way. An example is shown in Fig. 1. Note that with this choice, the projection which minimizes or maximizes a parameter varies with radius.

3 EFFECT OF RESOLUTION ON THE FORMATION OF SLOW ROTATORS

In this section, we briefly describe the properties of the simulated mergers with the three different resolutions. The complete set of analysis results can be found in Appendix A. We then focus the analysis on the simulations that show important differences, namely the cases producing slow rotators at high resolution.

3.1 Morphology and kinematics

Radial stellar density profiles are shown in Fig. 2. We then show, in Fig. 3, the projected stellar density maps, of the relaxed merger remnants in all simulations, choosing the flattest and roundest projections as well as a projection representative of the mean ellipticity in each case. The corresponding line-of-sight stellar velocity fields are presented in Fig. 4 for the same projections, the maps have been Voronoi binned (Cappellari & Copin 2003) to the same level of 15 particles minimum per bin. Further morphological or kinematics parameters are presented in Appendix A.

This analysis reveals various similarities or differences, depending on which merger is considered. The most notable results are as follows:

(i) *Mergers that produce fast-rotators at the highest resolution also result in fast rotating systems at the lower, standard resolution*. Overall, the apparent morphology for any projection of the Dry-Fast and Wet-Fast models is unaffected by the resolution (Fig. 3). The velocity fields are also quite similar (Fig. 4), with only minor misalignments between the apparent kinematic and photometric axes. Ellipticity and λ_R profiles, provided in Appendix A (see Figs A1 and A2), confirm these similarities and that all these merger remnants are fast rotators, with a rotational support that is largely independent from the numerical resolution.

(ii) *Strong kinematic misalignments and kinematically decoupled cores* (*KDCs*) are found only in slow-rotators, but really appear only at high resolution. The Dry-Slow model has a KDC at standard resolution, but its amplitude is significantly lower than the one observed in the high and highest resolution models. The Wet-Slow model has a KDC only at high/very high resolution. Overall, kinematic misalignments increase at high resolution, as illustrated for instance by the flattest projections of the Wet-Slow case.

(iii) *Morphological and kinematic differences are most important for mergers that produce slow-rotators at high resolution.* Striking morphological differences are seen in particular for the Wet-Slow case (Figs 2 and 3) and both the amplitude and the shape of the velocity field change with resolution for the Wet-Slow and Dry-Slow cases (Fig. 4). For instance, a rapidly rotating core is seen in the Wet-Slow merger remnant at standard-resolution, instead of a slow-rotating KDC at high and very high resolutions. The Dry-Slow remnant also shows up as a discy rotating system at standard resolution, in contrast with the observed remnant at higher resolutions. We also note on Fig. 2 that the stellar density profile is resolution-dependent in particular for the Wet-Slow case, with a much less concentrated merger remnant in the standard-resolution case (the mass within 5 kpc is about 25 per cent lower than at high or very high resolutions).

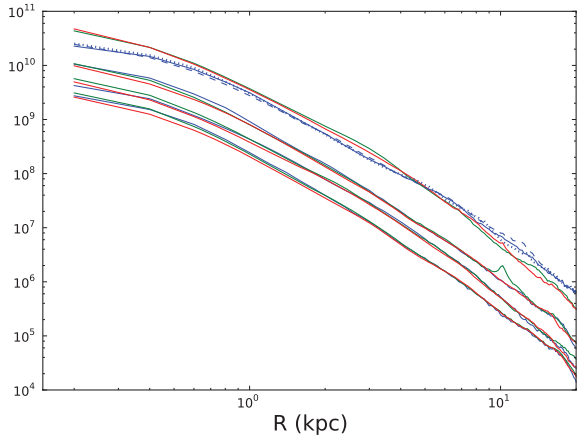

Figure 2. Stellar density profiles for the Wet-Slow, Wet-Fast, Dry-Slow and Dry-Fast simulations (from top to bottom, respectively). The density of the Wet-Fast, Dry-Slow and Dry-Fast cases has been divided by a factor of 5, 10 and 20, respectively, to improve the readability of the plot. Red lines correspond to very high resolution models, green lines to high-resolution cases and blue lines to standard-resolution models. The two alternative realizations of the Wet-Slow-Standard simulation (see Section 4.3) are shown in dashed and dotted lines.

3.2 Formation of *slow-rotators* at high resolution

We now focus on the detailed properties of the mergers for which the most important differences have been noticed, namely those producing slow rotators at the highest resolutions.

3.2.1 Morphology and kinematics

To better understand the differences seen in the morphology of the Wet-Slow simulations, we have examined the three included baryonic components of the merger remnants separately, namely the 'old' stars formed before the beginning of the merger event, the 'young' stars formed during/after the merger event, and the gas left over after the merger (see Fig. 5). Within the central 10 kpc, the *standard-res* remnant exhibits a prominent bar, the inner distribution of the gas and young stars being driven by this tumbling structure with e.g. a ring-like structure at a radius of ∼6 kpc. In the *high-res* and *very high-res*, the gaseous component and the young stars have a smoother distribution more closely following the overall old stellar distribution. In addition, many young star clusters are visible in the maps from the *very high-res*, a few in the *high-res* and none in the *standard-res*. High spatial resolution of course allows to resolve the formation of stellar clusters (see also Bournaud et al. 2008), but there is also a larger number of other young stellar substructures at increasing resolution, like filaments, tidal streams and a compact nucleus (Fig. 5).

The kinematic discrepancies discussed above in the velocity fields are quantified globally in the radial velocity and λ_R profiles (Fig. 6). The *standard-res* displays significant rotation inside 3–4 kpc (up to ∼85 km s^{-1}) and a decreasing rotation velocity at larger radii. There is a drop in the velocity dispersion in the central 2 kpc, and no sign of a KDC. This is in stark contrast with both the *high-res* and *very high-res* which overall show much lower rotational velocity support (below ∼50 km s^{-1} and particularly low in the central 2 kpc), and a KDC in the central 1 kpc. Overall, the *high-res* and *very high-res* have similar velocity rotation curves, apart from a more pronounced KDC signature in the *very high-res* (partly due to the KDC having a slightly different position angle in these two remnants).

The general discrepancies of the *standard-res* versus *high-res* and *very high-res* realizations are confirmed by the λ_R profiles (Fig. 6). The merger remnant made at *standard-res* is clearly a *fast-rotator*. The *high-res* and *very high-res* are both classified as

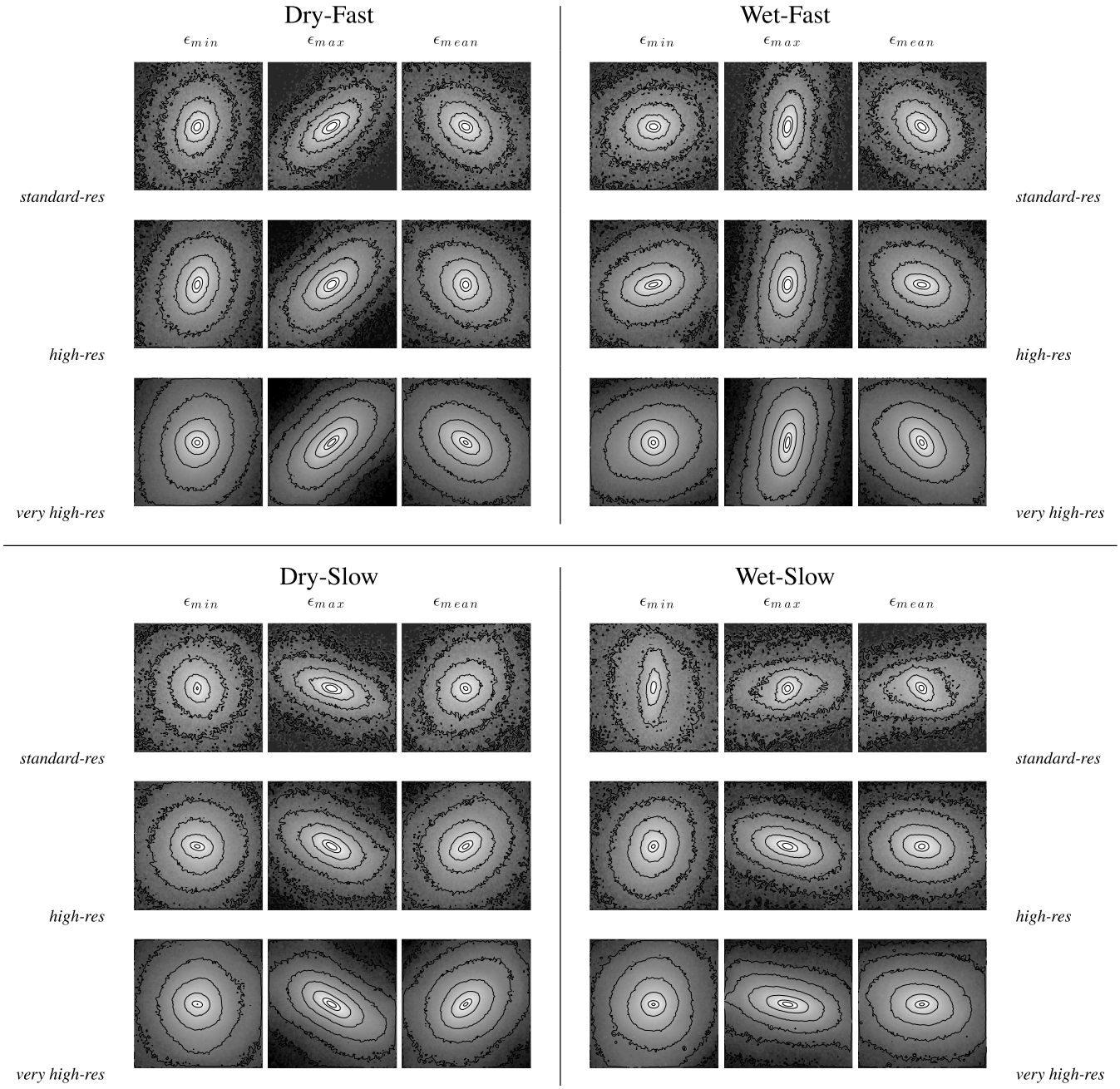

Figure 3. The 12 normalized projected surface density maps (in log), for the four sets of simulations at three different resolutions (labelled accordingly). The field of view is 16 × 16 kpc^2. For each simulation, the projections corresponding to the minimum, maximum and mean ellipticities are shown. The viewing angle of these projections are defined at *very high-res* and re-applied for the *standard-res* and *high-res* simulations: projections are thus established along the same line of sights for all resolutions. Luminosity contours are the same for all simulations and drawn with a spacing of 0.5 mag (except for the two inner contours with a step of 0.3). The effective radius is about at the edge of the fourth isophote for all simulations.

slow-rotators with, respectively, a maximum value of λ_R of 0.1 and 0.06 at one effective radius. The λ_R profile goes up somewhat more rapidly with radius in the *high-res* case than in the *very high-res*, but the difference remains of the order of the scatter between different projections of each case. The presence of a bar in the stellar component of the *standard-res* is likely a result of the significantly higher rotational support (see also Section 5).

Beyond one R_e, the λ_R profiles of the *high-res* and *very high-res* are rising: there is less angular momentum in the centre, which has been expelled outwards (see also E07). However, even at these large radii, the *slow-rotators* have less angular momentum than *fast-rotators* (see Fig. 6). Observations conducted up to two or three R_e (Coccato et al. 2009; Weijmans et al. 2009) would bring additional constraints on the formation scenario of slow-rotating early-type galaxies.

3.2.2 *Role of gas on the properties of merger remnants*

The Dry-Slow simulations show smaller differences in the stellar density maps and velocity fields. They also exhibit smaller differences in their λ_R profiles (Fig. 7). Nevertheless, the *standard-res*

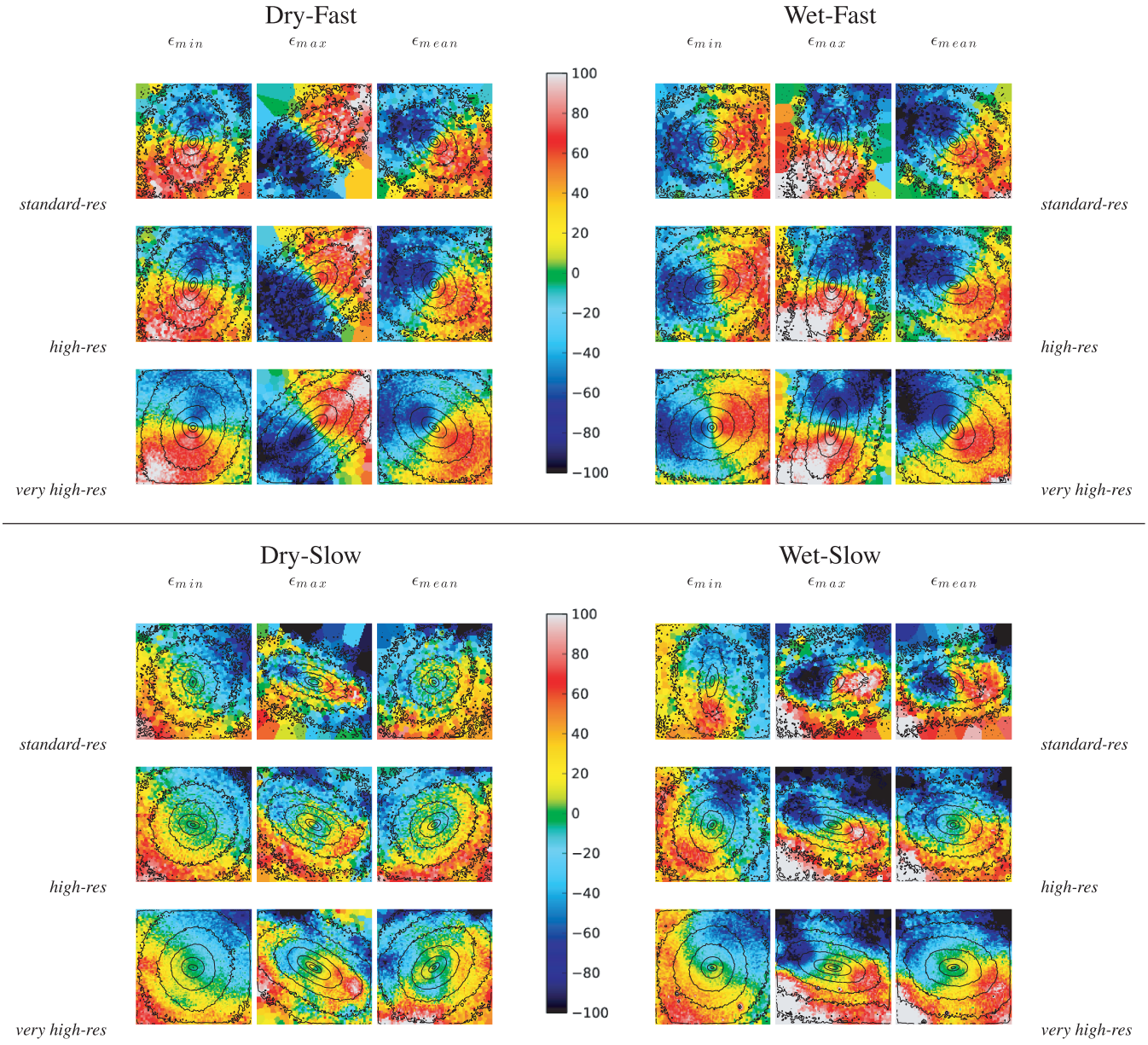

Figure 4. The 12 projected stellar velocity fields. The field of view is 16 × 16 kpc^2, projections and contours are the same as in Fig. 3.

simulation is again a faster-rotator than the *high-res* and *very high-res* cases at 1, 2 or 3 effective radii. A KDC is also found only in the *high-res* and *very high-res* cases, associated to a peak of λ_R inside one effective radius.

A lower specific angular momentum in the main stellar body at higher resolution is not only found in Wet-Slow mergers, but also in Dry-slow mergers, the differences being still much more pronounced in the Wet case.

Gas plays an important role in shaping merger remnants (Naab et al. 2006; Robertson et al. 2006; Hopkins et al. 2009) and it is interesting to compare the Wet-Slow and Dry-Slow merger remnants at fixed resolution, to better understand its specific impact (Figs 6 and 7).

(i) At *standard-res*, the Wet merger remnant has a much higher rotational support than the Wet case. This is consistent with the usually known effect of gas helping the survival of rotating stellar discs during major mergers, and/or rebuilding of discs after mergers (Robertson et al. 2006; Hopkins et al. 2009).

(ii) At *high-res* and *very high-res*, the rotational support of the merger remnant is not increased when gas is present. The angular momentum, traced by λ_R, is actually lower by about 20 per cent inside one effective radius in the *very high-res* Wet case, compared to the corresponding Dry merger.

It thus seems that the impact of gas on the global properties of major merger remnants is more complex than originally thought, and can even be weakened at high resolution. This suggests that the global dynamics of gas during the major merger or in a young merger remnant can be significantly affected by resolution. As seen in Fig. 5, gas at *standard-res* largely lies in smooth structures and the formation of new stars during the merger proceeds in a relatively smooth way. At increased resolutions, thinner gas structures are resolved during the merger, which can result in clustered star

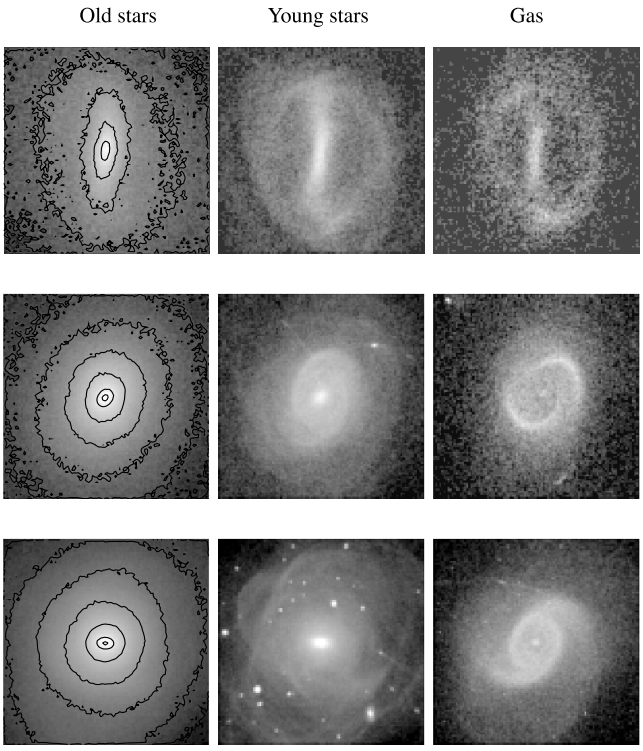

Figure 5. Projected density maps of the old stars, young stars and gas in the Wet-slow remnants; from top to bottom: *standard-*, *high-* and *very high-res* models, for the projection which minimizes the ellipticity ($\epsilon_{\rm min}$) as in Fig. 3. Old stars are those formed before the merger, young stars are formed during/after the merger. The field of view is 16 × 16 kpc^2 and the isocontours correspond to the projected old stellar component.

formation and the formation of numerous young stellar structures, as observed in the final merger remnant in Fig. 5.

3.3 Summary of the resolution tests

The resolution does not seem to significantly affect the morphology and kinematics of the mergers remnants that are fast rotators at high resolution: they are still fast rotators at lower resolution, with very similar morphological and kinematic properties. This contrasts with the fact that resolution has a major effect on the formation of slow-rotating systems. The systems that are slow rotators at high resolution rotate more rapidly when the resolution decreases, and can be observed as true fast rotators at *standard-res*. The effect is small in Dry mergers, but is dramatic in our Wet merger model. KDCs in these slowly rotating systems are also significantly better resolved at high resolution. The role of gas in shaping merger remnants is found to vary with resolution: at low resolution, gas rebuilds rotating disc components, increasing the overall disciness and rotational support. At higher resolution, the effect cancels out: a merger that forms a slowly rotating system in a Dry case still forms an equally slow or even a bit slower rotator in the corresponding Wet case.

The next section focusses on interpreting the origin of the resolution effect in the formation of slowly rotating ellipticals. We in particular show that it is not an artefact caused by different initial conditions or a bias in the simulated orbits, but a real effect related to the way the violent relaxation during the merger itself is treated.

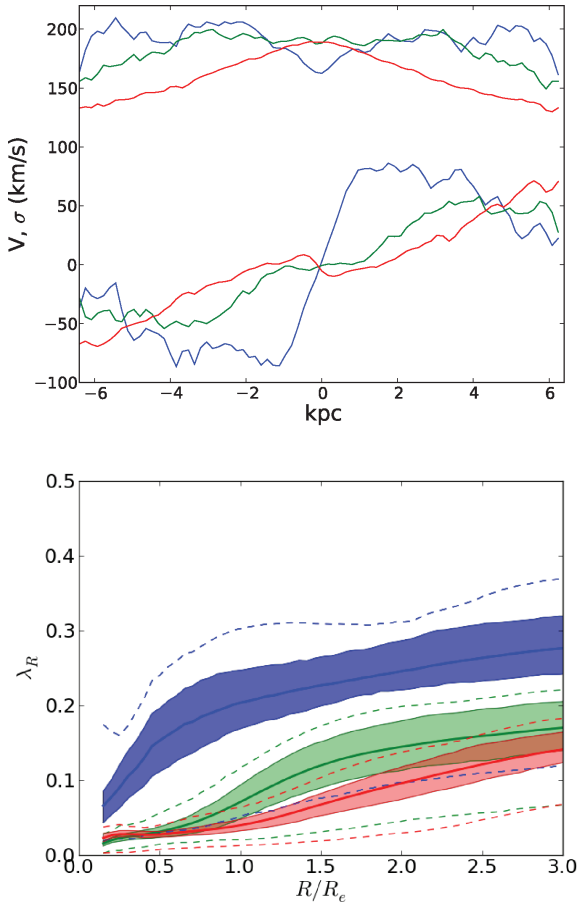

Figure 6. Top panel: radial line-of-sight velocity and velocity dispersion profiles (respectively bottom and top lines of the plot) for the mean ellipticity projection along the global kinematic position angle of the Wet-Slow simulation (right-hand panels of Fig. 4). Bottom panel: $\lambda_{\rm R}$ profiles as a function of $R/R_{\rm e}$, the minimum, median, maximum and quartiles values are presented as in Fig. 1. In both panels, the *standard-res* is represented in blue, the *high-res* in green, the *very high-res* in red.

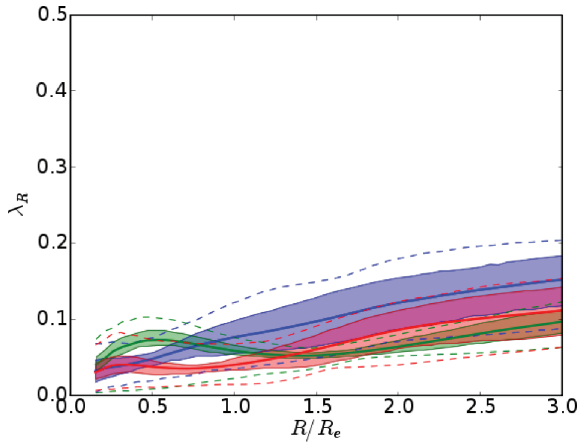

Figure 7. $\lambda_{\rm R}$ profiles as a function of $R/R_{\rm e}$ for the Dry-Slow simulation. The *standard-res* is represented in blue, the *high-res* in green, the *very high-res* in red.

4 ORIGIN OF THE RESOLUTION EFFECT

We here show that the above-mentioned discrepancies observed in the simulations that produce slow-rotating ellipticals at high resolution are really attributable to the physical modelling of the merging process. They are not artefacts related to initial conditions of the progenitor galaxies and/or interaction orbits that would vary with the resolution.

4.1 The progenitor galaxies

We first check that the progenitor galaxies are similar at any resolution. To this aim, we analyse their kinematic properties, in particular the λ_R profiles – ϵ and a_4/a parameters are less relevant for disc-dominated galaxies. Since the merger simulations were performed after an isolated relaxation of each progenitor galaxy (see Section 2), we analysed the progenitors from a snapshot right after this relaxation period, so that the results (Fig. 8) are representative of the conditions under which the mergers occur.

The two progenitor galaxies have quite similar angular momentum profiles (Fig. 8). There are some fluctuations, but they are not systematically corresponding to an increase or decrease of λ_R with resolution. They are also weaker than the discrepancies found in the final merger remnants. Actually, they result for a large part from the effective radius changing slightly with the resolution, and profiles of λ_R as a function of the absolute radius (in kpc) show smaller differences than the profiles in units of the effective radius. These fluctuations cannot therefore be the main cause for the observed resolution effects in the merger remnants.

4.2 Interaction orbits

Simulations at the three resolutions are started with the same relative position, velocity and inclination for the two interacting progenitors. However, varying the resolution may result in slight differences in dynamical friction and angular momentum exchanges, if these processes are resolved differently, and the interaction orbits might diverge before the merger actually takes place. If this were the case, our results would be attributable to different orbits rather than different treatments of the merging process itself.

We found that the positions at the first pericentric passage vary by 2.1 kpc on average and the velocities by 9 km s^{-1}. Although these differences seem small and no systematic variation with resolution appeared, we further investigated their potential effect. To this aim, we performed four new realizations for the Wet-Slow model at *high-res*, with variations of the position or the velocity twice larger than the average values above (i.e. $\pm$3.6 kpc and $\pm$18 km s^{-1}, respectively). The results are shown in Fig. 9 for the morphological and kinematic profiles of ϵ and λ_R. Changes are minor and differences arising in the interaction orbits cannot explain the variation of the results with resolution.

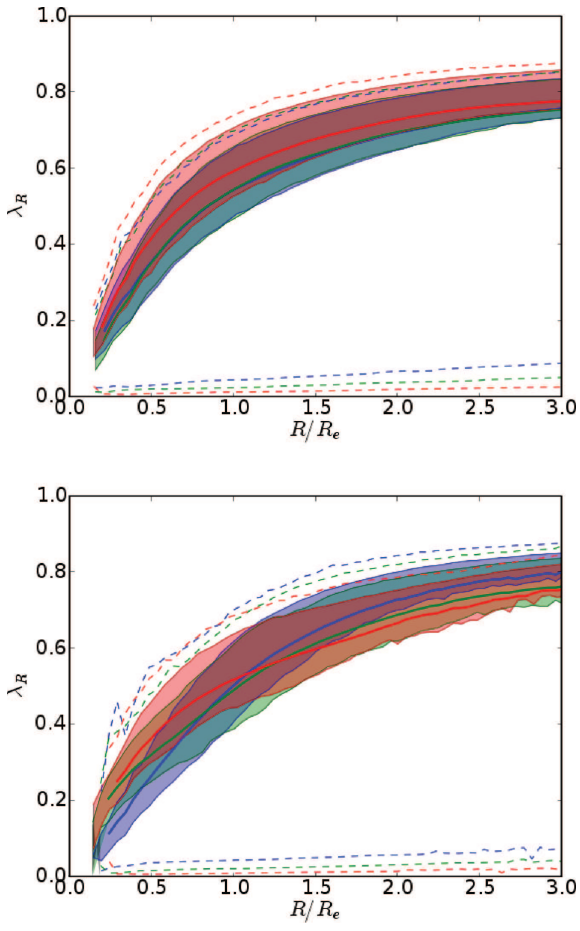

Figure 8. λ_R profiles of the two Wet progenitors as a function of R/R_e. Colours, as in previous figures, with the *standard-res* in blue, the *high-res* in green, the *very high-res* in red.

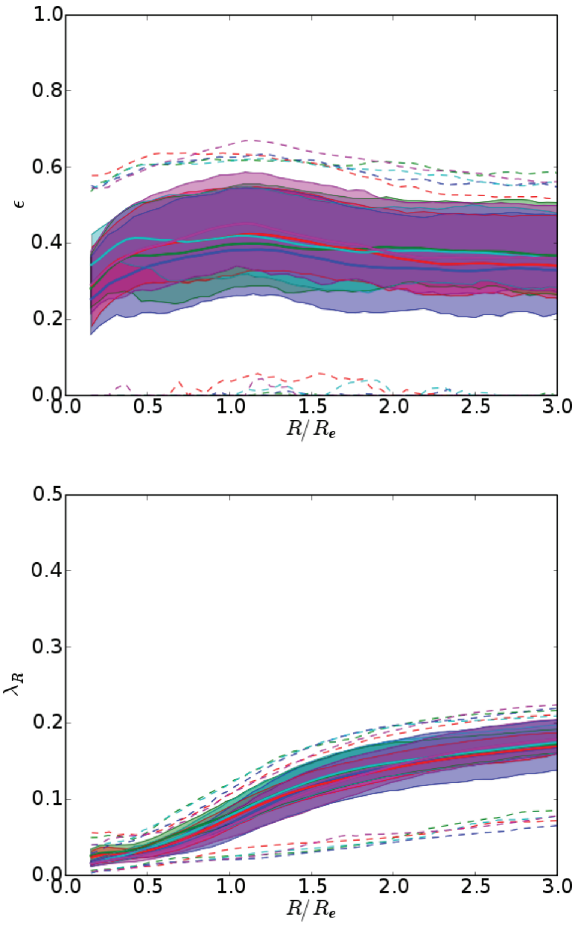

Figure 9. ϵ (top) and λ_R (bottom) profiles in function of R/R_e for five slightly different orbits for the Wet-Slow-High simulation.

4.3 Robustness of the Wet-Slow-Standard simulation

As the resolution effect found in the formation of slow rotators, in particular in the Wet-Slow model, cannot be attributed to a change in the initial conditions and interaction orbit, it likely relates to the physical treatment of the merging process itself. Nevertheless, we wanted to check whether or not this could still be attributed to the presence of particle noise, which is higher in the *standard-res* cases.

The Wet-Slow model at the *standard-res* shows a strong stellar bar, contrary to the *high-res* and *very high-res* cases. We wanted to make sure that this bar is a robust consequence of the high rotational support of the standard-resolution case, and is not a misinterpreted effect that arose from a particular realization of the particle noise.

To this aim, we performed two other Wet-Slow-Standard simulations with the same initial conditions but different, random realizations of the particle noise. The final stellar distribution, shown in Fig. 10 all show a similar bar, and the λ_R profiles are also relatively similar to the original Wet-Slow-Standard model – there are some variations, but the λ_R distributions of the three realizations overlap with each other, and the three systems are equally fast rotators. These two new realizations are also shown in dashed and dotted lines on Figs 2 and 11 and again share common properties with the initial Wet-Slow-Standard model, and hence the same differences compared to the higher resolution cases.

Thus, the role of bars and spiral patterns in redistributing the mass and angular momentum in the standard-resolution Wet-Slow model is robust, independent of a particular realization of the particle noise. We also find (see next subsection) that the time variations of the gravitational potential during the interaction and merger are similar for the three *standard-res* realizations.

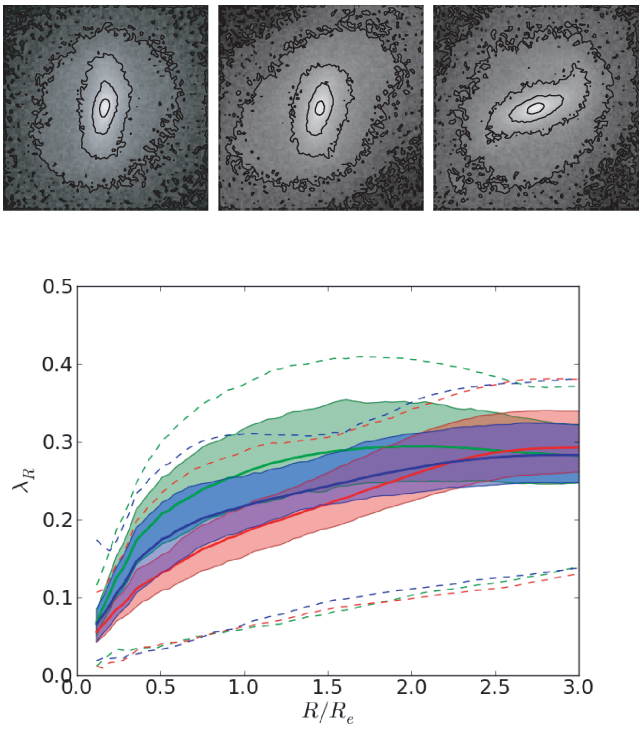

Figure 10. Top panel: stellar (old plus young) intensity maps for three different realizations of the Wet-Slow-Standard simulation. The field of view is 16 × 16 kpc^2. The simulation used in the study is in the left-hand panel. Bottom panel: λ_R profiles as a function of R/R_e of the three above simulations.

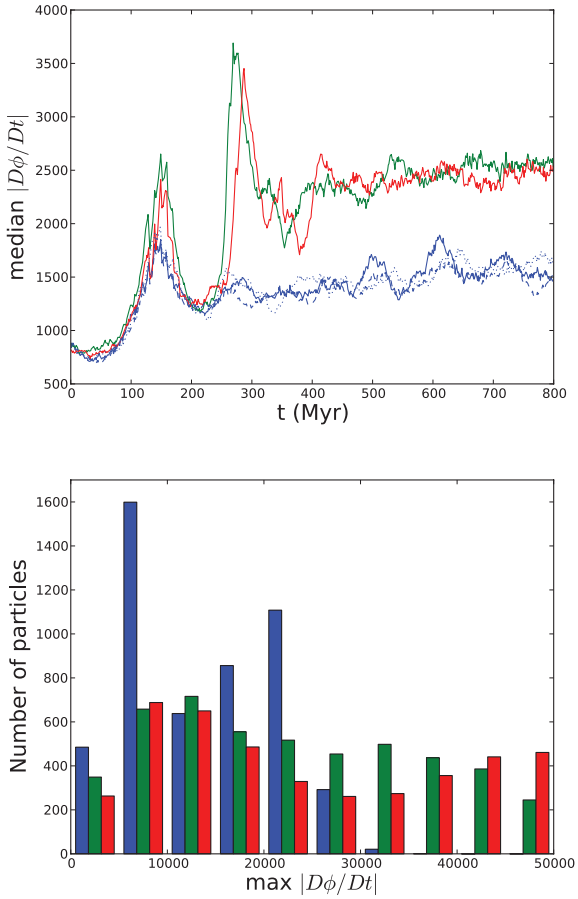

Figure 11. Top panel: median variations of the gravitational potential (in arbitrary units) over 5000 test particles as a function of time. The two other realizations of the Wet-Slow-Standard simulation are shown in dashed line. Bottom panel: histogram of the maximum variation of the gravitational potential (in arbitrary units) of each particle over the simulation.

4.4 The ongoing merger

At this point, we have established that the differences observed in the merger remnants do not result from variations in the initial conditions, interaction orbits or particle noise. The differences should then arise in the physical treatment of the merging process, which would mean that they are 'robust' effects, potentially affecting any simulation with any numerical code. Varying the spatial and mass resolution could affect the detailed evolution of the dissipative component (including star-forming structures), and this could in turn modify the overall orbital structure of the merger remnant (see Barnes & Hernquist 1996; Cox et al. 2006b; Naab et al. 2006). However, we have seen that the resolution effect does not completely disappear in Dry mergers. A more general effect can be the treatment of the violent relaxation, i.e. the rapid changes of gravitational potential that are responsible for the evacuation of energy and angular momentum from the main body of the merger remnant – these quantities being carried away by a low fraction of the mass expelled at large radii. This process of course plays a more important role in the formation of slow rotators than in the formation of fast rotators. The resolution effects are much more important for slow rotators than fast ones (Section 3), which suggests that they do actually relate to the violent relaxation process.

To quantify the importance of violent relaxation in our merger simulations, we followed, in the Wet-Slow models, the variations of

the gravitational potential $D\phi/Dt$ of 5000 randomly chosen 'test' particles, all of which are stellar particles existing at $t = 0$, all along the simulations. The derivate is Lagrangian, since it follows the motion of each particle. In an isolated galaxy, $D\phi/Dt$ relates to the variation of potential along the orbit of each particle, in particular their radial excursion in the potential well of the galaxy. During the interaction and mergers, peaks of $D\,\phi/Dt$ should trace the importance of scattering by local density fluctuations through the violent relaxation process.

The top panel of Fig. 11 shows the median value of $|D\phi/Dt|$ as a function of time – we take the absolute value for each particle, as a particle moving inwards or outwards can be considered with the same behaviour. Before the merging (i.e. before ∼150 Myr) the three resolutions are identical, meaning that there is no difference in the progenitors during the approach phase, modest values of $|D\phi/Dt|$ simply correspond to modest radial excursions of particle in the progenitor disc galaxies.

After the merger, each simulation shows a relatively constant $|D\phi/Dt|$ in a relaxed system, but the value is higher at *high-res* and *very high-res*, indicating larger radial excursions of stellar particles compared to the *standard-res* case. More radial orbits are indeed expected for slow rotators compared to the *standard-res* fast rotator. We note again that the different orbital structure does not only affect the gas and the young stars formed during the mergers, but also the old stars present before the merger itself (see also Fig. 5 and Section 3).

During the merging process, a first peak in the median $|D\phi/Dt|$ occurs at the first pericentre passage, after about 150 Myr, but is more pronounced at high(est) resolution. Another peak is found at the *high-res* and *very high-res* during the final coalescence at $t \sim 280$ Myr, but is much weaker in the *standard-res* case. The final coalescence does take place at the same moment for the three resolutions, but is a smooth process in the *standard-res* case, while it is accompanied by rapid variations of the potential undergone by stellar particles at high resolution. The bottom panel of Fig. 11 shows the maximum variation of $|D\phi/Dt|$ for each particle over all the simulation. The distribution at *standard-res* is very different from the distribution at *high-res* and *very high-res*. This confirms that the particles at *standard-res* undergo less rapid variation of the potential, i.e. lower peaks of gravitational forces.

This overall demonstrates that the relaxation process, during the merging of galaxies, is smoother at low resolution than at high resolution. We have shown previously that the *high-res* and *very high-res* simulations resolve much more dense substructures, like gas filaments, stellar clusters, compact cores, etc. Our interpretation is then that these local density peaks are accompanied by rapid variations of the gravitational potential, which scatter the stellar orbits, evacuate the angular momentum and form, for favourable orbits, slowly rotating elliptical galaxies. At low resolution, these rapid and local fluctuations of the density and potential are largely missed, hence the merging process is smoother and more angular momentum remains in the main stellar body of the merger remnant.

Density fluctuations are of course stronger in the dissipative component (gas) and the young stars formed therein, which likely explains why the resolution effect is stronger in Wet mergers. Nevertheless, old stars are clearly affected as well, as was shown above.

This also explains why the effect of gas in a Wet merger, compared to a Dry merger at fixed resolution, is different for standard-resolution models and high-resolution ones (Section 3.2.2). At *standard-res*, the gas remains relatively smooth, promotes the survival/rebuilding of a stellar disc component, thus increasing the rotational support in the final merger remnants. At higher resolution, the presence of gas forms many dense small-scale substructures of gas and young stars (consistent with observations, see e.g. Bournaud et al. 2008), these substructures increase the degree of relaxation during the merging process, not just for the gas and young stars but also for the old stars. Thus, while the presence of gas should still promote the survival/rebuilding of a disc component in the merger remnant (our high-resolution Wet-slow remnant does have a low-mass disc component of gas and young star), it also promotes orbital scattering and evacuation of the angular momentum for the whole baryonic mass, but the latter effect is missed if the resolution is too low. This explains why, at high resolution, the merger remnant (in the Wet-Slow case) does not have a higher rotation support or a more prominent disc component than the corresponding Dry-Slow case, and in fact even has a somewhat lower λ_R at one effective radius.

The high-resolution simulations, compared to the standard cases, resolve the formation of dense and relatively massive substructures (clusters, cores, filaments of 10^{5-7} solar masses) that scatter the stellar orbits and evacuate the angular momentum from the main body of the merger remnant. *Very high-res* simulations show a relatively reasonable convergence compared to the *high-res* ones: they resolve the same massive substructures, plus lower mass ones ($\sim 10^{4-5}$ solar masses) that are more numerous but are much less efficient to scatter the orbits and affect the relaxation of the merger remnant, as the corresponding relaxation time-scale is much longer. It is thus expected that results converge at a high-enough resolution.

4.5 Time-stepping and code specificities

Our results have been obtained with a given code and one can naturally wonder whether or not other codes would show the same resolution effect. We in fact expect no fundamental differences in the output from different codes, given that similar substructures are formed initially: this relaxation effect is mostly gravitational, and this should be treated rather similarly in grid-based and tree-codes. The main question remains then whether or not other codes would form substructures similar to those found in our simulations (e.g. with a similar mass spectrum, Bournaud et al. 2008): this a priori depends on the modelling of gas cooling and turbulence dissipation processes.

Another specificity of the code employed is its fixed time-step. A small time-step may better resolve the scattering of stellar orbits by dense substructures, in particular at high resolution. This would actually tend to increase the effect of resolution that we have found, which justifies studying the resolution effect at fixed time-step rather than decreasing the time-step at increasing spatial resolution. This way, the effects found can be robustly attributed to the spatial resolution. The time-step itself may have additional, separate effects, in our code or any other, that should be studied separately at fixed (high) resolution.

5 A SYSTEMATIC EFFECT IN THE FORMATION OF SLOW ROTATORS

To ensure that the resolution effect in the formation of slow rotators is a systematic one, and not specific to one simulated orbit, we have selected other major mergers that form slow rotators at high-enough resolution in a larger simulation sample (Bois et al., in preparation), and resimulated them at lower resolution. These three additional mergers were not simulated at the *very high-res* but at a resolution which is actually a bit higher than the *high-res*, with a spatial resolution of 58 pc and 2×10^6 particles per component

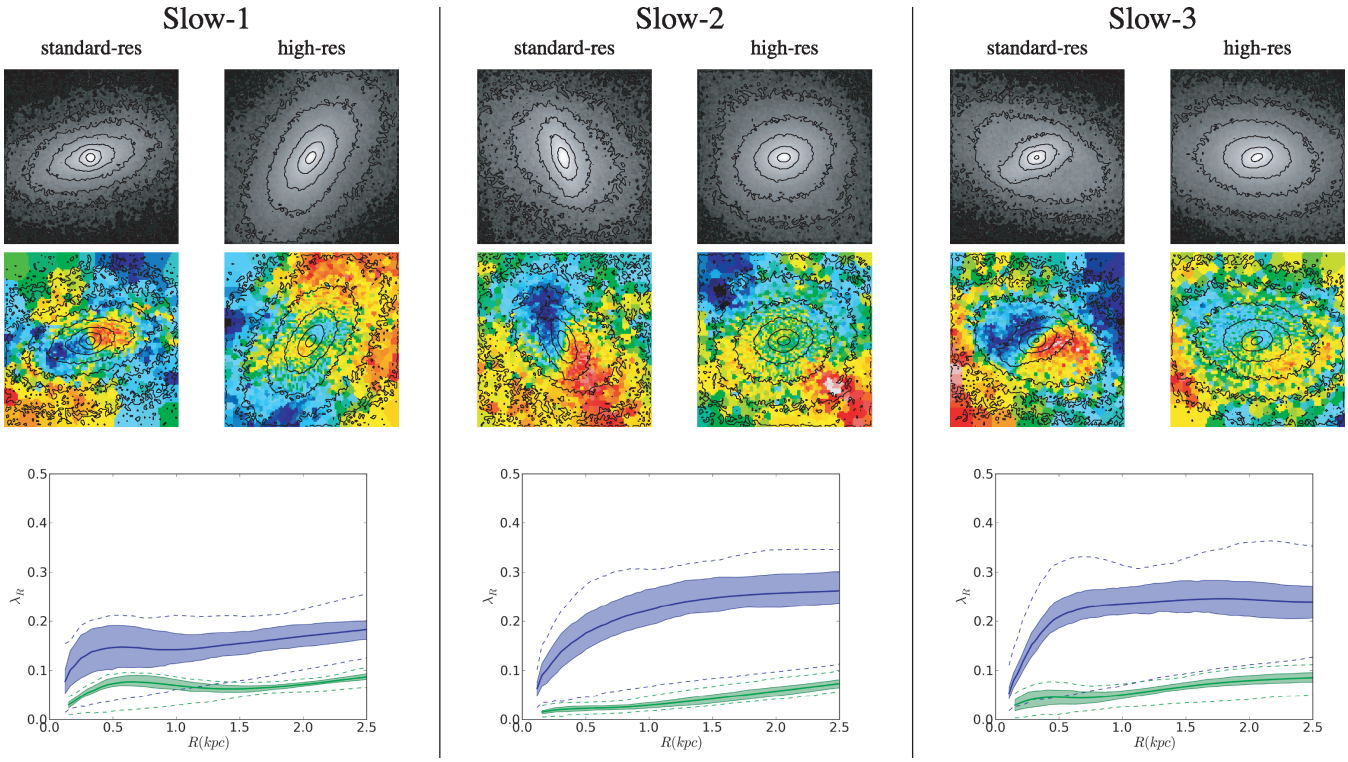

Figure 12. Projected density and velocity fields for the *standard-res* and *high-res* resolutions and their respective λ_R profiles (the *standard-res* in blue, the *high-res* in green) for the *slow-1, slow-2, slow-3* models (from left to right, respectively).

par galaxy (i.e. a total of 1.2×10^7 particles). They were also resimulated at the same *standard-res* level as the previous models. The gas fraction in these models is 10 per cent, so as to check that a high gas fraction is not required for the resolution effects to arise. Compared to the original slow-rotator simulation, one orbital parameter is changed in each case. Model *slow-1* has a retrograde orbit for both galaxies, model *slow-2* has a pericentre distance of 25 kpc, model *slow-3* has an orbit inclination of 25° for both discs.

The projected stellar density maps and line-of-sight velocity fields are shown for these models, at standard- and high resolutions, under the flattest projections in each case, on Fig. 12 (the λ_R profiles being also shown in this figure). These three merger remnants are slow rotators (at least at one effective radius) at *high-res*, but at *standard-res* they all have a much higher angular momentum λ_R, and a velocity field aligned with their morphological axis – the high-resolution slow rotators have important kinematic misalignments and KDCs.

These additional cases confirm the effect found and analysed in detail in the original slow-rotator model, with about the same degree of discrepancy between the standard-resolution and higher resolution models. Because we have spanned the four slowest rotators among the 1:1 mergers from the Bois et al. (in preparation) sample, the resolution effect seems to strongly affect the modelling of a significant number of slow-rotating ellipticals, if not all, even with modest gas fractions (here 10 per cent of the baryonic mass).

6 DISCUSSION AND CONCLUSION

In this paper, we have studied the effect of numerical resolutions (spatial and mass resolution) on the global properties of merger remnants. Our simulations at 'standard' resolution are comparable to the majority of merger simulation samples published in the last few years: the spatial resolution (gravitational softening and typical hydrodynamical smoothing lengths) is 180 pc, and the number of particles $\sim 10^5$ per galaxy and per component (gas, stars and dark halo). These simulations have been compared to models of the same mergers with increased resolution, up to 32 pc and almost 10^7 particle per galaxy and per component.

We have analysed the morphology and kinematics of the relaxed merger remnants. In particular, we have studied whether they are 'fast rotators', with an apparent spin parameter $\lambda_R > 0.1$ and have small misalignments between the morphological and kinematic axes, i.e. in broad terms early-type galaxies with significant flattening and rotational support. At the opposite end, 'slow rotators' are systems with a low $\lambda_R \leq 0.1$ (at one effective radius), large kinematic misalignments, i.e. early-type galaxies dominated by (anisotropic) pressure support and low residual rotation. Such slow rotators usually have central KDCs in our high-enough resolution simulations.

Our main findings can be summarized as follows:

(i) The formation of *fast-rotators* is not significantly affected by numerical resolution. Models that produce fast rotators at the highest resolution also result in fast rotators at lower resolution, with some random fluctuation of their properties but no sign of systematic variation in the morphology or angular momentum profile against resolution.

(ii) The formation of *slow-rotators* is greatly affected by numerical resolution. Models that produce slow rotators at the highest resolution result in much faster rotators at lower, standard resolution. The effect is present, but relatively minor, in purely collisionless Dry mergers. Discrepancies become major in Wet mergers, even in cases with modest gas fractions like 10 per cent of the baryonic mass.

(iii) These effects cannot be attributed to our choice of initial conditions or interaction orbits, but actually relate to the physical treatment of the merging process itself. In particular, small-scale density fluctuations increase at high resolution, and they participate to scattering stellar orbits and largely influence the final degree of relaxation and orbital structure in the merger remnants.

(iv) The effect of gas on the properties of merger remnants is generally considered to consist in preserving a higher angular momentum, in particular through enhancing the survival/rebuilding of disc components in merger remnants. We find that this picture is incomplete: at high resolution, gas still reforms discy components, but also forms a large number of dense substructures (massive star clusters, dense nuclei, tails, and filaments, etc.) that trigger rapid variations of the gravitational potential and the degree of relaxation of the final system. This effect is missed with a too low resolution. At high-enough resolution, adding gas to a given merger does not necessarily increase the rotational support of the final merger remnant; we even find a case of a Wet merger with 20 per cent of gas that has a final angular momentum parameter λ_R slightly lower than the corresponding Dry merger.

At the present stage, our results do not indicate how frequently real slowly rotating ellipticals were formed by binary (Wet) mergers of disc galaxies, but they show that this can be a robust pathway for their formation. In the course of the ATLAS^{3D} project, we are conducting, analysing and comparing a large set of numerical simulations for various formation mechanisms, in order to derive which is (are) the main formation mode(s) of real slow rotators in the nearby Universe. Our present results already indicate the limitations of existing samples of galaxy merger simulations, and will then serve to estimate the required resolution, the limitations of numerical models and their possible biases.

More generally, the immediate implications of these findings on our understanding of early-type galaxy formation are:

(i) High resolution in simulations of major mergers does not just allow to resolve small-scale structures like nuclear systems and star clusters, but impacts the whole global properties of the elliptical-like merger remnants, at least for the slow-rotating ones.

(ii) The formation of slow-rotating elliptical galaxies can be achieved through a major merger relatively more easily than previously believed. It can be frequent even in Wet mergers with relatively high gas fraction, and with late-type, disc-dominated progenitor galaxies.

(iii) Repeated mergers and/or Dry mergers of galaxies that are already early-type systems are thus not the only theoretical path to produce slow-rotating galaxies. Major mergers of two dic galaxies, including Wet mergers, can produce slow-rotating early-type galaxies. Further studies are needed to determine how common this formation mechanism is for slow-rotators.

(iv) Quantitative comparisons of major merger simulation results with the observed properties of real early-type galaxies require high-resolution models. A typical requirement, according to our study, would be a spatial resolution better than 100 pc for both the gravitational *N*-body aspects (i.e. softening length) and the hydrodynamical ones (for instance, the size of groups of particles with other quantities are smoothed in smoothed particle hydrodynamics models). The mass resolution should correspond to at least $\sim 10^6$ particle per galaxy per component, which typically corresponds to a mass resolution $\sim 10^4\,M_\odot$ for the gas discs of bright spiral galaxies. We find reasonable convergence above this resolution, but cannot rule out that some systematic effects still exist; in any case, simulations below this resolution level show clear and strong resolution effects. Unfortunately, most published samples of major merger simulations are below this typical resolution limit.

(v) The small-scale properties of interstellar gas and clustered star formation are important for the global, large-scale properties of merger remnants. Simulations directly resolving gas cooling down to low temperatures, the formation of cold (molecular) gas clouds and star formation therein, are highly desirable to understand the whole process of early-type galaxy formation. Modern hydrodynamic codes are promising in this respect (e.g. Bournaud et al. 2009; Kim et al. 2009).

ACKNOWLEDGMENTS

We are most grateful to the referee, Joshua Barnes, for constructive comments that very significantly improved the presentation of our results. This work was supported by Agence Nationale de la Recherche under contract ANR-08-BLAN-0274-01. Simulations were performed at CEA-CCRT using HPC resources from GENCI, grant 2009-042192.

REFERENCES

Barnes J. E., 1992, ApJ, 393, 484
Barnes J. E., Hernquist L., 1996, ApJ, 471, 115
Bendo G. J., Barnes J. E., 2000, MNRAS, 316, 315
Bournaud F., Combes F., Jog C. J., 2004, A&A, 418, 27
Bournaud F., Jog C. J., Combes F., 2005, A&A, 437, 69
Bournaud F., Jog C. J., Combes F., 2007, A&A, 476, 1179
Bournaud F., Duc P.-A., Emsellem E., 2008, MNRAS, 389, L8
Bournaud F., Elmegreen B. G., Martig M., 2009, ApJ, 707, L1
Burkert A., 1995, ApJ, 447, L25
Burkert A., 2006, Comptes Rendus Phys., 7, 433
Burkert A., Naab T., Johansson P. H., Jesseit R., 2008, ApJ, 685, 897
Cappellari M., Copin Y., 2003, MNRAS, 342, 345
Cappellari M. et al., 2007, MNRAS, 379, 418
Chilingarian I., Di Matteo P., Combes F., Melchior A.-L., Semelin B., 2010, preprint (arXiv:1003.3243)
Coccato L. et al., 2009, MNRAS, 394, 1249
Cox T. J., Jonsson P., Primack J. R., Somerville R. S., 2006a, MNRAS, 373, 1013
Cox T. J., Dutta S. N., Di Matteo T., Hernquist L., Hopkins P. F., Robertson B., Springel V., 2006b, ApJ, 650, 791
Cox T. J., Jonsson P., Somerville R. S., Primack J. R., Dekel A., 2008, MNRAS, 384, 386
Di Matteo P., Combes F., Melchior A.-L., Semelin B., 2007, A&A, 468, 61
Di Matteo P., Bournaud F., Martig M., Combes F., Melchior A.-L., Semelin B., 2008, A&A, 492, 31
Elmegreen B. G., Scalo J., 2004, ARA&A, 42, 211
Emsellem E. et al., 2007, MNRAS, 379, 401 (E07)
Hernquist L., 1990, ApJ, 356, 359
Hernquist L., Barnes J. E., 1991, Nat, 354, 210
Hopkins P. F., Hernquist L., Cox T. J., Dutta S. N., Rothberg B., 2008, ApJ, 679, 156
Hopkins P. F., Cox T. J., Younger J. D., Hernquist L., 2009, ApJ, 691, 1168
Jesseit R., Naab T., Burkert A., 2005, MNRAS, 360, 1185
Jesseit R., Naab T., Peletier R. F., Burkert A., 2007, MNRAS, 376, 997
Jesseit R., Cappellari M., Naab T., Emsellem E., Burkert A., 2009, MNRAS, 397, 1202
Khochfar S., Burkert A., 2006, A&A, 445, 403
Kim J. H., Wise J. H., Abel T., 2009, ApJ, 694, 123
Krajnović D., Cappellari M., Tim de Zeeuw P., Copin Y., 2006, MNRAS, 366, 787
Krajnović D. et al., 2008, MNRAS, 390, 93
Li Y., Mac Low M.-M., Klessen R. S., 2004, ApJ, 614, L29
Mac Low M.-M., 1999, ApJ, 524, 169
McDermid R. M. et al., 2006, MNRAS, 373, 906

Mihos J. C., Hernquist L., 1994, ApJ, 437, 611
Mihos J. C., Walker I. R., Hernquist L., Mendes de Oliveira C., Bolte M., 1995, ApJ, 447, L87
Naab T., Burkert A., 2003, ApJ, 597, 893
Naab T., Jesseit R., Burkert A., 2006, MNRAS, 372, 839
Naab T., Johansson P. H., Ostriker J. P., Efstathiou G., 2007, ApJ, 658, 710
Navarro J. F. et al., 2010, MNRAS, 402, 21
Robertson B., Bullock J. S., Cox T. J., Di Matteo T., Hernquist L., Springel V., Yoshida N., 2006, ApJ, 645, 986
Weijmans A.-M. et al., 2009, MNRAS, 398, 561
Wetzstein M., Naab T., Burkert A., 2007, MNRAS, 375, 805

APPENDIX A: ADDITIONAL MORPHOLOGICAL AND KINEMATIC PARAMETERS FOR THE MERGER REMNANTS

In this appendix, we provide further details on the morphology and kinematics of the four merger remnants analysed in the present paper.

A1 Morphology

The ellipticity ϵ and a_4/a profiles are shown in Fig. A1 as a function of R/R_e. The apparent differences sketched in Section 3.1 are confirmed quantitatively in the radial ellipticity profiles. Within $1.5R_e$, there are small differences in the Dry/Wet-Fast and Dry-Slow simulations. The ellipticity outside $1.5R_e$ is however quite similar at all resolutions for these three simulations: the minimum ellipticity is basically 0, the mean is 0.33 ± 0.03 and the maximum is 0.55 ± 0.05 at $2R_e$ for all three *standard-res*, *high-res*, *very high-res*.

The Wet-Slow simulation shows much larger differences. Outside $0.5\,R_e$, the *high-res* and *very high-res* are similar. The ellipticity profile of the *standard-res* has then a completely different appearance: between 0.6 and $2R_e$, 75 per cent of the projections have an ellipticity higher than 0.4, and the reached maximum in ϵ is 0.75 (versus $\sim$0.6 for the other two resolutions). In the outer part ($R > 2R_e$), the ellipticity of most of the projections is decreasing but its maximum is still larger than 0.7.

The same trends are observed in the a_4/a profiles. In the Dry/Wet-Fast and Dry-Slow simulations at all three resolutions, the mean a_4/a is around 0. Then, 50 per cent of the projections are between -2 and 2 per cent. The *high-res* Wet-Fast and the *very high-res* Dry-Fast simulations are only slightly more boxy. The a_4/a profile of the Wet-Slow simulation dramatically confirm what we observe for the ellipticity. The *standard-res* clearly departs from the *high-res* and *very high-res*, which are quite similar. Between 0.5 and $1R_e$, the projections of the *standard-res* span a very large range of a_4/a. Between 1 and $2R_e$, 75 per cent of the projections have a discy shape, and the isophotes of the merger remnant become then increasingly boxy going outwards.

A2 Kinematics

The Wet-Slow simulation has been treated in the paper, we will thus focus on the three other simulations.

Left-hand panels of Fig. A2 show the velocity and velocity dispersion curves for the mean–ellipticity projection along the global kinematic position angle. In the Dry-Fast simulation, the central slope of the rotation curve at *very high-res* is slightly shallower, and the dispersion about 15 per cent smaller, but in the outer part the velocity amplitude is similar at all three resolutions, with a velocity of about 60 km s^{-1} at 6 kpc, and dispersion values going to about 150 km s^{-1}. The Wet-Fast simulations show consistent velocity profiles at all three resolutions, with a velocity amplitude of 60 km s^{-1} at 6 kpc, and dispersion decreasing outwards down to $\sim$125 km s^{-1}. Again, the velocity curves for the Dry-Slow simulation are all very similar, but these profiles clearly reveal the previously observed KDC which appears here as a kpc-size core counter-rotating with respect to the outer part. Note the *standard-res* dispersion profile which is about 10 per cent smaller than for the other two higher resolutions.

In right-hand panels of Fig. A2, we now compare the simulations using the apparent angular momentum λ_R. These figures clearly show that the Dry/Wet-Fast simulations (top and second from top) both result in *fast-rotators*, the mean values of λ_R is 0.2 and the maximum about 0.25 at $1R_e$ for the three resolutions. This confirms our previously mentioned results that the spatial and mass resolutions do not seem to have a significant effect on these merger remnants.

The analysis of the morphology and kinematics of the Dry-Slow simulation did show mild differences in the remnants for varying resolutions, the λ_R profiles exacerbate these small discrepancies. At *standard-res*, λ_R is an increasing function of radius, with 75 per cent of all projections having values below 0.1 at $1R_e$ and 25 per cent above 0.1. However, if we are taking into account the projection which maximizes λ_R, the *standard-res* remnant should be classified as a *fast-rotator*. In the same context, both the *high-res* and *very high-res* are classified as *slow-rotators*. They have not the same profiles but have a similar overall behaviour: λ_R first increases up to about $0.5R_e$, and then decreases (up to $1.5R_e$ for the *high-res* and $1R_e$ for the *very high-res*). Outside $1.5R_e$, λ_R increases again outwards. Such a λ_R profile is the clear signature of large-scale KDCs as mentioned in Emsellem et al. 2007 (see also McDermid et al. 2006).

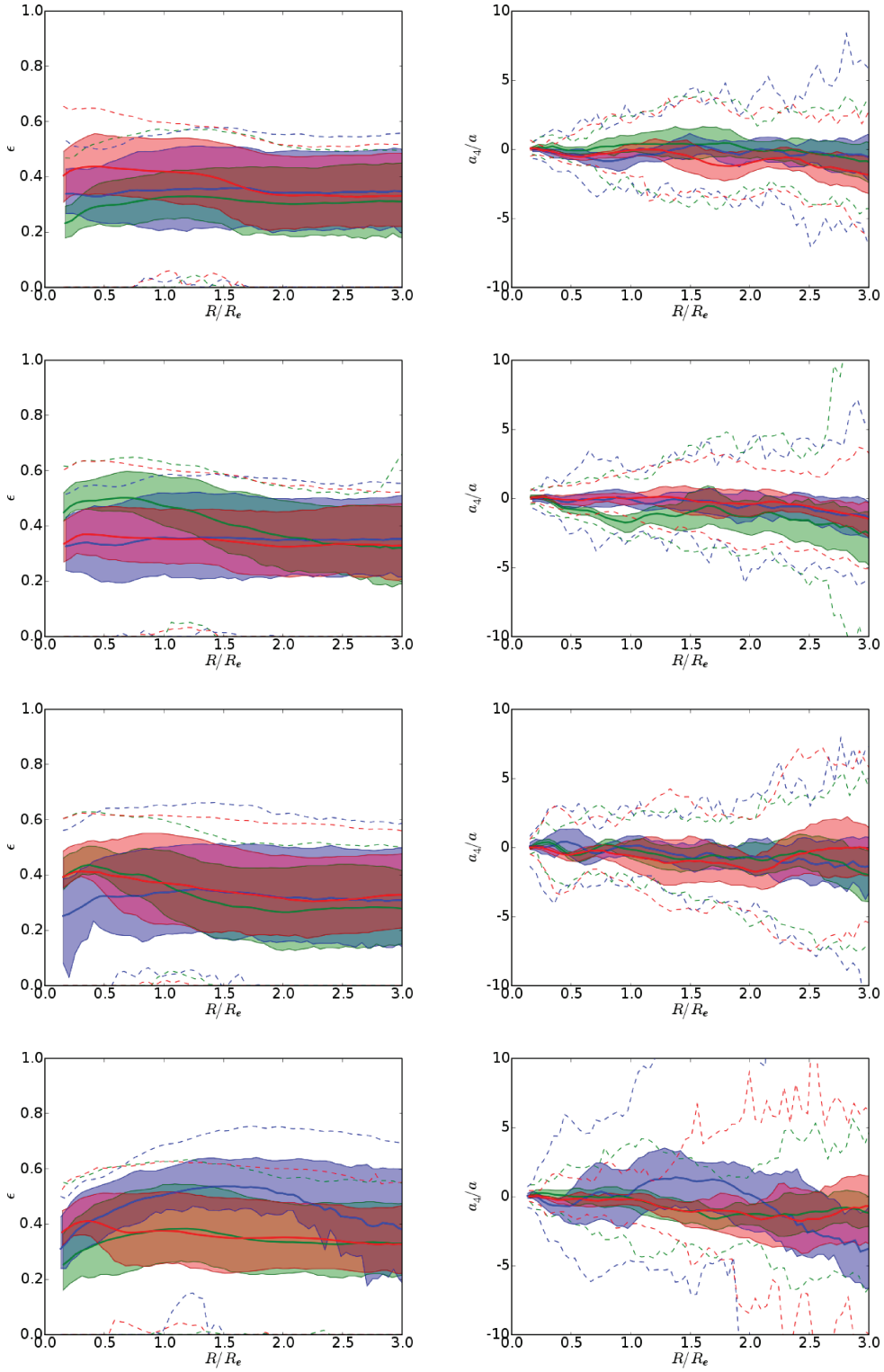

Figure A1. Ellipticity and a_4/a profiles (left- and right-hand panels, respectively) of the four simulations as a function of R/R_e. From top to bottom: simulations Dry-Fast, Wet-Fast, Dry-Slow and Wet-Slow. The three resolutions are shown with different colours: the *standard-res* in blue, the *high-res* in green and the *very high-res* in red. For each resolution, we plot five lines which correspond to the minimum and maximum at each radii (dashed lines), the mean value (thick solid lines) and the first and third quartiles (thin solid lines). The interquartile space (which corresponds to 50 per cent of all projections) is filled with the colour associated with the resolution.

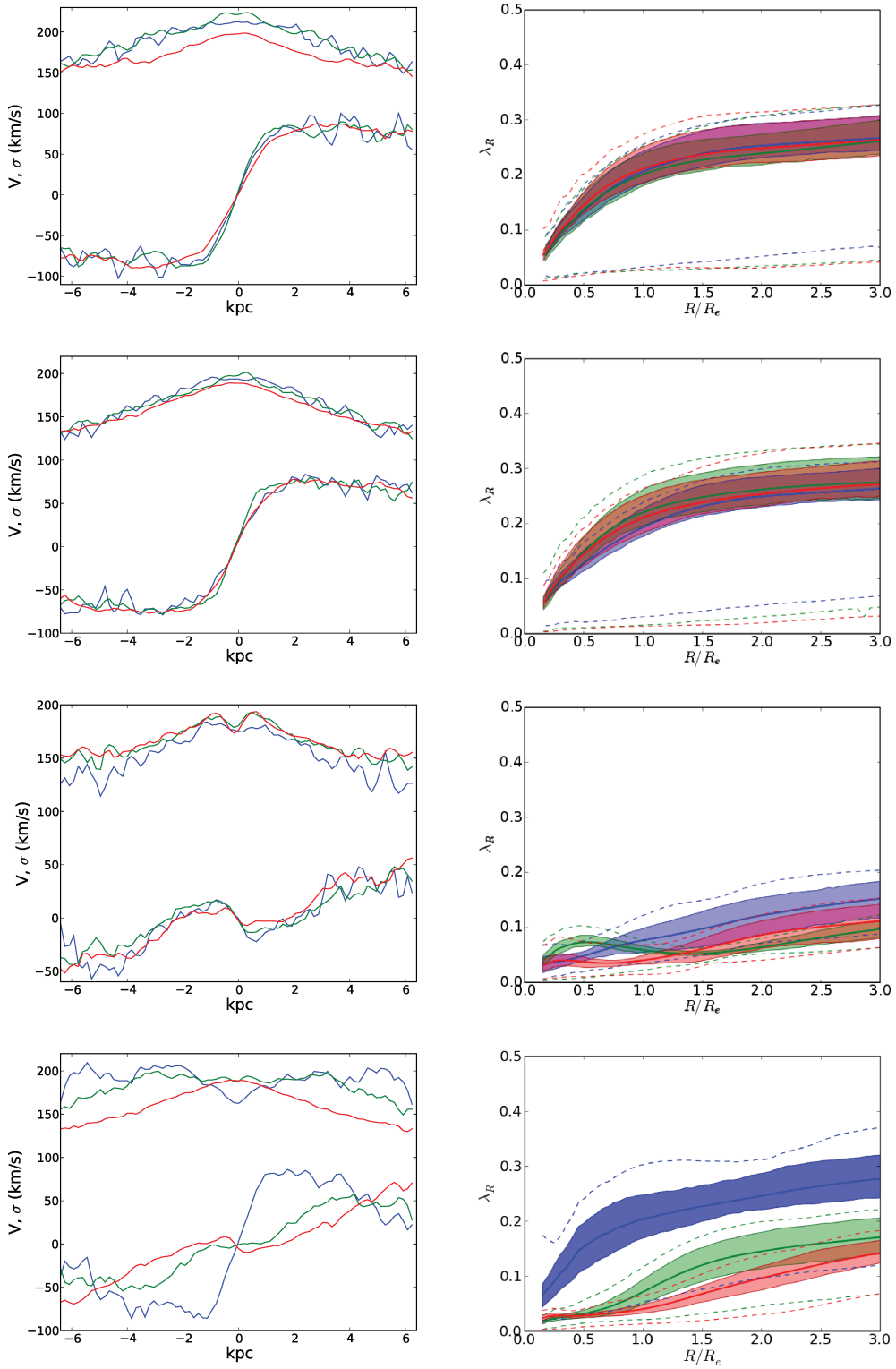

Figure A2. Left-hand panels: the radial velocity and velocity dispersion profiles (in km s^{-1}) for the mean ellipticity projection along the global kinematic position angle (radius in kpc). Right-hand panels: λ_R profiles as a function of R/R_e. From top to bottom: simulations Dry-Fast, Wet-Fast, Dry-Slow and Wet-Slow. The three resolutions are shown with different colours: the *standard-res* in blue, the *high-res* in green and the *very high-res* in red.

This paper has been typeset from a TEX/LATEX file prepared by the author.

Chapter 3

Numerical simulations of binary mergers of disc galaxies

Contents

Galaxy mergers affect the morphology and the kinematics of galaxies: they are the main driver for the formation of ETGs (see Section 1.1). In this chapter, we then study the morphological and kinematical properties of galaxies originating from equal-mass and nearly equal-mass binary mergers of spiral galaxies.

I first present the need for understanding the formation of the slow and fast rotators families. After a Section describing the code, the simulations and the parameters used in this study, I present the results we obtained on the formation of fast rotators, slow rotators and KDCs. In the last Section, I compare these results with other recent studies to test the convergence of this sample of simulations.

Part of this chapter has been submitted to MNRAS in Bois et al. (2011).

3.1 Understanding the formation of slow and fast rotators

Numerical simulations, intensively used for more than two decades, have clearly shown that the global characteristics of the remnants of binary mergers between two equal-mass spiral galaxies, called major mergers, resemble those of Early-Type Galaxies (ETGs) [Toomre & Toomre 1972, Hernquist & Barnes 1991, Barnes 1992, Mihos *et al.* 1995, Springel 2000, Naab & Burkert 2003, Bournaud *et al.* 2005]. Remnants with properties similar to ETGs can also be recovered via multiple minor mergers with the total accreted mass being at least half of the initial mass of the main progenitor [Weil & Hernquist 1994, Weil & Hernquist 1996, Bournaud *et al.* 2007]. This picture of the formation of ETGs via accretion and merging of stellar bodies would fit well within the frame of the hierarchical assembly of galaxies provided by ΛCDM cosmology.

The SAURON survey [de Zeeuw *et al.* 2002] has introduced a new view of ETGs, classifying them in two families – the fast and the slow rotators – according not only to their morphology, but also to their kinematics [Emsellem *et al.* 2007, Cappellari *et al.* 2007]. These two classes are intrinsically different and seem to correspond to different populations of galaxies: while the fast rotators present regular rotation patterns aligned with the photometry, the slow rotators have low angular momentum and show misalignments between the photometry and the velocity axes. Furthermore, slow rotators often exhibit KDCs.

To further constrain the formation scenarios for these two classes, an ambitious program – ATLAS^{3D} – is being conducted, combining a multi-wavelength observational survey of a complete volume-limited sample of ETGs with various numerical simulations and modelling efforts. The ATLAS^{3D} project[1] [Cappellari *et al.* 2010] aims to quantify the distribution and kinematics of the stellar and gaseous components of a statistically significant sample of ETGs to relate their detailed properties to their mass assembly, star formation history and evolution. In the context of the ATLAS^{3D} project, an extensive set of numerical simulations is being conducted to support the survey: cosmological simulations, semi-analytic modelling and idealized binary galaxy mergers.

In the present chapter, I am leading the effort to build and analyze a large sample ($\sim$ 70) of binary mergers of disc galaxies at an unprecedented resolution, sufficient to properly follow the merging process and the resulting galaxy remnant (see previous Chapter). I aim to constrain the formation of the slow and fast

[1] http://purl.org/atlas3d

rotators revealed by the SAURON and ATLAS^{3D} surveys. For this purpose, I further examine the role of the initial conditions (impact parameter, incoming velocities, inclination and spins of the progenitors) on the global characteristics of the remnants of binary galaxy mergers. I then propose to study their morphology and kinematics: I build two-dimensional momentum (intensity, velocity and velocity dispersion) maps of the merger remnants and analyse their apparent properties, directly linked with their orbital structures [Jesseit *et al.* 2005].

3.2 Simulations and Analysis

In this Section, I describe the code used to simulate galaxy mergers, the sample of simulations and the parameters used for the analysis of the merger remnants.

3.2.1 Method

3.2.1.1 Code

We have simulated galaxy mergers using the same PM – sticky particle code of the resolution study (see Section 2.2). All simulations were performed with a softening length (*i.e.* spatial resolution) of 58 pc.

3.2.1.2 Set-up for initial parameters

We have simulated binary mergers of discs galaxies (i.e., "spiral-spiral" mergers) with mass ratios of 1:1, 2:1, 3:1 and 6:1. The main parameters are summarized in Table 3.1 for the progenitor galaxies and Table 3.2 for the orbital parameters.

Initial progenitor galaxies Our sample consists of binary mergers of disc galaxies, i.e. "spiral-spiral" mergers. The first progenitor, which is defined as the most massive for unequal-mass mergers, has a baryonic mass of 1.3×10^{11} $M_{\odot}$. The bulge fraction is $B/T = 0.20$ and the gas fraction in the disc is usually 10 per cent (33 per cent in some m21 simulations). The initial disc has a Toomre profile[2] with a scale length of 4 kpc, consistent with observations of nearby disc galaxies [Fathi *et al.* 2009], truncated at 10 kpc. The gas has a scale length of 8 kpc and a truncation radius of 20 kpc. The bulge has a Hernquist profile [Hernquist 1990] with a scale length of 700 pc. The dark matter halo is modelled with a Burkert

[2]The profile rapidly evolves into a quasi-exponential profile with a slightly smaller exponential scale length.

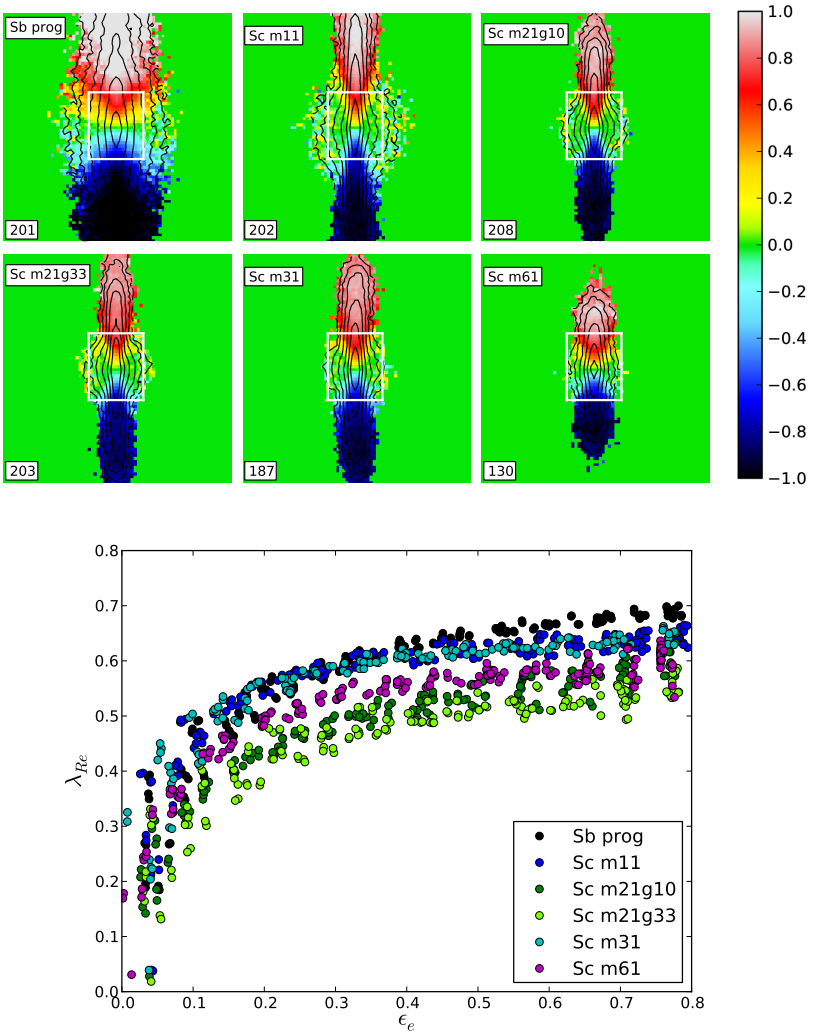

Figure 3.1: Top: Projected stellar velocity maps for the Sb progenitor and the different Mass ratio Sc companions, the black contours represent the iso-magnitude contours, they are equally spaced in magnitude and are the same for all progenitors. Each subpanel is labelled with the name of the progenitor and with the maximum velocity V_{max}, the colorbar goes from -V_{max} to +V_{max}. The field of view is 15×15 kpc^2 (15 kpc $\simeq$ 6 R_e). The white rectangle indicates a typical field covered by the instrument SAURON and corresponds to a field of $41'' \times 33''$ for a galaxy at a distance of 20 Mpc, its orientation follows the photometric position angle taken at $3R_e$. Bottom: $\lambda_R - \epsilon$ diagram for the progenitors of binary mergers. The Sb progenitor (black points) is the same in all simulations, the other colours correspond to the Sc companion at different mass ratios (m11 in blue, m21g10 in green, m21g33 in light green, m31 in cyan, m61 in magenta). All projections (200 per remnant) are plotted.

profile [Burkert 1995] with a 7 kpc scale-length and a truncation radius of 70 kpc, inside which the dark matter mass is 3×10^{11} $M_{\odot}$. This initial galaxy is representative for an Sb spiral galaxy, given its bulge fraction in particular, and is denoted as the *Sb* spiral progenitor throughout the paper.

The other progenitor, which has the lower mass in unequal mass mergers, has its total mass determined by the mass ratio. Apart from the bulge which was reduced to $B/T = 0.12$, all components have their mass scaled by a factor equal to the mass ratio, and all sizes and scale lengths scaled by the square root of the mass ratio, thus keeping the central density of their discs constant. The gas fraction is 10 per cent, except for the lower-mass companions used in 6:1 mergers where a gas fraction of 15 per cent is used. The main difference with the first progenitor is thus the lower bulge fraction, and this progenitor galaxy is denoted as the *Sc* spiral progenitor.

The Sb spiral is modelled with 2×10^6 particles for each component (stars, gas, and dark matter). The Sc spiral is modelled with a number of particles scaled by the mass ratio. Equal-mass mergers thus use a total of 12 million particles.

The progenitors are initialized as perfectly axisymmetric disc galaxies. Such galaxies will unavoidably develop substructures such as spiral arms and bars. We need to avoid this spontaneous, intrinsic evolution to take place during the merger, otherwise the effects of the merger itself can not be disentangled. We also need to avoid the artificial consumption of gas that could result from applying the Schmidt law during the transition from an axisymmetric gas disc to a spiral disc. To this aim, each progenitor galaxy was evolved in isolation and without star formation for about two rotations of the outer stellar disc, so that a reasonable steady state in its structure and gas density distribution is reached. At this point, we remark that the Sb progenitor is more concentrated and dynamically stable than the Sc galaxy. The merger simulation is then started, with star formation and feedback, using these pre-evolved progenitors – see [Martig & Bournaud 2008] for further discussion of this technique.

The initial properties of our pre-merger spiral galaxies, after their initial relaxation in isolation, are shown in Fig. 3.1. We in particular compare the isophotal ellipticity ϵ to their angular momentum tracer λ_R at the effective radius R_e for 200 different projections (see Sections 3.2.2.1 and 3.2.2.2 for details on projection effects). Small differences between the progenitors arose during the initial relaxation as galaxies with different sizes and bulge fractions behave somewhat differently in isolation; these properties are essentially stabilized (on time-scales

Name	Prog 1$^{(1)}$	$B/T^{(2)}$	$f_{gas}^{(3)}$	$m_B^{(4)}$	Prog 2$^{(1)}$	$B/T^{(2)}$	$f_{gas}^{(2)}$	$m_B^{(3)}$
m11	Sb	0.2	10%	1	Sc	0.12	10%	1
m21g10	Sb	0.2	10%	1	Sc	0.12	10%	0.5
m21g33	Sb	0.2	33%	1	Sc	0.12	33%	0.5
m31	Sb	0.2	10%	1	Sc	0.12	10%	0.33
m61	Sb	0.2	10%	1	Sc	0.12	15%	0.17

Table 3.1: Main physical parameters used to model the initial progenitor galaxies in our merger models. (1) Spiral Hubble type (2) M_{stars} in the bulge / total M_{stars} (3) Fraction of the baryonic mass in gas (4) Baryonic mass in unit of 1.3×10^{11} $M_\odot$.

Name	V_∞ $^{(1)}$	i $^{(2)}$	R $^{(3)}$
0	120	45	60
im	120	25	60
ip	120	75	60
Rm	120	45	35
Vm	70	45	60
Vp	200	45	60

Table 3.2: The different initial conditions for the mergers. (1) The relative incoming velocity V_∞ (in km s^{-1}) of the Sc companion computed at infinite distance. (2) Inclination i (in $^\circ$) for each galaxy with respect to the orbital plane. (3) Impact parameter R at infinite distance (in kpc).

of a few 10^8 yr) when the merger simulations are started.

Merger orbits The different orbits used for the merger simulations are described in Table 3.2. They are all parabolic or hyperbolic, with an initial total energy $E > 0$ or $E \simeq 0$, corresponding to initially unbound galaxy pairs. Such orbits are representative of the most common mergers in ΛCDM cosmology [Khochfar & Burkert 2006].

The fiducial orbit "0" has a velocity at infinite distance of V_∞=120 km s^{-1}, an inclination i=45° for each galaxy with respect to the orbital plane, and an impact parameter (*i.e.* the perpendicular distance between the two velocity vectors of the progenitors at the beginning of the simulation) of R=60 kpc. The six other orbits correspond to one of the three parameters V, R, i being changed compared to the fiducial values, one at a time. The nomenclature denotes the parameter

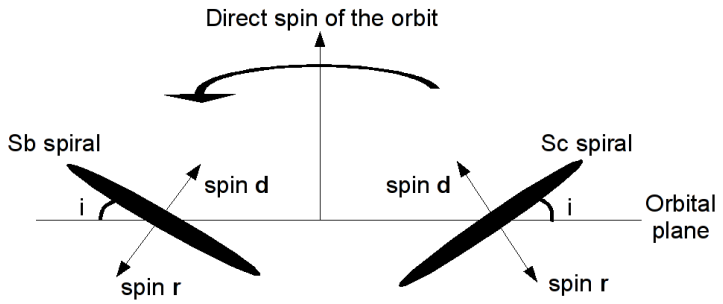

Figure 3.2: Orbital configuration of the binary merger remnants. The orbit always has a direct spin, the progenitors can have a direct or retrograde spin. The initial inclination of the progenitors is initialised as shown.

varied and whether it is increased (p: plus) or decreased (m: minus), as detailed in Table 3.2. We have then a total of 70 simulations of galaxy mergers.

In addition of the three listed parameters, we identify the spin of the progenitors which can be either direct (prograde) **d** or retrograde **r** with respect to the orbital angular momentum. The first letter refers to the spin of the first progenitor (Sb) and the second letter to the Sc companion. The orbital configuration is sketched in Fig. 3.2.

Our nomenclature also indicates the type (mass ratio) of the modelled merger, as defined in Table 3.1. For instance, the simulation labelled *m31rdVm* refers to a 3:1 merger with a retrograde orientation for the main Sb progenitor and a direct orientation for the Sc companion on an orbit with lowered initial velocity.

The chosen orbits do not cover all the parameter space of initial conditions: the goal of this study is to understand the formation of slow and fast rotators, and not to build a full library of binary merger remnants.

3.2.2 Analysis

We analysed all merger remnants about 600-800 Myr after the central coalescence. The central body of the ETG-like systems formed in the mergers are thus relaxed within several effective radii when the analysis is performed, even if tidal debris is present at larger radii. We checked in several cases that the measured morphological and kinematical parameters were stabilized by comparing the ellipticity and the λ_R parameter to earlier snapshots.

3.2.2.1 Projected velocity moment maps

Similarly to the study on the resolution effects in numerical simulation (see Section 2.2), we have built two-dimensional maps indicating the stellar surface density, stellar velocity and stellar velocity dispersion for various projections. The intensity and velocity moment maps are built to cover a 20×20 kpc^2 field of view centred on the stellar density peak of each system (figures show the inner 15×15 kpc^2 area). This covers at least about four effective radii R_e to enclose most of the baryonic mass of early-type galaxies, the average effective radius of our merger remnants being 2.3 kpc. Each projection was computed on a 100×100 pixel grid, giving an effective resolution consistent with the SAURON data of the ATLAS^{3D} survey. The maps have been Voronoi binned [Cappellari & Copin 2003] to have a minimum number of 400 particles per bin.

To obtain statistically representative results rather than analysing a particular projection, we have produced velocity moment maps and performed the subsequent analysis for 200 isotropically distributed viewing angles for each merger remnant. The choice of 200 projections ensures a sampling smaller than 10 degrees in any direction, so that intermediate viewing angles would not show significant differences.

3.2.2.2 Extracted parameters

The analysis assumes a constant stellar mass-to-light ratio, which should be a reasonable approximation for relatively old ETGs. Furthermore, our main results will show that the classification of merger remnants into slow and fast rotators, and the presence of KDCs, do not significantly depend on the youngest stellar populations formed during the merger, but rather on how the populations from each progenitor galaxy are distributed with respect to each others.

Our analysis is mainly based on two simple morphological and kinematical parameters, a choice motivated by the fact that these parameters are often used as standards in studies of nearby ETGs, see *e.g.* [Jesseit *et al.* 2009] or Section 2.2 of this thesis. These two parameters are the ellipticity ϵ, probing the morphology, and the λ_R parameter, which is a robust proxy for the stellar projected angular momentum. These parameters were also computed for the study on the resolution effects in numerical simulation (see Section 2.2), however, their measurement and definition have changed. I then briefly described the new procedure.

To quantify the global morphology, we measured the ellipticity $\epsilon = 1 - b/a$, where a and b are the semi major- and minor-axes, respectively. To measure a

profile of a, b and ϵ as a function of the radius r (and subsequently an ϵ profile), we selected all pixels encircled by a given isophote and computed the inertia matrices as in *e.g.* [Cappellari *et al.* 2007]. The diagonalisation of these matrices provides ϵ and the Position Angle (PA) of the projected density map at different radii r. We also derive the effective radius R_e from the stellar surface density as the radius encompassing half of the total stellar light (or stellar mass).

To quantify the global kinematics of each system, using the velocity and velocity dispersion maps, we measure the λ_R parameter defined in [Emsellem *et al.* 2007], hereafter E+07:

$$\lambda_R \equiv \frac{\langle R\,|V|\rangle}{\langle R\,\sqrt{V^2+\sigma^2}\rangle}$$

We hence obtain $\lambda_R(r)$ profiles for all projections of all merger remnants.

In E+07, λ_R was used to reveal two families of early-type galaxies, the slow rotators with $\lambda_R \leq 0.1$ and the fast rotators with $\lambda_R > 0.1$ at one effective radius R_e. However, the SAURON survey was based on a representative sample of ETGs but biased towards the upper end of the luminosity function. The ATLAS^{3D} survey probes a complete sample of ETGs in the Local volume [Cappellari *et al.* 2010]. This led to a refined criterion for the separation between fast and slow rotators with $\lambda_R = 0.31 \cdot \sqrt{\epsilon}$ at one effective radius R_e (see [Emsellem *et al.* 2011]).

The main analysis performed in this study is then based on the $\lambda_R - \epsilon$ diagram plotted at one R_e. When the merger remnant presents a strong bar and/or spiral arms, the ellipticity is computed at $3R_e$ to better account for the "real" ellipticity and avoid being contaminated by the flattening of the bar (the difference being significant only for a small fraction of the projections), and λ_R always being computed at R_e. This is the same procedure applied to the real ATLAS^{3D} galaxies in [Emsellem *et al.* 2011] and makes our results directly comparable to the observations (see Chapter 5).

The right panel of Fig. 3.1 shows the values of ϵ and λ_R for the 200 projections of the various disc progenitors. A few generic statements, valid for any of our spiral progenitors as well as for our fast rotator merger remnants (see Section 3.3), can be made (see also [Jesseit *et al.* 2009]):

- The edge-on view (high ϵ) of the progenitors has, as expected, the highest λ_R value;
- as the galaxy is inclined (lower ϵ) the value of λ_R slightly decreases, and

- as the viewing angle gets nearly face-on, the value of λ_R drops abruptly, reaching $\lambda_R \simeq 0$ for $\epsilon \simeq 0$ as expected.

3.3 Build-up of fast and slow rotators in binary galaxy mergers

This section is devoted to the analysis of the remnants of binary mergers of disc galaxies, which in our sample are Sb+Sc mergers with various orbits and mass ratios. We study under which conditions slow and fast rotators are formed, according to the criterion defined in Section 3.2.2.2. We also study which of the merger remnants harbour a KDC, and study the influence of the internal and orbital parameters of the mergers in determining such properties.

3.3.1 General results: populations of slow and fast rotators

The $\lambda_R - \epsilon$ diagram is a useful tool to quantify the global properties of ETGs: it relates the angular momentum and flattening at one effective radius R_e, and disentangles fast and slow rotators. Fig. 3.3 shows this diagram for our complete sample of 70 binary disc merger simulations, including the 200 independent projections analysed for each relaxed merger remnant. The threshold defined by $\lambda_R = 0.31 \cdot \sqrt{\epsilon}$ separating slow and fast rotators as suggested by the ATLAS^{3D} observations is shown [Emsellem *et al.* 2011]. Each set of projections for a given simulation span a range of $\lambda_R - \epsilon$ values: this is shown in Fig. 3.3 and individual examples are presented in Fig. 3.4 as well as in Fig. 3.5 for various mass ratios. Fig. 3.4 also shows examples of velocity moment maps for several fast and slow rotators formed in 1:1, 2:1 and 3:1 mergers.

The $\lambda_R - \epsilon$ distribution for our entire sample of binary merger remnants is shown in Fig. 3.3 for galaxies with and without a KDC, respectively. The detection of KDCs has been conducted by visually inspecting the velocity moment maps. The merger remnants can be seen from Fig. 3.15 to 3.19 in the Appendix, the colour code in the different panels presents in black the fast rotators, in red the slow rotators with KDC and in green the slow rotators without KDC. Fig. 3.3 shows evidence for a tight relation between the presence of a KDC and the slow versus fast rotator classification. All fast rotators presented in Fig. 3.4 show a clear and regular rotation pattern at all radii, and most slow rotators exhibit KDCs.

We can then sketch the following general results regarding the formation of fast and slow rotators and the presence of a KDC from our sample of binary disc

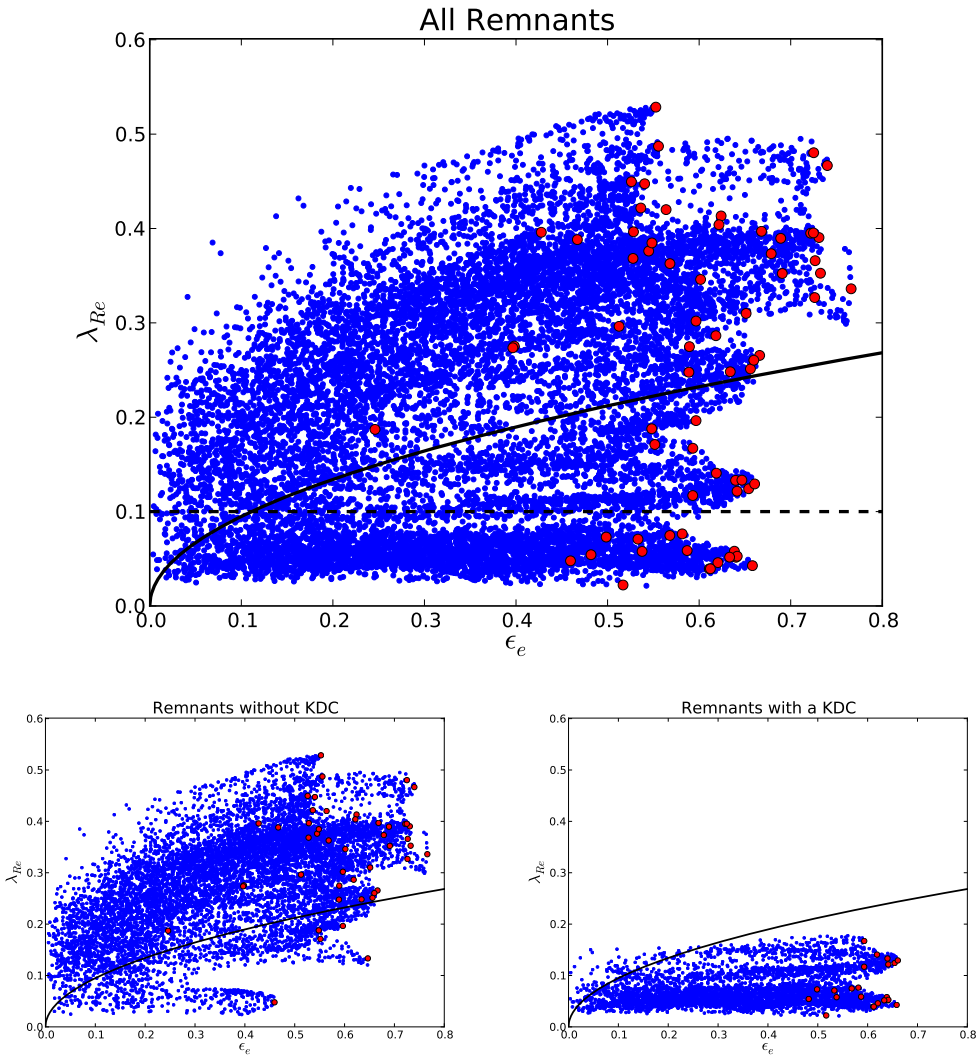

Figure 3.3: Top: $\lambda_R - \epsilon$ diagram for all simulations of binary mergers of disc galaxies. All projections (200 per remnant) are plotted in blue, the red symbols corresponding to the maximum ellipticity (*i.e* edge-on view) of a remnant. The limits defining the slow/fast categories from ATLAS^{3D} (solid) and from SAURON (dashed, only for the top panel) are plotted in black. Bottom left: Same diagram for the simulations which do not present a KDC in their velocity fields. Bottom right: Same diagram for the simulations which present a KDC in their velocity fields.

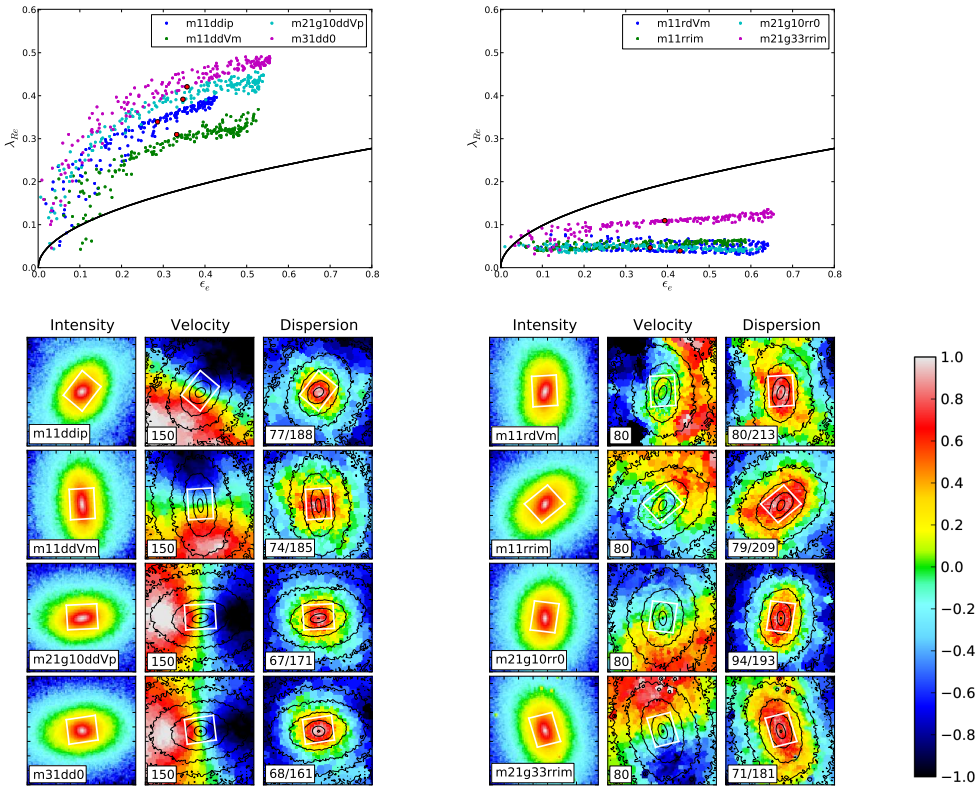

Figure 3.4: $\lambda_R - \epsilon$ for four fast rotators (left panels) and for four slow rotators with a KDC (right panels). The 200 projections of each merger are represented by a coloured point (see the legend in the figure for the name of the merger), the red point corresponds to the projection with an ellipticity closest to the mean ellipticity. The intensity, velocity and velocity dispersion fields of the previous red point projections are plotted below the $\lambda_R - \epsilon$ diagram. The name of the merger is written in the intensity map, the maximum value of the velocity V_{max} and the minimum/maximum values of the velocity dispersion are written in their respective maps. The colorbar goes from -V_{max} to +V_{max} and can also be used as an indicator for the intensity and the velocity dispersion ("-1" corresponding to the lower value, "1" to the maximum value). The field of view is 15×15 kpc^2 (15 kpc $\simeq 6R_e$). The white rectangle indicates a typical field covered by the instrument SAURON and corresponds to a field of $41'' \times 33''$ for a galaxy at a distance of 20 Mpc, its orientation follows the photometric position angle taken at $3R_e$.

mergers:

- We find both fast and slow rotators in our sample of relaxed remnants of binary disc mergers. An apparent bimodality is observed in the global $\lambda_R - \epsilon$ distribution of the sample and in the presence of a KDC in the remnants, but this could likely result from the specific choices of simulated mass ratios and the limited number of simulated incoming orbits.

- In our sample of merger remnants, fast rotators all have aligned kinematic and photometric axes, while slow rotators frequently exhibit kinematic misalignments (see Section 5.2.3 and examples in Fig. 3.4), and obviously exhibit weak rotational support. This is similar to what is observed in the ATLAS^{3D} sample [Krajnović *et al.* 2011]. This suggests that slow rotators are not velocity-scaled down versions of members of the fast rotator population.

- Slow rotators remain slow for nearly all viewing angles, and fast rotators remain fast. Even nearly face-on projections of fast rotators are rarely classified as "slow". This result was already pointed out by [Jesseit *et al.* 2009] while using a constant threshold for λ_R between slow and fast rotators as in E+07. The simulations allow here to further explore various projections of a given merger remnant: they confirm that the combination of the λ_R and ϵ parameters, together with the refined definition for fast and slow rotators recently proposed by [Emsellem *et al.* 2011] (see Section 3.2.2) allow a robust classification of ETGs, which is almost independent of the viewing angles.

- Another intrinsic difference between fast and slow rotators is that none of the fast rotators harbours a KDC, while the majority of slow rotators do harbour a clear KDC. Only for a few slow rotators we could not detect a clear KDC (with sufficient rotation amplitude or misalignment angle). This strong trend brings further support to the relevance of the definition of fast and slow rotators as emphasising two families with different intrinsic properties. With the low noise level and very high velocity resolution of our simulations, we notice that KDCs in slow rotators are visible for the vast majority of projections, but sometimes with rather low velocity amplitudes which would be hard to detect in observations.

- Slow rotators have relatively high edge-on ellipticities (0.45 to 0.65), with the ones for fast rotators being only slightly larger (generally 0.5 to 0.75).

The mean ellipticities over random projections show a somewhat more significant though still mild difference, being around 0.35 for slow rotators and 0.45 for fast rotators. The fast rotators with the highest edge-on ellipticities ($\epsilon > 0.7$) are remnants of some of the less violent 3:1–6:1 mergers; those which tend to appear rounder formed with high orbital inclinations. We also note that the majority of fast rotators have a bar, and 6:1 merger remnants often have weak spiral arms associated with the bars.

- The typical λ_R profile of a fast rotator (see Fig. 3.15 to Fig. 3.19 in the Appendix) increases rapidly within 1 to 2 effective radii, and then exhibits a shallower positive slope. As for slow rotators, we observe two general types of λ_R profiles. (1) It can remain constant with a low value within 1.5 or 2 R_e and then starts to slightly increase outwards or (2) λ_R shows a local maximum around 0.5 R_e, decreasing from there to $\sim 1R_e$, with a subsequent outward increase: such a λ_R profile is the clear signature of large-scale KDC as mentioned in E+07 (see also [McDermid *et al.* 2006]). In both cases, λ_R never reaches the level of fast rotators at very large radii: the mean value of λ_R over the edge-on projections at $3R_e$ is 0.6 for the fast rotators and 0.25 for the slow rotators. The radial λ_R profiles of slow and fast rotators are therefore significantly different both at small and large radii.

The definition of slow and fast rotators seems to robustly disentangle two families of ETGs with different intrinsic properties, with *e.g.*, the formation of KDCs in slow rotators only. To further understand the influence of various initial parameters, we now explore the impact of the mass ratio, orbital parameters, gas fraction and nature of the spiral progenitors, on the properties of the merger remnants.

3.3.1.1 Influence of the mass ratio

Fig. 3.5 shows the $\lambda_R - \epsilon$ diagram for different mass ratios, and different gas fractions in the cases of 2:1 mergers. 1:1 and 2:1 mergers form slow rotators in about 60 per cent of our simulations, the lowest λ_R systems being formed in equal-mass mergers (the fraction of slow rotators directly reflecting the initial orbital parameters, see Section 3.3.1.3 and Fig. 3.6). The formation of slow rotators is unlikely in 3:1 mergers, and does not occur in 6:1 mergers. This is consistent with the conclusions of previous samples of merger simulations, see *e.g.* [Naab & Burkert 2003, Bournaud *et al.* 2004, Jesseit *et al.* 2009].

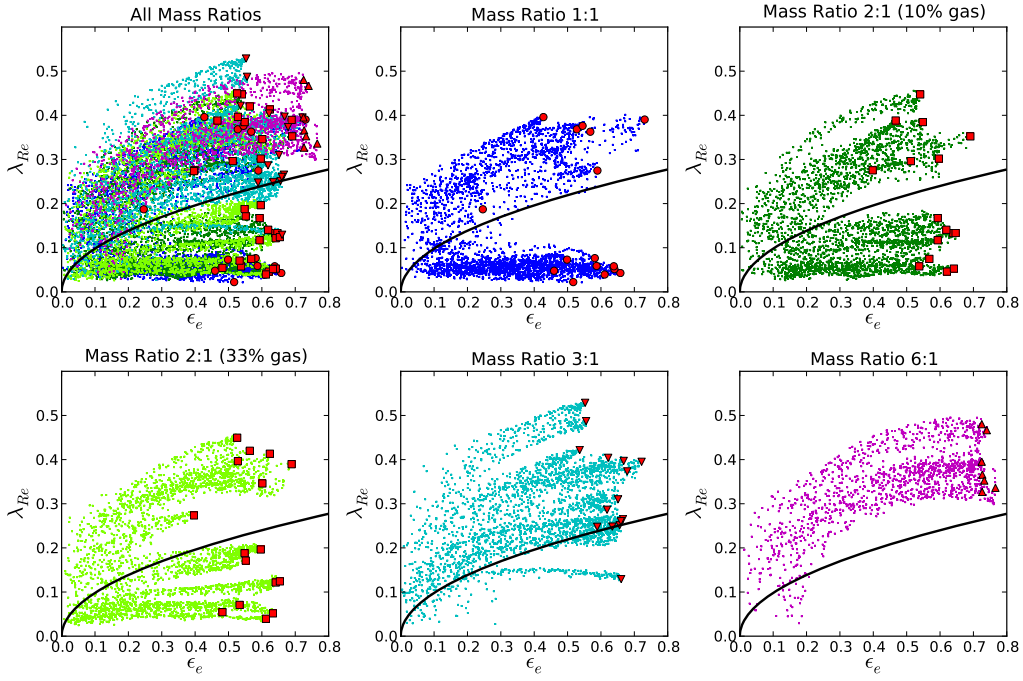

Figure 3.5: $\lambda_R - \epsilon$ diagram for all simulations of binary mergers of disc galaxies. Top left: All projections of all mass ratios as in Fig. 3.3, colours correspond to the different mass ratios. Top middle: All projections of mergers remnants for mass ratio 1:1. Top right: All projections of mergers remnants for mass ratio 2:1 with 10 per cent of gas. Bottom left: All projections of mergers remnants for mass ratio 2:1 with 33 per cent of gas. Bottom middle: All projections of mergers remnants for mass ratio 3:1. Bottom left: All projections of mergers remnants for mass ratio 6:1. The red symbols are for the projection which maximizes the ellipticity for a given remnant. The limit defining the slow/fast categories from ATLAS^{3D} is plotted as the solid black line.

[Bournaud *et al.* 2004] showed that spheroid dominated galaxies with little rotating disc components could be formed only during the so-called "major" mergers (1:1–3:1), while "intermediate" mergers with mass ratios between 4:1 and 10:1 did not perturb the galaxies much from the initial disc-like morphology and kinematics. [Naab & Burkert 2003] found that mass ratios of 3:1 and above formed discy systems. Our present conclusions therefore confirm these results, but with a larger and higher-resolution sample of simulations and new analysis parameters.

3.3.1.2 Influence of the gas fraction

2:1 mergers were simulated with gas fractions of 10 and 33 per cent. Both subsamples show similar distributions of λ_R, ϵ, and presence of a KDC. The gas fraction thus seems to have no major impact on the global properties of the merger remnants, although we did not explore the context of very high-redshift mergers ($z \sim 2$ and above) which could involve extreme gas fractions, *e.g.* above 50 per cent [Daddi *et al.* 2010a, Tacconi *et al.* 2010]. Mergers with very low gas fractions ($f_{gas} \sim 0$ per cent) should not be associated with spiral-like progenitors, which is the topic of the present section, but with ETG-like progenitors (see Section 4.1).

One could a priori expect that a relatively high gas fraction eases the immediate re-building of massive rotating disc components during or soon after the merger. A few studies suggested that gas-rich mergers could form discy fast rotating systems, or even spiral galaxies, *e.g.* [Springel & Hernquist 2005, Robertson *et al.* 2006, Hopkins *et al.* 2009b]. The relatively stable morphology and kinematics of the 2:1 merger remnants with 10 and 33 per cent of gas could a priori seem conflicting with these earlier results: the value of λ_R at 1 R_e averaged over all 2:1 mergers varies only from 0.17 to 0.19 when the gas fraction is increased from 10 to 33 per cent and the average value of the ellipticity ϵ varies from 0.39 to 0.38. Actually, a separate study by [Bournaud *et al.* 2010a] shows that a high gas fraction does not easily reform massive and extended disc components in major mergers. This occurs provided that most of the ISM is modelled as a cold medium supported by supersonic turbulence, which is the case in our present sticky particle simulations[3] and in the AMR models of [Bournaud *et al.* 2010a], rather than being supported by a high thermal pressure as it is often the case in existing SPH simulations. This probably explains the differences between our results and the published works mentioned above.

[3] A difference being that turbulence dissipation in local shocks is "sub-grid" in sticky-particle models, while it is explicitly captured in high-resolution AMR models.

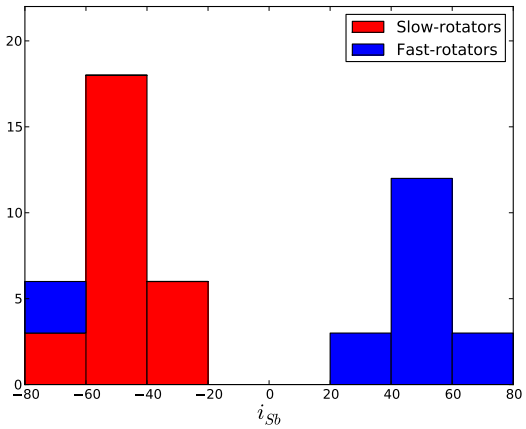

Figure 3.6: Fraction of slow/fast rotators as a function of the inclination of the main progenitor with respect to the merger orbital plane for mass ratio 1:1, 2:1g10, 2:1g33. The negative inclination occurs when the spin of the Sb progenitor and the spin of the orbital angular momentum are anti-parallel, so that -25° and 25° represent the same inclination for the galaxy but on retrograde orbit.

3.3.1.3 Influence of orbital parameters

We now examine, for mergers with mass ratios 1:1 and 2:1 which form the majority of slow rotators, how the orbital parameters influence or determine the slow/fast nature of the merger remnant and the associated presence/absence of a KDC.

Fig. 3.6 shows the distribution of fast and slow rotators as a function of the orbital inclination/orientation with respect to the Sb progenitor galaxy for the 1:1 and 2:1 merger remnants. We remind the reader that the Sb progenitor is the "main" (most massive) progenitor in the 2:1 mergers. Mergers with a direct (prograde) orbit with respect to the Sb progenitor all produce fast rotators. Mergers with a retrograde orbit with respect to the Sb progenitor almost exclusively produce slow rotators regardless of the spin of the Sc galaxy. This shows that mergers with a high total angular momentum (orbital momentum + internal momentum of each progenitor) do not produce slow rotators, as even violent relaxation fails to efficiently expel a significant fraction of the (baryonic) angular momentum from the central part of the merger remnant.

In contrast to this result, having the Sb progenitor on a retrograde orbit (the main one for 2:1 mergers) represents a sufficient condition to form a slow rotator

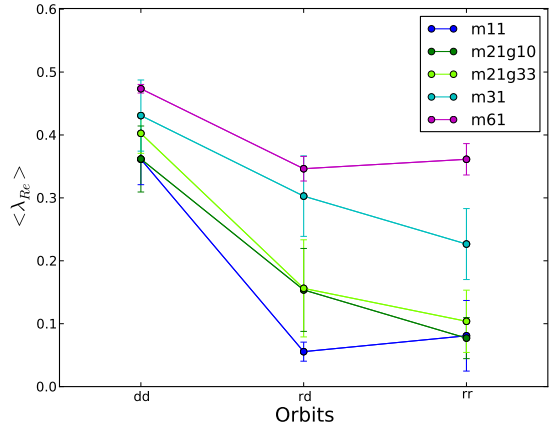

Figure 3.7: Average λ_R as a function of the spin of the progenitors for the different mass ratios.

(see also next Section). The formation of a slow rotator therefore requires a relatively low total angular momentum, without requiring *e.g.*, that the progenitors both are on retrograde orbits. The formation of a slow rotator may then be a likely event in a 1:1 or 2:1 merger of spiral galaxies: if the main requirement is to have a retrograde orbit for the main progenitor, the relative fraction of slow and fast rotators should directly reflect the spin distribution of the progenitors (with respect to the orbit, Fig. 3.5).

These conclusions are further assessed by Fig. 3.7: it presents the average λ_R value as a function of the orbital orientation for both progenitor galaxies (*i.e.*, **dd**, **rd** and **rr** orbits) for all mass ratios. It shows that, while **rr** orbits result in a somewhat lower angular momentum at 1 R_e than **rd** orbits (or similar for 1:1 and 6:1 mass ratios), most of the angular momentum removal is already obtained for **rd** orbits, where the orbit is **r**etrograde for the main Sb progenitor but **d**irect (prograde) for the Sc companion.

3.3.1.4 Influence of the Hubble type of the progenitor spiral galaxies

We noted above from Fig. 3.6 that having the main progenitor prograde or retrograde largely determines the fast or slow rotator nature of the merger remnant, while the orbit orientation with respect to the companion has a weaker effect. This is expected for unequal mass mergers, and in particular for 6:1 mass ratios, where the companion mass and momentum are naturally much lower than those

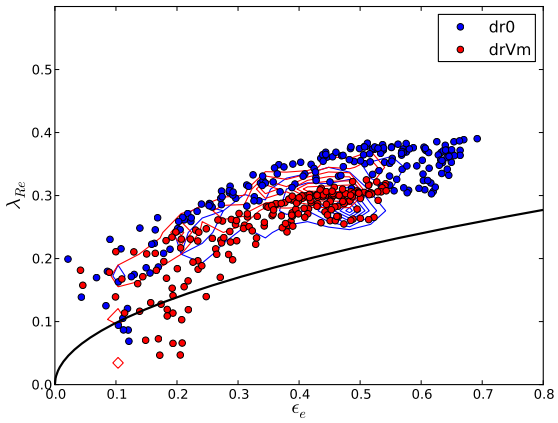

Figure 3.8: $\lambda_R - \epsilon$ diagram for the *m11dr0* (in blue) and for the *m11drVm* (in red). The contours represent the distribution of the 200 projections of the *m11dd0* (in blue) and *m11ddVm* (in red) simulations.

of the main progenitor. This is however more surprising for 1:1 mergers. Indeed, these equal-mass mergers end-up with a relatively similar λ_R as long as the Sb progenitor has a retrograde orientation, regardless of the orientation of the Sc progenitor.

This could be the consequence of a "saturation" effect: the final angular momentum of the merger remnant could be dominated in the centre by one retrograde galaxy with the other (retrograde) galaxy contributing very little. However, the central properties of merger remnants which exhibit relatively high angular momentum obtained via a prograde orientation of the Sb progenitor show little variation whether the Sc progenitor is on a prograde or retrograde orientation. This suggests that the Sb and Sc progenitors do not have symmetric roles in determining the properties of the merger remnant. We first examined whether or not this is an artefact from the initial positioning of the two spiral galaxies in the simulation box and/or the initial orientation of their spin axis with respect to the numerical grid. To test this, we reversed the initial positioning of the Sb and Sc progenitors and changed the grid orientation in a re-simulation of the *m11rd0* merger: we observe no significant difference in the merger remnants. This confirms that our results do not depend on the simulation box size and grid orientation.

We then simulated mergers in which the Sb progenitor is on a direct orbital orientation, and the Sc progenitor is on a retrograde orientation, *i.e.* **dr** mergers –

so far our sample comprised only **rd** mergers with a retrograde Sb and a direct Sc progenitor. Given that the *m11rd0* and *m11rdVm* orbits resulted in quite typical slow rotators, we performed the corresponding *m11dr0* and *m11drVm* simulations. The $\lambda_R - \epsilon$ profiles are shown on Fig. 3.8. The *m11dr0* and *m11drVm* remnants are fast rotators, relatively typical compared to the fast rotators produced on **dd** orbits. The outputs of **dr** and **rd** orbits are therefore widely different. This shows that while the angular momentum of a merger remnant largely depends on the total available (baryonic) angular momentum, *i.e.* the sum of the orbital angular momentum and the internal spin of each progenitor galaxy, the Hubble type of the progenitor galaxies – *i.e* their central concentration and dynamical stability – has a significant impact. A retrograde orbit around an early-type spiral, such as our so-called Sb galaxy, is efficient in producing slow rotators (for 1:1 and 2:1 mergers). A retrograde orbit around a late-type spiral, such as our so-called Sc galaxy, does not significantly impact the angular momentum remaining in the central body of the merger remnant (see Fig. 3.8 and Section 3.3.2.3 for the interpretation).

3.3.2 Formation mechanisms for KDC via major mergers

In this section, we focus on the processes involved in the formation of a KDC in our simulations, and we thus examine the relative contribution of the different components, namely the old stars, the young stars and the gas associated with the KDC observed in the merger remnant.

3.3.2.1 The contribution from old stars

To probe the contribution of the old stars in the slow rotator remnants with a KDC, we have separated the old stars which belong to the Sb progenitor from the ones of the Sc companion. The intensity and velocity fields of six analysed cases (m11, m21g10, m21g33 with **rd** orbit and m11, m21g10, m21g33 with **rr** orbit) are shown in Fig. 3.9. The projections used in that figure have been selected to emphasise the respective contributions of the progenitors in the final remnant and do not specifically correspond to edge-on or face-on views of the galaxy.

There seem to be two qualitatively different types of KDCs which can in fact be associated with different initial orbits. In the **rd** cases, a KDC is visible within 1 R_e and results from the luminosity weighted average of two counter-rotating stellar systems. In the **rr** orbits, the KDC is more prominent and extended, and is visible in the *individual* contributions of both progenitors, at least for the 1:1

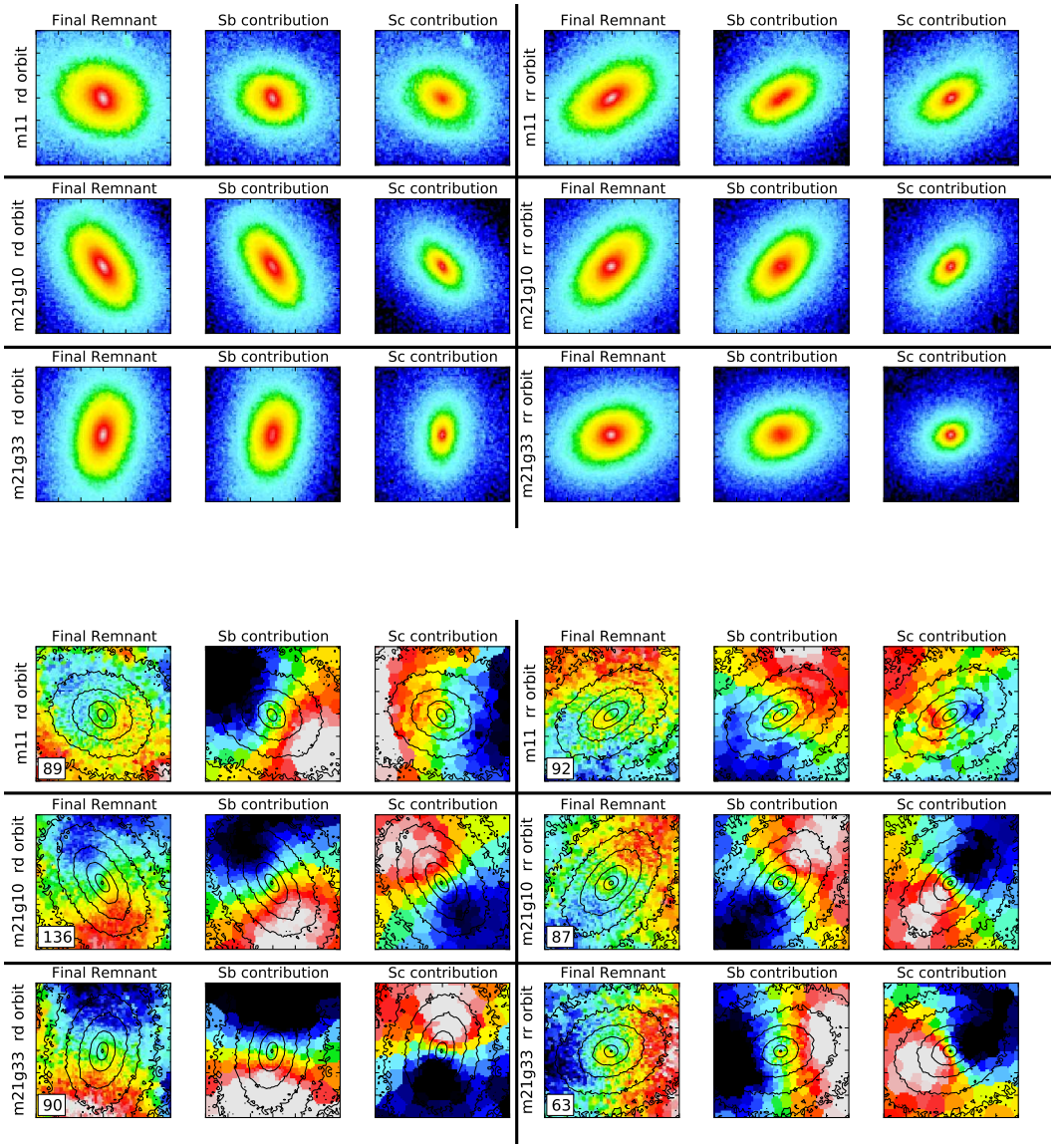

Figure 3.9: Intensity (three top panels) and velocity (three bottom panels) fields of the old stars for the final merger remnant, for the stars belonging to the Sb progenitor in the remnant, for the stars belonging to the Sc companion in the remnant. The cuts in magnitude and velocity are computed from the Final remnant and applied to the Sb and Sc progenitor contributions. The field of view for each panel is 15×15 kpc^2.

mergers. This can be understood by following the Sb and Sc progenitor in turn.

The Sb progenitor remains, within the central region, mostly unaffected by the merger, even for large mass ratios (1:1). This is true except at $R < R_e$ for the **rr** orbit: when the Sc companion has a negative spin (with respect to the orbit) the Sb progenitor is more severely affected. This is consistent with the picture developed by [Renaud *et al.* 2009] which suggests that retrograde galaxy orbits allow more material to be available for later interactions when galaxies get closer to each others.

The Sc progenitor is, in stark contrast with the Sb progenitor, almost entirely disrupted during the merging event and will basically adopt part of the orbital angular momentum (the rest being transferred to the dark matter component) and its sign. The final contribution of the Sc progenitor in the remnant therefore mostly reflects that choice of orbit, which was assumed as prograde (positive) as a reference. When the Sc progenitor itself is on a prograde orbit, this will add up to produce a rapidly rotating stellar component to the remnant. When the Sc progenitor is on a retrograde orbit, and considering that the close interaction time between stars of the Sc and the global potential of the Sb is then shortened [Renaud *et al.* 2009], some stellar material with the initial angular momentum sign will remain in the remnant potentially producing a rather large stellar KDC (from old stars).

We can therefore naturally expect a KDC to form as soon as the Sb progenitor is on a retrograde orbit, due to the superposition of a positively rotating contribution from the companion, and the counter-rotating stellar contribution of the main Sb progenitor. When the Sc is on a retrograde orbit, it more violently affects the Sb progenitor which then exhibits a KDC. The Sc is then also transformed into a stellar system with rather disturbed and complex dynamics resulting from the superposition of the orbital wrapping (following the galaxy orbit) and the initial angular momentum of the stars (in the opposite sense).

This process is valid for both the 1:1 and 2:1 mergers. However, the Sc companion in an unequal mass mergers has obviously a smaller influence on the Sb progenitor and is itself more easily destroyed which explains why it appears as having fully adopted the sign of the orbital angular momentum vector. This is nicely illustrated in Fig. 3.9. In the case of a 2:1 **rr** merger, the two contributions have roughly the same mass profiles within the central kpc. The velocity map of

the remnant is then composed of the superposition of the counter-rotating component of the Sb progenitor and the contribution from the Sc companion. At larger radii (r $>$ 1 kpc), the Sb galaxy is dominant in mass and leads the velocity field of the merger remnant. An apparent KDC is then visible in the merger remnant. The small ($\sim$ 1 kpc) decoupled core in the centre of the Sb progenitor is also smaller than in 1:1 mergers because the companion is lighter and does not affect the central stars of the Sb progenitor much. However, as also pointed out in the 1:1 merger cases, the decoupled core is larger than in the **rd** case as the mass of the companion falling in the centre is bigger.

We can now easily extend this analysis to the **dd** and **dr** cases which produce fast rotators. In the case of a **dd** orbit, the two spins of the progenitors are aligned with the spin of the orbital angular momentum. This maximises the (positive) angular momentum, which naturally produces a flattened fast rotator. The output of the case of the **dr** orbit can be extrapolated from the **rr** case: the Sc companion has a spin anti-parallel with respect to the orbital angular momentum vector. During the approach, the companion is violently disturbed and its stars (most of them in 1:1 and all of them in 2:1 mergers) merge with the Sb progenitor with the spin of the orbit (and of the Sb progenitor). The final merger remnant is then composed of two components with the same sense of rotation and is then a fast rotator, just slightly rounder than for a **dd** orbit.

3.3.2.2 The contribution from young stars and gas

In Fig. 3.10 we present the velocity fields of the gas and the young stars of the projections used for Fig. 3.9, the iso-magnitude contours of the old stars being superimposed. We can see that the gas and the young stars share the sense of rotation with the outer part of the final remnants. The gas does not show much sign of a disturbed morphology or kinematics in the centre. The young stars exhibit some misalignments in the very centre of the galaxy, these misalignments being roughly at 90° with respect to the photometric major-axis of the remnant. The gas, and the associated star formation, thus do not play a role in the KDC itself, although the concentration of gas and young stars in the central part of the merger remnant bring an additional central density which could influence the evolution of the KDC.

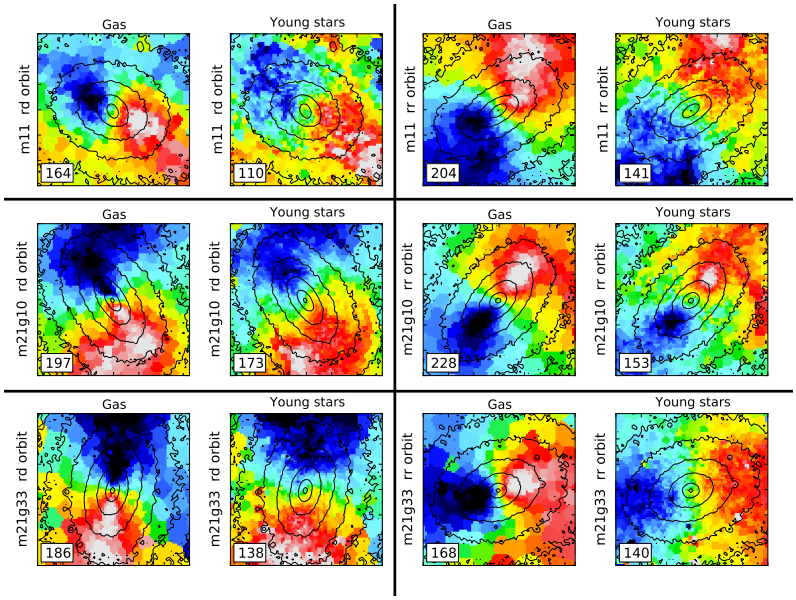

Figure 3.10: Velocity fields of the gas and the young stars in the final merger remnant, iso-magnitude contours of the old stars of the final remnant are superimposed. The field of view for each panel is 15×15 kpc^2.

3.3.2.3 Summary

The KDCs in the merger remnants are mostly seen in the old stars, with only a weak signature in the young stars (none in the gas). Moreover, most of the KDCs formed in the major mergers (1:1, 2:1) do not correspond to physically distinct stellar components (see also the study of [van den Bosch *et al.* 2008]), except in the case of 1:1 binary disc mergers on a **rr** orbit. These "apparent" KDCs result from the superposition of two counter-rotating stellar components where one disc is dominating the mass profile in the centre while the second disc is dominating outwards. This scenario seems to hold even when the two progenitor discs have the same sense of rotation but with a spin which is retrograde with respect to the orbital angular momentum. The formation of an apparent counter-rotating core (CRC) with two initial retrograde progenitors has also been probed by [Balcells & Quinn 1990] in a 5:1 merger of oblate ETGs: the companion adopts the sign of the orbital angular momentum during the merger to form a CRC when the two galaxies merge. The physical process invoked to form CRCs in [Balcells & Quinn 1990] appears consistent with the one witnessed in the present study, although we only form here CRCs in remnants of major (1:1 or 2:1) merg-

ers.

As pointed out in Section 3.3.1.4, the two progenitors have a different influence on the output of the merger. Our so-called Sb progenitor is more concentrated and dynamically stable, and most of its stars keep their original orientation during the merger. The so-called Sc progenitor is colder, less concentrated and responds more efficiently to potential disturbances.

Our study on the formation of the KDCs in binary mergers of disc galaxies should therefore be completed by probing mergers with various morphological types, *e.g.* Sb–Sb or Sc–Sc. The detailed role of the Hubble type for disc progenitors in galaxy mergers is an important issue which will be examined in a future study.

3.4 Convergence with other studies

We have focused our analysis on the central part of the merger remnants to study in details the formation of the slow and fast rotators (and the formation of the KDCs). In this section, we compare our sample of galaxies with other similar recent studies to test the convergence of the different results.

3.4.1 TreeSPH Gadget-2

We here specifically compare our results with two other sets of simulations, namely the work of [Jesseit *et al.* 2009] and [Hoffman *et al.* 2010]. They have both performed a suite of simulations using the TreeSPH code Gadget-2 [Springel 2005] with a gravitational softening length of 140 pc. In these simulations, [Hoffman *et al.* 2010] included radiative heating and cooling, star formation, feedback from supernovae and active galactic nuclei and used a total of 4×10^5 particles while [Jesseit *et al.* 2009] "only" included star formation and stellar feedback but with a total of $\sim 10^6$ particles. We discuss in the following some relevant differences between these studies and ours.

[Jesseit *et al.* 2009] emphasised the formation of slow and fast rotators with their sample of simulations. They have simulated binary mergers of disc galaxies with mass ratios from 1:1 to 4:1 as well as galaxy remergers. We find some significant differences with their results:

- 75 per cent of their 1:1 mergers, but only 10 per cent of their 2:1 are slow rotators. This can be compared with 60 per cent for both 2:1 and 1:1 mergers in our sample.

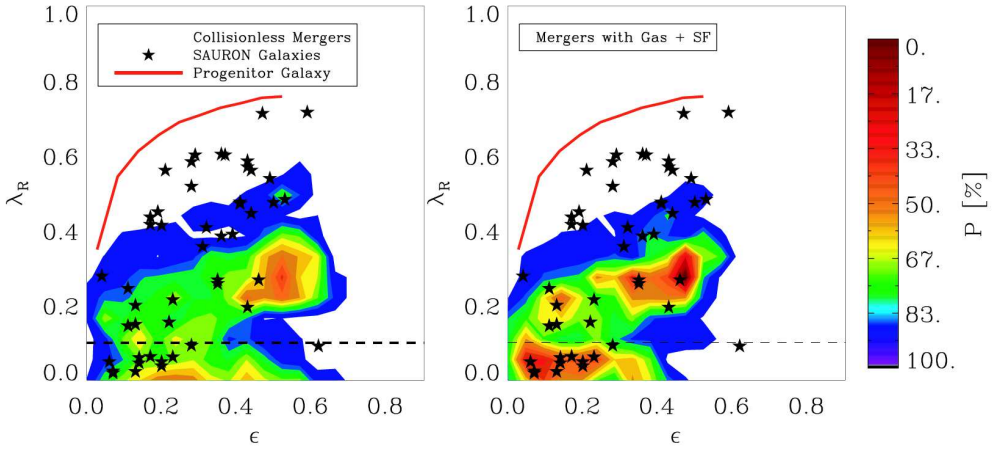

Figure 3.11: (Extracted from [Jesseit *et al.* 2009]) Left: 2D probability contours of collisionless 1:1 and 3:1 remnants in $\lambda_R - \epsilon$ diagram. The SAURON galaxies are indicated by black stars. High-λ_R galaxies are resembling more the progenitor galaxy than 3:1 merger remnants. Right: the same plot, but this time with merger remnants which formed with gas.

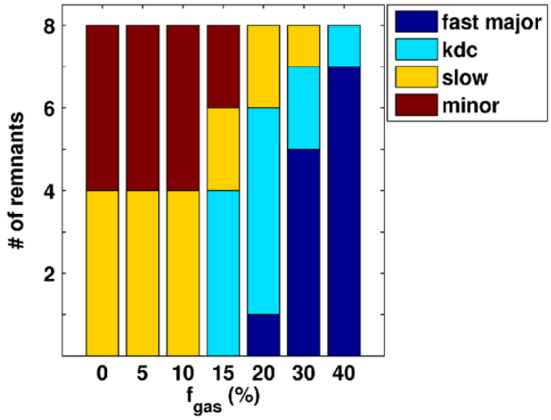

Figure 3.12: (Extracted from [Hoffman *et al.* 2010]) Classification of the remnant kinematics. The eight remnants of each gas fraction were categorized as (1) showing rapid major-axis rotation, (2) slowly rotating with a disk-like KDC, (3) slowly rotating throughout, or (4) showing rapid minor-axis rotation, based on visual inspections of their velocity maps.

- Overall, their merger remnants are rounder than ours (see Fig. 3.11. Their progenitors have $\epsilon < 0.5$ and their slow rotators have $\epsilon < 0.4$, their dry remnants are flatter but do not have $\epsilon > 0.6$. The distribution of λ_R and ϵ for their fast rotator remnants are consistent with the fast rotators described in the present study.

- The ellipticity and λ_R distributions of their 1:1 disc-disc merger remnants are "hardly distinguishable" from their ETG-ETG merger remnants. From our sample of ETG-ETG mergers (see Section 4.1), the difference is very clear, our ETG-ETG merger remnants are rounder and are classified as fast rotators, and we do not produce slow rotators with very low λ_R values from re-merging of disc binary mergers.

These differences can be mainly explained by variations in the initial parameters of the disc galaxies and the initial conditions of the mergers. The progenitors in [Jesseit *et al.* 2009] have a more massive bulge ($B/T = 1/4$, as compared to $B/T = 1/5$ and $1/8$ for our study), and their bulges are non-rotating. The distance between the two progenitors at the pericentre is about two disc scale-lengths ($\sim$ 7 kpc) while this distance is on average 5–10 disc scale-lengths in our study. Due to their low pericentric distance, the mergers are more direct and thus violent which may produce rounder remnants. These remnants are also classified as slow rotators, which may be again linked with the absence of rotation of the bulges in their progenitors and the low angular momentum of orbits with low pericentric distances.

In the present study, we have also simulated binary mergers with an impact parameter R decreased from 60 to 35 kpc. In this range of R values, there is no significant difference in the shapes of the merger remnants we obtain, for all mass ratios and initial spins of the progenitors, when the value of R is decreased. Our lower value of R remains large compared with the one used for [Jesseit *et al.* 2009] and simulations with an even lower impact parameter ($\sim$ 10 kpc) should be considered for further comparison. Orbits with large impact parameters and pericentric distances, as in our study, seem statistically more representative of hierarchical merging in ΛCDM context [Khochfar & Burkert 2006]. However, the presence of an external gravitational field (in dense environment) may significantly impact the orbit of the two progenitors, decreasing the pericentric distance (Martig, private comm.): this will be examined in more detail in a forthcoming paper.

[Hoffman *et al.* 2010] have simulated binary mergers of disc galaxies of mass

ratio 1:1 at different gas fraction (from 0 to 40 per cent of gas). Again, there are several differences between their results and ours:

- From 0 to 10 per cent of gas, their remnants are all slowly rotating. They do not have KDCs, the slow rotator galaxies are dominated by box orbits or by minor axis rotation. With 15 and 20 per cent of gas, most of their remnants have a KDC. When reaching 30 and 40 per cent of gas, most of their remnants are all fast rotators (see Fig. 3.12). They do not find any strong trend between the initial condition of merging (*e.g* the orientation of the discs) and the formation of slowly rotating early-type galaxies.

- Their KDCs are small discs of young stars coming from the gas in rotation in the centre. When the fraction of gas is increased, the size of the final disc of gas –and thus the disc of young stars – is also increased and it creates a fast rotator. Their fast rotators are purely dominated by the young stars created in this large disc of gas in rotation. In our sample, the KDC is an apparent KDC (except for the 1:1 merger with **rr** orbits) and is seen only in the old stars. The gas does not show any sign of counter-rotation. Our KDCs do not depend on the gas fraction, as we do not find any significant difference between the remnants with 10 or 33 per cent of gas.

In [Hoffman *et al.* 2010], the stars in the spiral progenitors are only distributed on a disc (*i.e.* without a bulge or spheroid), they also used a impact parameter of 7.1 kpc. These initial conditions are far from ours and lead to a very different merging process. We speculate that, as the orbit leads to a more rapid and direct collision, the two discs are destroyed and strongly influenced by violent relaxation and are not expected to keep a trace of the original disc dynamics (except at large radii as pointed out in their paper). This may explain why none of their low gas fraction mergers shows signs of rotation around the short-axis of the remnants.

The treatment of the gas and the resolution used for the simulations are also different between this study and the one presented here. During my thesis, I showed that at high resolution, thinner gas structures are resolved during the merger, which can result in structured and clustered star formation. These local density peaks are accompanied by rapid variations of the gravitational potential, which help scatter stellar orbits and evacuate the angular momentum. A gas-free and a gas-rich merger should differ not only with the reformation of a disc of gas in the centre of the remnant as seen in [Hoffman *et al.* 2010], but also at all radii with different stellar orbits (see also [Bournaud *et al.* 2010a]). These results emphasized the need for high spatial and mass resolution (see also

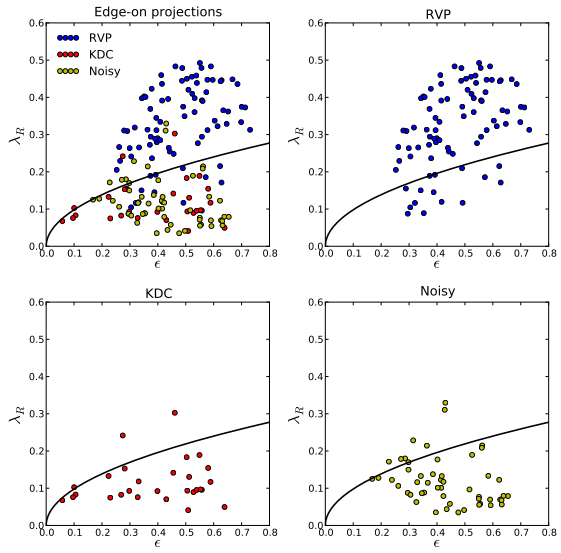

Figure 3.13: $\lambda_R - \epsilon$ diagram of an edge-on projections of the GalMer merger remnants. Upper left: all the galaxies, upper right: galaxies classified as RVP, lower left: galaxies with a KDC, lower right: Noisy galaxies.

[Powell *et al.* 2010, Teyssier *et al.* 2010] and Section 2.2 of this thesis) and for realistic physical inputs: *e.g.* the treatment of the gas with models capable of resolving the main dense gas clouds/SF regions, see [Governato *et al.* 2009] in a cosmological context.

3.4.2 GalMer sample

The GalMer project consists of one of the largest – if not the largest – publicly available sample of numerical simulations of interacting galaxies (see [Di Matteo *et al.* 2007, Chilingarian *et al.* 2010]): with a high number of simulations but a relatively low resolution. They employed a TreeSPH code with a total number of particles of 1.2×10^5 and a softening length of 280 pc. The progenitors for these simulations are either spiral or elliptical galaxies. For the comparison with our sample of galaxy mergers in this Chapter, we have only selected progenitors which are spiral galaxies with a Hubble type typical for a Sa, Sb and Sd galaxies. Details on the progenitors and the initial conditions for the mergers can be found in [Chilingarian *et al.* 2010].

As it has been done for our sample of binary mergers, we have visually inspected the 2D velocity maps for different projections of the GalMer merger rem-

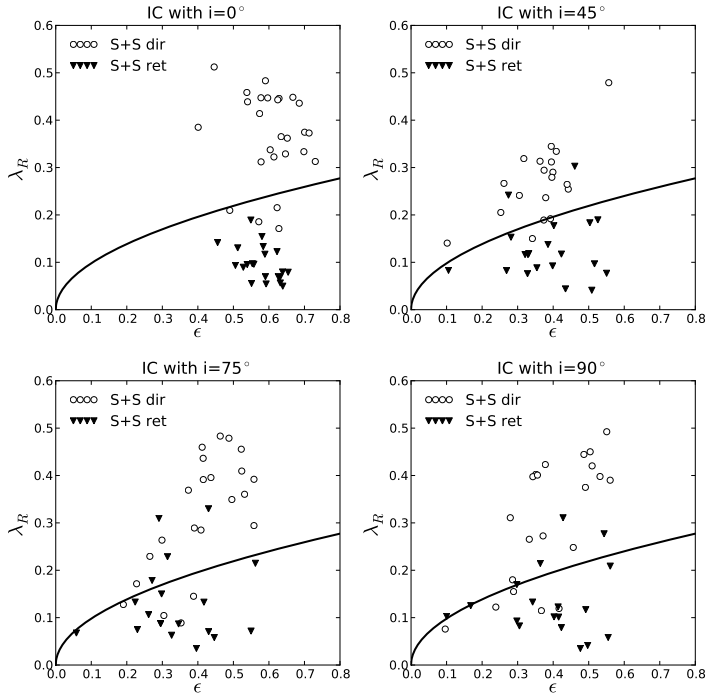

Figure 3.14: $\lambda_R - \epsilon$ diagram of an edge-on projection of the GalMer merger remnants. The white symbols represent the Spiral-Spiral mergers, the black symbols the ETG-Spiral remnants. The points represent the **dd** orbits and the triangles the **rr** orbits. The four panels correspond to four different initial conditions, the spin of the first progenitor is always aligned with the orbital angular momentum while the spin of the second progenitor have an inclination of: 0° (top left), 45° (top right), 75° (bottom left) and 90° (bottom right) with respect to the orbital angular momentum.

nants. I have classified the remnants in three families: the galaxies with a regular velocity pattern (named *RVP* galaxies), the galaxies with a KDC (named *KDC* galaxies) and the galaxies with no regular velocity pattern and a very noisy velocity field (named *Noisy* galaxies). The noise in the galaxies with no regular velocity pattern is a direct consequence of the low resolution level of the simulations. We also applied our analysis routines to compute the ellipticity ϵ and λ_R at one effective radius.

Fig. 3.13 shows the $\lambda_R - \epsilon$ diagram for an edge-on projection of the GalMer merger remnants sorted by their kinematical classification (RVP, KDC, Noisy). The RVP galaxies span a large range of ellipticities: from round (ϵ = 0.25) to very flat (ϵ = 0.7) remnants, and a large range of λ_R values: from 0.07 to 0.5. These remnants are mostly classified as fast rotators but 15 of these should be classified as slow rotators. The remnants with a clear KDC and the Noisy galaxies share the same properties: they span a large range of ellipticities and, except for very few cases, are classified as slow rotators. Fig. 3.14 presents the $\lambda_R - \epsilon$ diagram for the same projections but sorted by their initial conditions. The remnants of two co-planar (*i.e.* i = 0°) spiral galaxies are very flat. The remnants become rounder when the second progenitor is inclined (the first progenitor is always in the orbital plane): the ellipticity can be as low as 0.2 when the angle is larger than 75°. Similarly to our sample of simulations, we note a pronounced relation between the orbit of merging and the formation of the slow and fast rotators: two progenitors with a direct-direct orbit will globally lead to a fast rotator and two progenitors with a retrograde-retrograde orbit to a slow rotator.

Using the simulations of the GalMer database, we find the same process of formation for the slow rotators than in our present study. But there is a large scatter in the results of the GalMer simulations: *e.g.* four mergers remnants – with co-planar spiral progenitors in a **dd** orbit as initial conditions – are visually classified as RVP galaxies but are below the limit defining the slow and fast rotators. The resolution in the GalMer simulations is clearly too low to properly resolve the different kinematic features observed in galaxies with low velocity amplitudes but it seems to provide relatively good recipes (in term of initial conditions) for the formation of the round slow rotators which are missing in our sample of simulations. The main difference between the GalMer sample and ours being the choice of initial conditions.

The GalMer database could then be a good springboard for simulations at higher resolution. To test these conclusions, we can easily imagine a sample of high-resolution simulations – using *e.g.* our PM-sticky code – selected to repro-

duce the initial conditions of some of the GalMer simulations.

3.5 Conclusions

We have simulated 70 binary mergers of disc galaxies at an unprecedented resolution for such a sample of simulations. We have studied the effect of different initial parameters on the global properties of merger remnants, varying: the mass ratio (from 1:1 to 6:1), the initial conditions of the mergers (incoming velocity, impact parameter, inclination in the orbital plane), the spins of the progenitors. We have also compared our work with previous established samples of numerical simulations. Our main conclusions can be summarized as follows:

- We obtain both fast and slow rotators. The fast rotators can be observed at all mass ratios while the slow rotators are formed only for mass ratios between 1:1 and 2:1, in agreement with [Jesseit *et al.* 2009]. We confirm that the limit separating the two families of ETGs defined by the ATLAS^{3D} survey is meaningful, as our simulated slow and fast rotators present distinct characteristics: the fast (*resp.* slow) rotators have a high (*resp.* low) angular momentum content, their photometric and kinemetric position angle are aligned (*resp.* misaligned), they present (*resp.* do not present) regular velocity patterns. An important difference is the presence (or absence) of a KDC: none of the fast rotators hold a KDC while most of the slow rotators do.

- The two parameters which constrain the formation of the KDCs are (1) the mass ratio between the initial spirals, as we form a KDC only with 1:1 and 2:1 mergers, and (2) the orientation of the initial spin axis of the earliest-type (Sb) disc progenitor with respect to the orbital angular momentum (its spin has to be anti-parallel). The spin of the later-type (Sc) progenitor has less importance as this galaxy is mostly disrupted during the merging process. For a 1:1 merger, if the two progenitors are retrograde, the KDC is intrinsically decoupled from the external part of the merger remnant. For all other initial conditions leading to the formation of a slow rotator, the KDC is only an apparent KDC formed via the superposition of two counter-rotating discs.

- The Hubble type of the initial spiral progenitors seems to play a prominent part in the formation of slow rotators and additional simulations are needed to further constrain its role.

- To test the importance of the presence of gas, we have simulated binary mergers with mass ratio 2:1 with either 10 or 33 per cent of gas. We do not find major differences in the morphology and the kinematics of the merger remnants. There are some visible differences (*e.g.* the number of newly formed globular clusters) but it does not impact much the kinematics of the remnants and the comparison with the ATLAS^{3D} sample. Higher gas fractions representative of mergers at high redshifts could have a larger impact, though.

Appendix: Velocity fields and λ_R profiles

All simulations used for this study are listed here. For each simulation, an edge-on view of the velocity field (with the iso-magnitude contours in black) and its associated λ_R profile are plotted. The simulations are classified in this way:

- A figure corresponds to mergers with the same mass ratio, *e.g* Fig. 3.15 shows the binary mergers of mass ratio 1:1
- A group of six projections associated to their λ_R profiles correspond to a specific orbit of merging (**dd**, **rd** or **rr** orbits)
- The six projections correspond to the different initial conditions for a specific orbit of merging (*0*, *im*, *ip*, *Rm*, *Vm*, *Vp*, see Table 3.2)
- The label of the simulation (*e.g* m31ddip) and the velocity cut are noted in the projected velocity maps: the colour of the text indicates if the galaxy is classified as a fast rotator (black), a slow rotator with a KDC (red) or a slow rotator without KDC (green); the KDC may not be visible under the edge-on projection but is visible for most of the others.
- The colour of the text indicates if the galaxy is classified as a fast rotator (black), a slow rotator with a KDC (red) or a slow rotator without KDC (green)

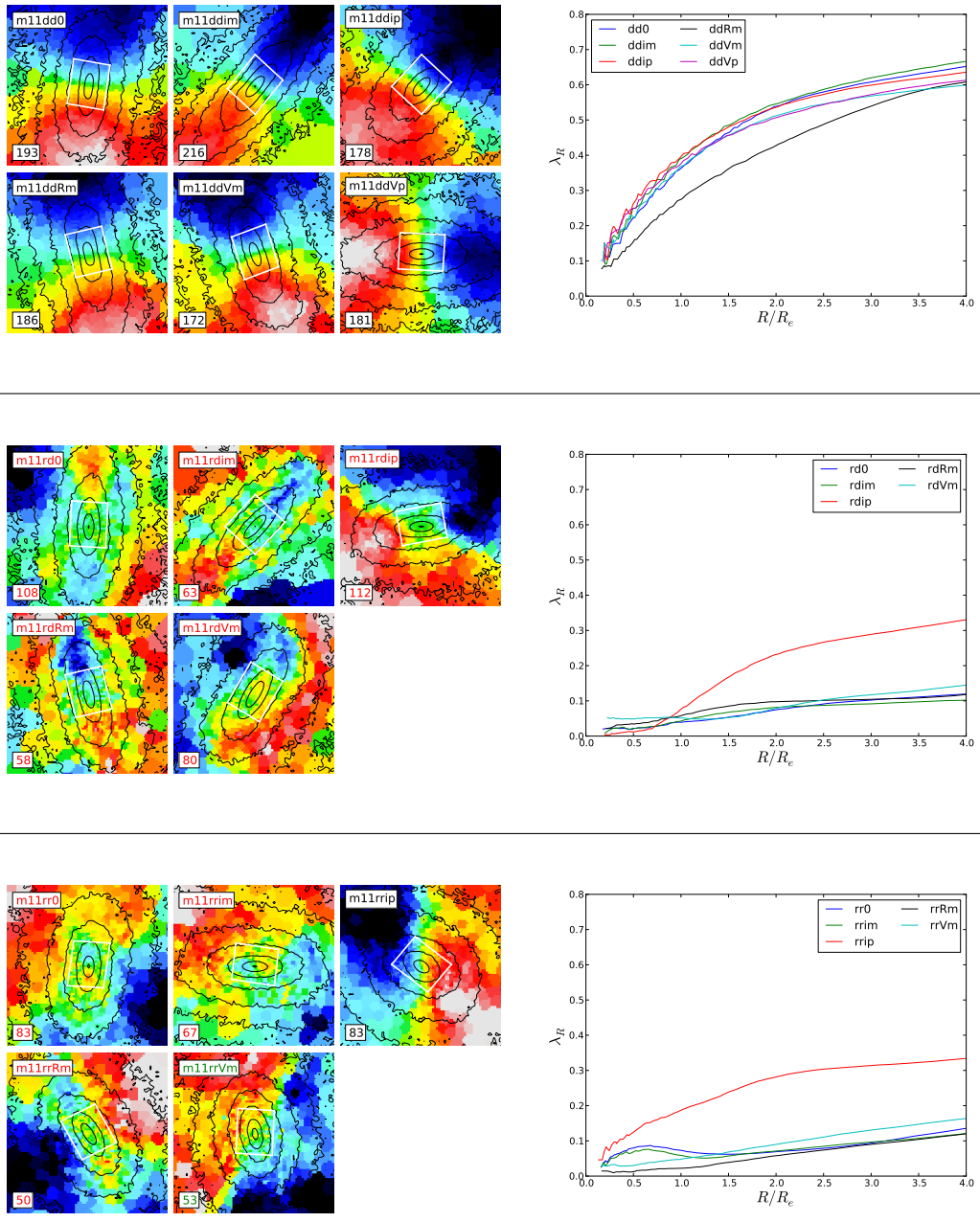

Figure 3.15: **Left:** Edge-on projection of the velocity field for the binary mergers of mass ratio 1:1 for the 3 type of orbits (top: **dd** orbit, middle: **rd** orbit, bottom: **rr** orbit). The black lines correspond to the iso-magnitude contours. The field of view is 15×15 kpc^2. The white rectangle indicates a typical field covered by the instrument SAURON and corresponds to a field of $41'' \times 33''$ for a galaxy at a distance of 20 Mpc, its orientation follows the photometric position angle taken at $3R_e$. **Right:** The corresponding λ_R profiles as a function of the radius R divided by the effective radius R_e of the edge-on projection.

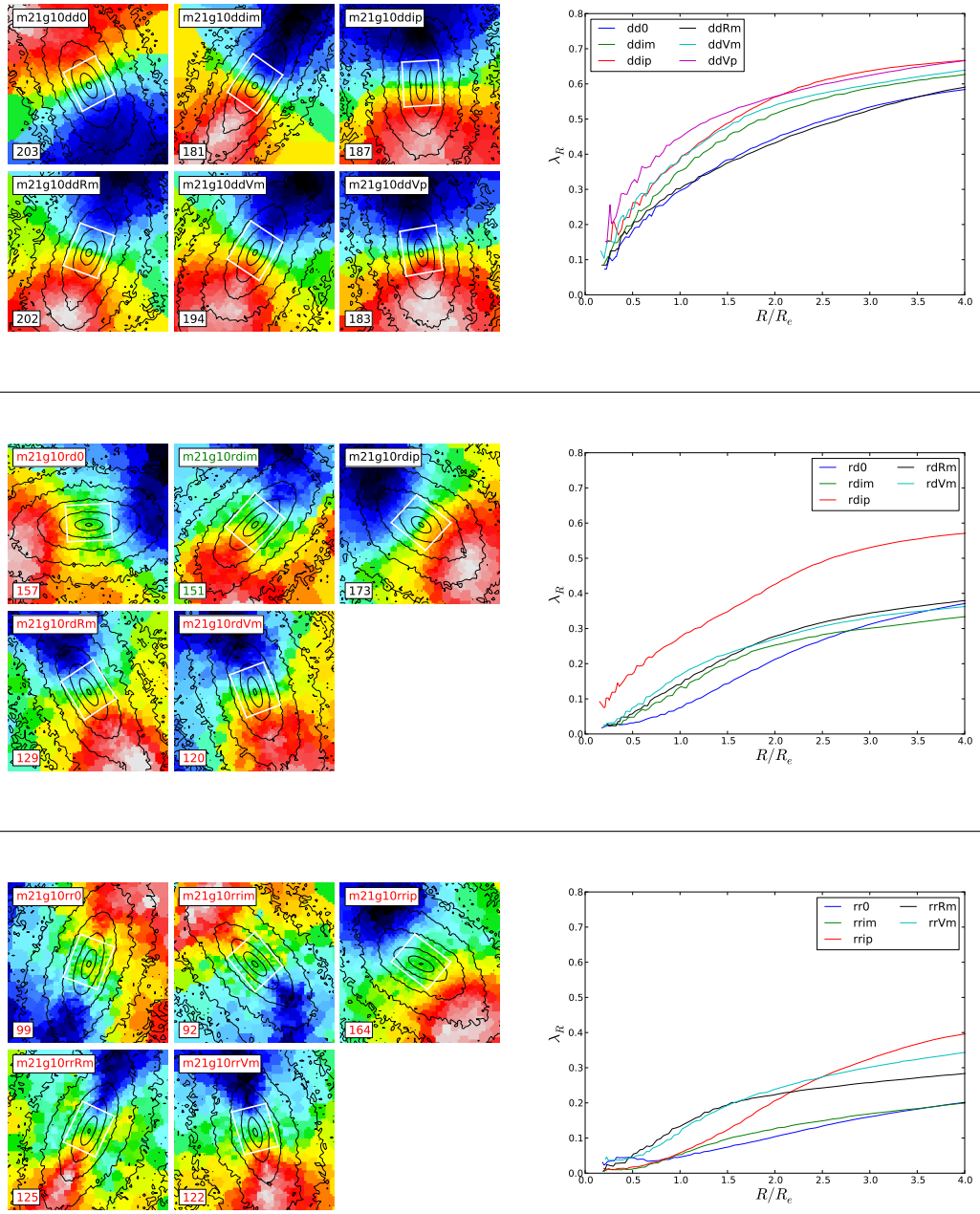

Figure 3.16: Same as Fig. 3.15 for the binary mergers of mass ratio 2:1 with 10 per cent of gas.

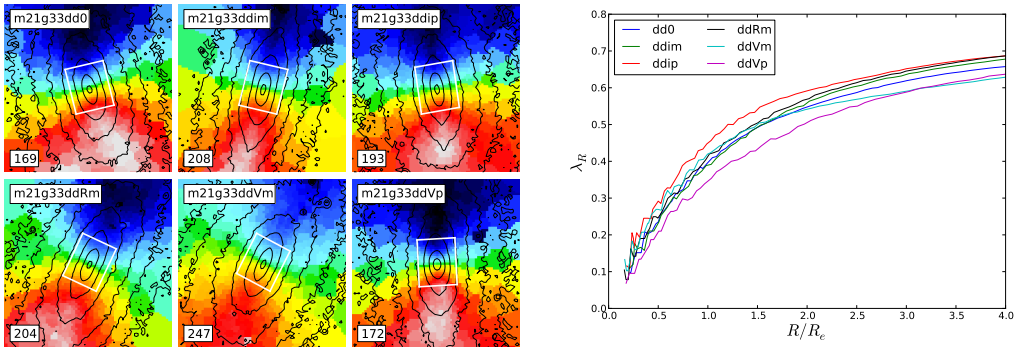

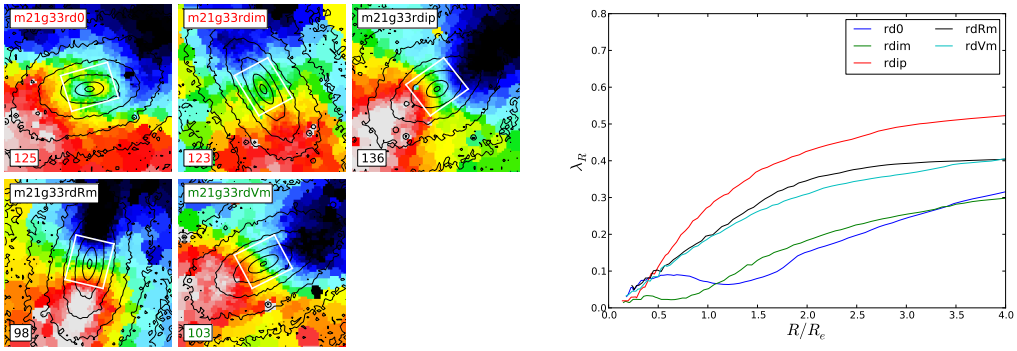

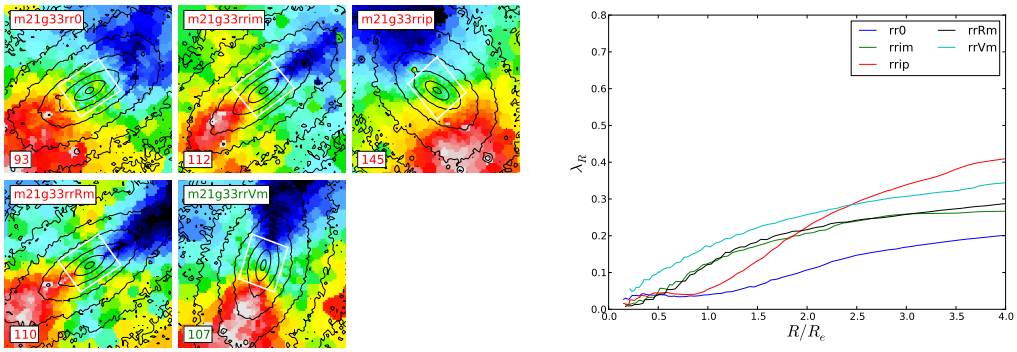

Figure 3.17: Same as Fig. 3.15 for the binary mergers of mass ratio 2:1 with 33 per cent of gas.

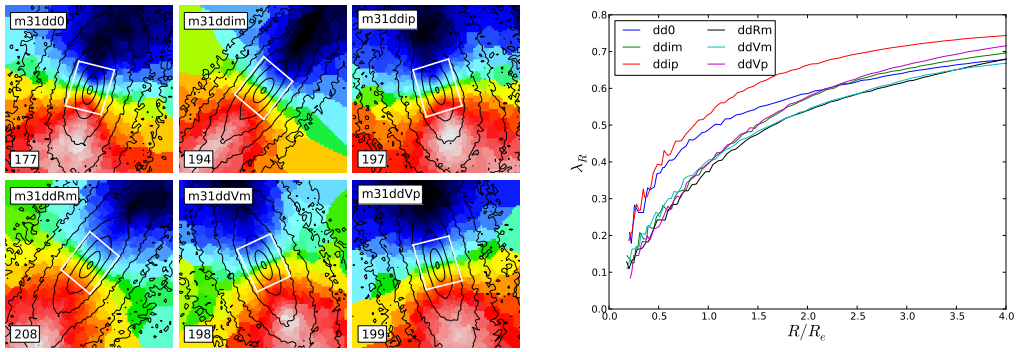

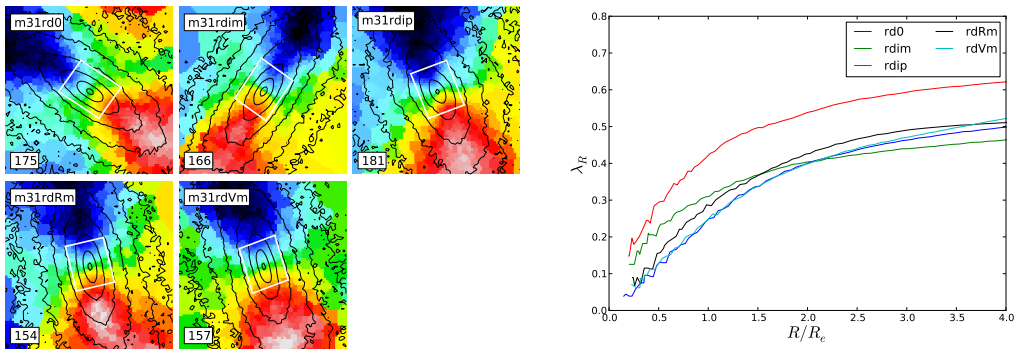

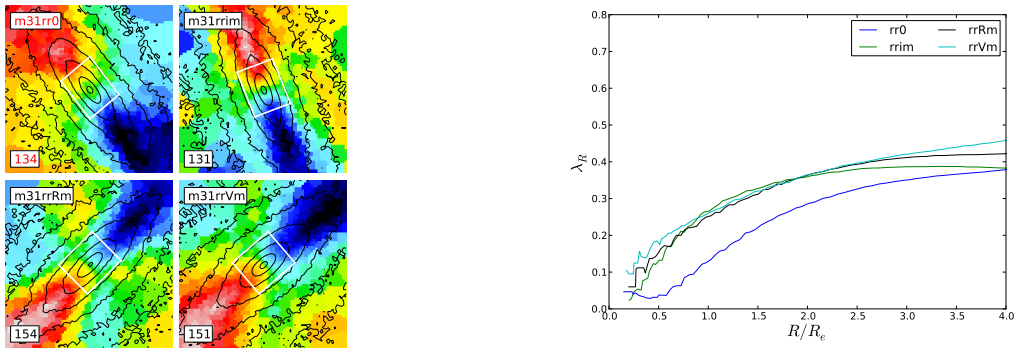

Figure 3.18: Same as Fig. 3.15 for the binary mergers of mass ratio 3:1.

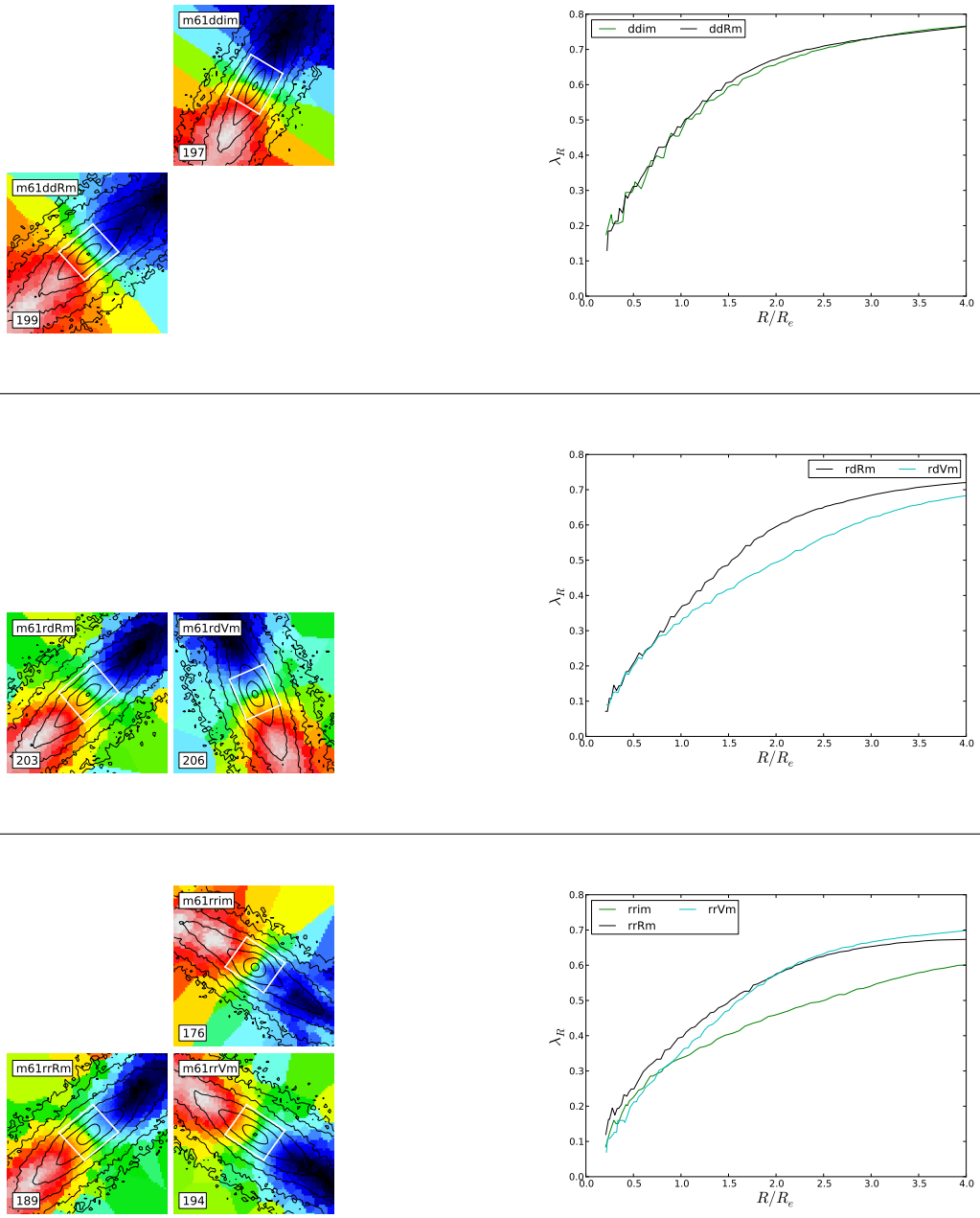

Figure 3.19: Same as Fig. 3.15 for the binary mergers of mass ratio 6:1.

Chapter 4

Numerical simulations of multiple galaxy mergers

Contents

The most massive galaxies in the Universe are not formed only via a binary merger of spiral galaxies: they have a more complex history of formation, including several mergers. This chapter will then be devoted to the analysis of mergers between an early-type galaxy and other galaxies (either spiral or ETG), called galaxy remergers.

In the first section, I analyse the morphological and kinematical properties of ETG equal mass remerger remnants and show that these always end-up with a regular velocity pattern without a KDC. In the second section, I perform simulation of remergers between an ETG with a central KDC and a lower mass spiral galaxy to study the destruction and the survival of the KDCs. In the last section, I analyse a cosmological simulation of a field galaxy to understand the different processes involved in the formation of these ETGs.

4.1 Early-type galaxy equal mass remergers

[Naab *et al.* 2006b] suggested that mergers of ETGs play an important role in the assembly of massive galaxies. Moreover, [Naab & Ostriker 2009] showed, with a study on stellar populations, that giant ETGs could not be formed only via a merger of disc galaxies. Similar trends have been found with simulations in a cosmological context. [Khochfar & Burkert 2003] have shown that the last major merger of bright present-day ETGs ($M_B \lesssim 21$) was preferentially between bulge-dominated galaxies, while those with $M_B \simeq 20$ have mainly experienced last major mergers between a bulge-dominated and a disc-dominated galaxy. They also indicated that the last major merger was probably dry (see also [Hopkins *et al.* 2007, Khochfar & Silk 2009]).

This section thus introduces binary galaxy mergers of ETGs, or "remergers", with the goal to examine the morphology and kinematics of such remnants. This section is included in the submitted paper Bois et al. (2011).

4.1.1 Sample of galaxy remergers

We have simulated galaxy remergers using the same code as for the resolution study (see Section 2.2). All simulations were performed with this particle-mesh code with a softening length (*i.e.* spatial resolution) of 58 pc. The progenitors we used for this analysis are themselves the remnants of binary disc mergers described in the previous Chapter.

Table 4.1 details the remergers we have performed. We ran simulations for four pairs of progenitors with different orbital configurations (**dd**, **dr**, **rd**, **rr**). The first three pairs have been drawn from simulations with three respective initial mass ratios, namely m11, m21g10 and m21g33. In these three cases, the orbital configurations that generated the progenitors were kept the same for a given remerger configuration, *e.g* for a **dd** remerger orbit we always use progenitors coming from rd0 (primary) and rr0 (secondary) orbits. The progenitors for the fourth pair (fourth remerger set) are m21g10 and a spiral.

4.1.2 Towards the round fast rotators

Fig. 4.1 presents the $\lambda_R - \epsilon$ diagram for the remergers, the four subplots correspond to the four different types of remergers (rem2x11, rem2x21g10, rem2x21g33, rem21g10+S) and the four colours in each subplots corresponding to the orbit of remerging (**dd**, **dr**, **rd**, **rr**). From the results of binary galaxy disc

Name	Orbit(1)	Progenitors(2)	Prog Type(3)
rem2x11	dd	rd0 - rr0	Slow - Slow
rem2x11	dr	rrim - ddip	Slow - Fast
rem2x11	rd	rrVp - ddVm	Slow - Fast
rem2x11	rr	rd0 - dd0	Slow - Fast
rem2x21g10	dd	rd0 - rr0	Slow - Slow
rem2x21g10	dr	rrim - ddip	Slow - Fast
rem2x21g10	rd	rrVp - ddVm	Slow - Fast
rem2x21g10	rr	rd0 - dd0	Slow - Fast
rem2x21g33	dd	rd0 - rr0	Slow - Slow
rem2x21g33	dr	rrim - ddip	Slow - Fast
rem2x21g33	rd	rrVp - ddVm	Slow - Fast
rem2x21g33	rr	rd0 - dd0	Slow - Fast
rem21g10+S	dd	rr0 - S	Slow - Fast
rem21g10+S	dr	rdim - S	Slow - Fast
rem21g10+S	rd	rdVp - S	Slow - Fast
rem21g10+S	rr	dd0 - S	Fast - Fast

Table 4.1: Details of the characteristics of the remergers: (1) Spin of the progenitors with respect to the orbital angular momentum, (2) Galaxy remnants of binary merger of spirals as progenitors for the remerger, (3) Slow/Fast classification from Section 3.3.1

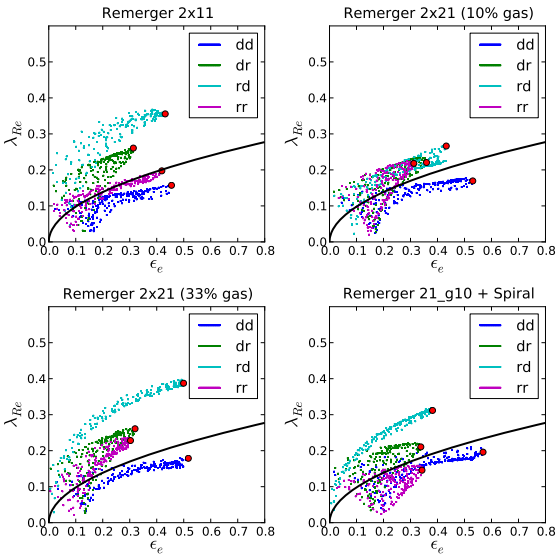

Figure 4.1: $\lambda_R - \epsilon$ diagram for all projections for all simulations of remergers. The 4 panels represents the 4 different remergers, the four colours in each subplot correspond to the orbit of remerging (**dd**, **dr**, **rd**, **rr**)

mergers (see Section 3.3.1), we could presume that the **rr** orbit would produce the slowest rotators of this sample of remergers. In fact, the **dd** cases are the ones to produce the slowest systems for the four different types of remergers. In the **dd** cases of galaxy remergers, both progenitors are slow rotators and hold a KDC. The progenitors acquire angular momentum from the orbit, resulting in merged galaxies with large-scale rotation, and the KDCs have been destroyed. The remnant is classified as a slow rotator but is very close to the dividing line separating slow and fast rotators. The remnant does not present any sign of a KDC and has its photometric and kinematic axis aligned. Velocity maps of all remerger remnants are shown in Fig. 4.2 to 4.5 in the Appendix. In the other cases (**dr**, **rd**, **rr**), the main progenitor is a slow rotator with a KDC and the companion is a fast rotator. During the merger, the main progenitor – with no global rotation – acquires some angular momentum from the orbit while the companion – similar to the behaviour of the spiral Sb progenitor – keeps the initial orientation of its spin, the contribution of which determines and dominates the final spin of the remnant. None of these remergers exhibit a stellar KDC: the KDCs which were present in the progenitors have been destroyed and none are created during the merger. The final remnants of these remergers are rounder than binary disc merger remnants

and all have regular kinematics. As mentioned, a few of these (mostly the **dd**) lie just below the limit between the slow and fast rotators, emphasising the potential small overlap between the two families ([Emsellem *et al.* 2011]).

As seen in our sample of galaxy remergers, and in agreement with the results of [Di Matteo *et al.* 2009]: slow or non rotating galaxies can gain central angular momentum through mergers via a transfer of the orbital angular momentum and start to rotate, destroying the initial KDC. The final state of a merger remnant is the combination of internal+orbital angular momentum: starting with one or two slow rotators can thus leads to a rotating merger remnant. To form a round slow rotator via ETG mergers, one should need two fast rotators on a favourable (*e.g* **rr**) orbit. Repeated minor mergers may preserve the initial KDC of the initial ETG and heat the external parts of the galaxy [Bournaud *et al.* 2007, Qu *et al.* 2010]: this could end up with a round slow rotator, this scenario is tested in the next section.

Appendix: Velocity fields and λ_R profiles

All simulations used for this study are listed here. For each simulation, an edge-on view of the velocity field (with the iso-magnitude contours in black) and its associated λ_R profile are plotted. The simulations are classified in this way:

- A figure corresponds to remergers of two remnants of binary mergers with the same initial mass ratio, *e.g* Fig. 4.2 shows the remergers of two remnants of binary mergers of mass ratio 1:1.
- The four subpanels of a figure correspond to the four different orbit of merging (**dd**, **dr**, **rd** or **rr**)
- The label of the simulation (*e.g* rem21g10+Sdd) and the velocity cut are noted in the projected velocity maps.

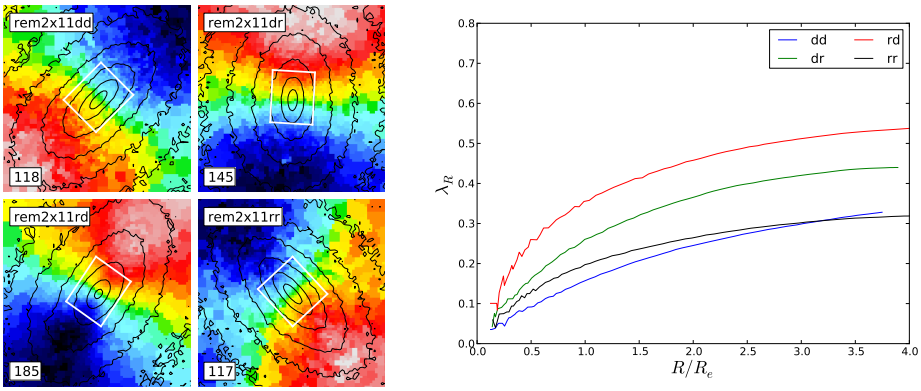

Figure 4.2: **Left:** Edge-on projection of the velocity field for remergers of two remnants of binary mergers of mass ratio 1:1. The black lines correspond to the iso-magnitude contours. The different initial angular momentum spins and velocity cuts are noted in the sub-panels. The field of view is 15×15 kpc^2. The white rectangle indicates a typical field covered by the instrument SAURON and corresponds to a field of $41'' \times 33''$ for a galaxy at a distance of 20 Mpc, its orientation follows the photometric position angle taken at $3R_e$. **Right:** The corresponding λ_R profiles as a function of the radius R divided by the effective radius R_e of the edge-on projection.

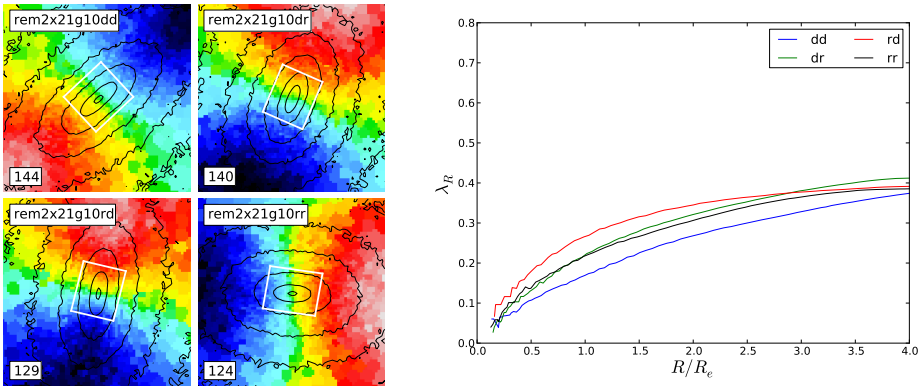

Figure 4.3: Same as Fig. 4.2 for remergers of two remnants of binary mergers of mass ratio 2:1 with 10 per cent of gas.

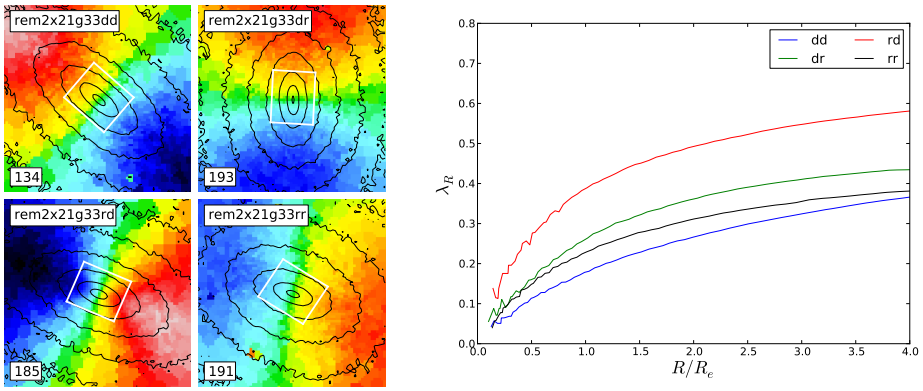

Figure 4.4: Same as Fig. 4.2 for remergers of two remnants of binary mergers of mass ratio 2:1 with 33 per cent of gas.

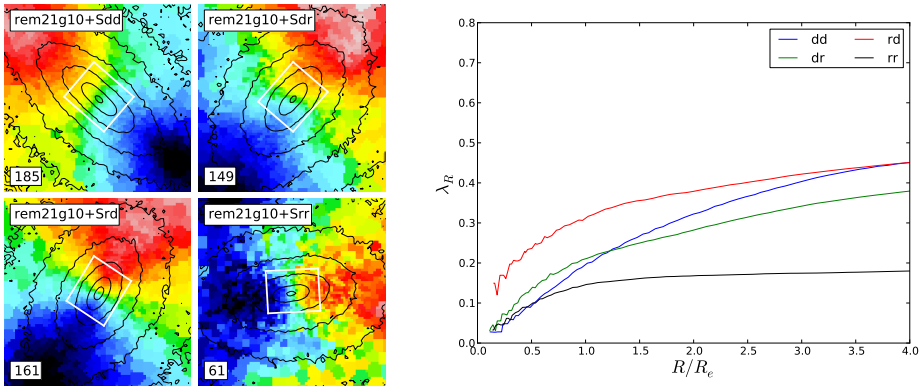

Figure 4.5: Same as Fig. 4.2 for remergers between a remnant of binary mergers of mass ratio 2:1 with 10 per cent of gas and a spiral galaxy.

4.2 Destruction and survival of KDC

We have seen in the previous section that a major remerger (*i.e.* a merger of two equal mass ETGs) destroy the initial KDC present in the ETG progenitor and that none is reform in these relatively gas-poor events. The observed slow rotators with a KDC in the ATLAS^{3D} survey have a low intrinsic ellipticity (with $\epsilon < 0.4$, [Emsellem *et al.* 2011]) and our sample of binary (re)mergers can not account for these galaxies (see also section 5.2). Slow rotators could therefore be the result of a single major merger but then with significantly more violent initial conditions (*e.g.* with a very small impact parameter, Duc et al. 2011, *in prep*) or must have experienced further interactions: a sequence of small satellite mergers may produce rounder remnants and at the same time preserve the KDCs. Such accretion of low-mass objects should be much more frequent than major mergers and are therefore expected (see *e.g.* [Khochfar & Silk 2006, Naab *et al.* 2007, Bournaud *et al.* 2007, Genel *et al.* 2008, Naab *et al.* 2009, Genel *et al.* 2010, Hopkins *et al.* 2010, Oser *et al.* 2010, Qu *et al.* 2010, Abadi *et al.* 2010], ΛCDM models).

In this section, we test the impact of a merger of a small spiral galaxy (with mass ratios from 5:1 to 15:1) on a previously simulated slow rotator holding a KDC. The simulations have been made using the previous described code (see Section 2.2), using the same spatial resolution of 58 pc. The first galaxy – holding the KDC – used for these simulations is always the same: the *so-called* m11rr0 (see Section 3.3). The second progenitor is typical for a spiral galaxy and has been simulated at four different mass ratios: 5:1 (*i.e.* the spiral is 5 times lighter than the slow rotator), 8:1, 12:1 and 15:1. Each different mass ratios have been simulated on three different initial conditions: the previously called **dd**, **dr** and **rr** orbits, leading to 12 mergers. The spin of the progenitor with the KDC (*i.e.* two counter-rotating components) is defined according to the rotation at large radius. The spirals are pure collisionless galaxies (*i.e.* without gas): in this way, we directly test if a KDC can survive to violent relaxation. If the initial KDC is destroyed, we avoid the possible process of re-formation of a new KDC dominated by the recently formed stars. Similarly to the study on binary mergers (see Section 3.2.2), we then analyse the morphology and the kinematics of the merger remnants using the ellipticity and the λ_R parameter, and we visually inspect the velocity maps to see if the initial KDC has survived or not the merger.

The $\lambda_R - \epsilon$ diagram for these simulations is shown in Fig. 4.6. We first see that the remnants coming from the **dd** and **dr** orbits are very similar at all mass

ratios. They have λ_R values higher than the progenitor at mass ratios 5:1 and 8:1, slightly higher at mass ratio 12:1 and somehow similar to the progenitor at mass ratio 15:1. However, the angular momentum added in the remnants remains small and they are all classified as slow rotators. The ellipticity of the **dd** and **dr** remnants is similar to the one of the progenitor at the four different mass ratios. Contrarily to these orbits, the **rr** merger remnants have λ_R values and ellipticities lower than the progenitor at all mass ratios and are therefore still classified as slow rotators. In the range of mass ratios of 5:1 to 15:1, we then do not see any trend with the mass of the spiral progenitor but we see a clear trend with the orbit of merging.

This result is confirmed by looking at the velocity fields of the merger remnants in Fig. 4.7. This figure shows the 2D velocity maps of the edge-on projection of the remerger remnants and the contribution in the remnant of the stars coming from the initial galaxy with the KDC and the spiral progenitor (similarly to Fig. 3.9). We can make the following statements:

- At each mass ratio, the remnants of the **dd** and **dr** orbits are nearly identical. In these remnants, we do not see any KDC in the remnants. The KDC is not "hidden" under the rotation pattern of the spiral galaxy but physically destroyed: there is no trace of it in the contribution of the ETG progenitor.

- In the **dd** and **dr** initial conditions, the spiral galaxy had different spin axis. But in the merger remnants of these orbits, the spiral contribution has the same angular momentum orientation. We thus confirm what we stated in Section 3.3.2: the spiral is entirely disrupted during the merging event and will adopt part of the orbital angular momentum and its sign.

- At all mass ratios, the remnants of the **rr** orbits exhibit a KDC: the KDC of the initial slow rotator has survived the merger. It still can be observed in the contribution of the initial slow rotator.

- Surprisingly, in this **rr** configuration, the spiral contribution ends up with the same angular momentum vector than (the outer part of) the initial slow rotator. They both started with a retrograde spin and, according to Section 3.3.2, the spiral should have adopted the direct spin of the orbit.

This study on the destruction/survival of the KDC in slow rotators is only starting with these 12 simulations. With this sample in hand, some results remain not understood but we already have some hints about the survival of the KDC via

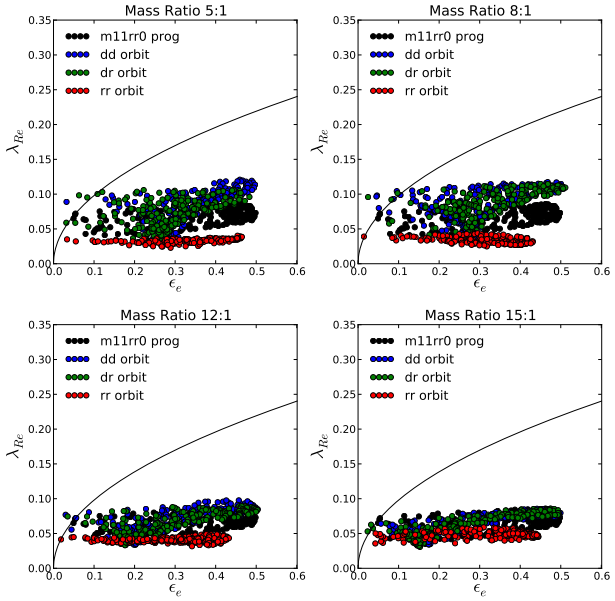

Figure 4.6: $\lambda_R - \epsilon$ diagram for the remnants of a remerger between a galaxy with a KDC and a small spiral galaxy. Each subplot show a different mass ratio (top left: mass 5:1, top right: 8:1, bottom left: 12:1, bottom right: 15:1). The black points show the initial galaxy with the KDC, the blue (*resp.* green, red) points show the merger remnant of the **dd** (*resp.* **dr**, **rr**) initial configuration.

minor mergers: mass ratios in the range from 5:1 to 15:1 do not seem to matter much and the orbit of merging of the spiral progenitor appears important. However, our sample of simulations is too small and there are many open questions: what does role the gas play ? What about larger mass ratios (20:1, 30:1) ? Is the impact parameter important ? What about simultaneous minor mergers ? These questions may be solved with a larger sample of simulations covering a larger parameter space of initial conditions.

4.3 Summary on galaxy remergers

In this Chapter, I have studied numerical simulations of multiple galaxy mergers. Firstly, we have simulated equal-mass ETG remergers with the goal to understand the formation of the most massive slow rotators. With a sample of 16 major remergers, we found that all of the remnants present a clear rotation pattern and are classified as fast rotators (or very close to the boundary of the slow/fast

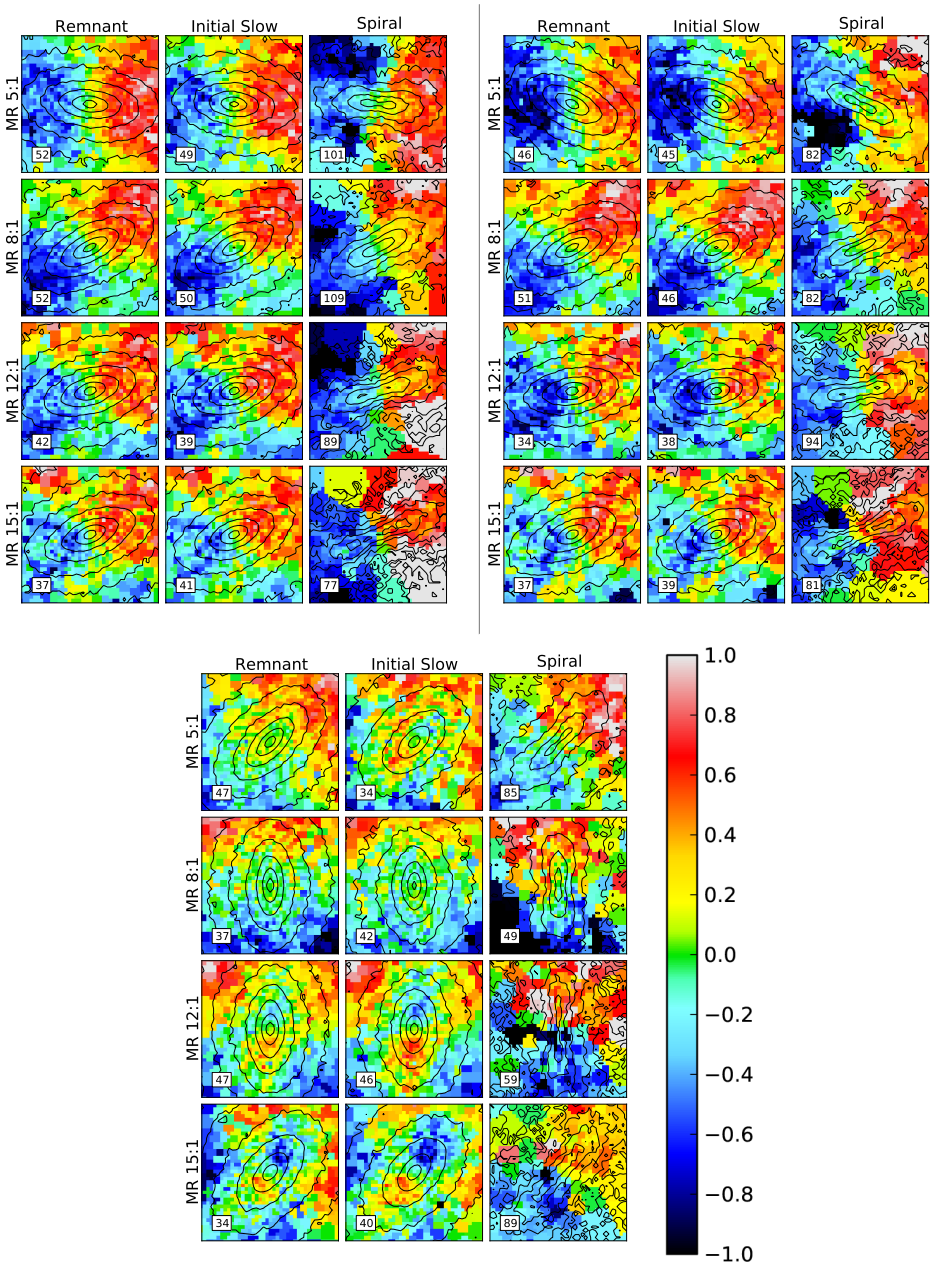

Figure 4.7: The three panels represent the three different initial orbits, top left: **dd** orbits; top right: **dr** orbits, bottom: **rr** orbits. On each panel: the left column shows the 2D velocity map of the remnants, the middle column shows the contribution of the stars coming from the galaxy with the KDC, the right column shows the contribution of the stars coming from the spiral galaxy (similarly to Fig. 3.9). One each panel: the lines correspond to different mass ratios, from 5:1 (top) to 15:1 (bottom). The field of view of the 2D maps is 8×8 kpc^2. The cuts in velocity are written in the respective maps. The field of view is 8×8 kpc^2. The black lines correspond to the iso-magnitude contours.

families). During the remergers, the KDCs in the initial ETG progenitors have been destroyed and none have been re-formed. Due to the transfer of angular momentum from the orbit to the galaxies, initial slow rotators started to rotate and so do the remnants.

Secondly, we have simulated minor remergers (*i.e.* a remerger between an ETG and a smaller spiral companion) with the goal to determine for which conditions the initial KDC of an ETG can survive a merger. We have then simulated 12 minor remergers with four different mass ratios and three different initial conditions (varying the orientation of the spins of the progenitors). We found that if the spin of the initial ETG is parallel to the spin of the orbit, the KDC is destroyed while if the spin of the initial ETG is anti-parallel to the spin of the orbit, the KDC is preserved. The mass ratio does not seem to influence significantly the resulting remnant. However, these results should not be taken at face value: we still need to understand the different behaviours observed in these simulations.

To clearly understand how to form the most massive ETGs with a KDC, a larger sample of simulations is needed. However, the parameter space of initial conditions is very (and maybe too) large. Starting from our sample of 16+12 simulations, we can imagine to run other simulations to restrict the space of parameters:

- A major remerger between two slow rotating ETGs leads to a fast rotator remnant due to the transfer of orbital angular momentum in internal angular momentum. If the orbital angular momentum is smaller, with *e.g.* a smaller impact parameter, the remnant should gain less rotation and may be ends up as a slow rotator, preserving its initial KDC.

- Two spiral galaxies on a retrograde orbit can produce a slow rotating ETG with a KDC. Is this possible with two fast rotating ETGs as progenitors ?

- A KDC can survive to a minor remerger, could it survive to several minor ones ?

- A KDC can also be destroyed via minor remergers. This is also due to the transfer of orbital to internal angular momentum. We also know, from cosmological simulations, that minor mergers can occur simultaneously: if two smaller galaxies interact with the slow rotating ETG on different orbits, how efficient is this transfer of angular momentum ?

- The presence of gas during a minor remerger can also influence the final

state of the remnant. As seen in the study of the resolution in galaxy mergers (see Section 2.2), the gas can form stellar clusters which help to evacuate the angular momentum and form slow rotating ETGs.

To apprehend the formation history of the massive ETGs, we can also use an other method. Cosmological simulations follow the time evolution of a galaxy from high redshifts to nowadays. Selecting an ETG at $z = 0$ and tracing its history of merging and interactions would help us to understand its formation processes. I present in the next section the analysis of such a cosmological simulation.

4.4 Zoom on a cosmological simulation

We have so far simulated mergers in an "idealized" view of the Universe: two relaxed galaxies merging on a non disturbed orbit. As already mentioned, these idealized simulations are a powerful tool to constrain physical processes involved in galaxy mergers, as *e.g.* the formation, destruction and survival of KDCs as in this manuscript. Real massive galaxies are known to have experienced many interactions through the ages (see *e.g.* [Naab *et al.* 2007]) and simulating their full cosmological history of interactions is essential to understand their formation.

Besides the work made on simulations of binary mergers, I have analysed one numerical simulation of galaxy formation in a cosmological context made by Marie Martig. I will first briefly described the new technique of simulation she developed during her PhD. thesis, and then describe the simulation and their associated results.

4.4.1 Re-simulating at higher resolution

To take into account the full cosmological context of the galaxies, we need to simulate a big part of the Universe. When using such a large simulation box, the mass and spatial resolutions are very low compared to the resolution needed to properly resolve galaxy-galaxy interactions. But to study the specific formation of a given galaxy, the analysis of the full volume of the box is not required. "Zoom simulations" (called also re-simulations) have been developed for that purpose: it consists of re-simulating at high resolution a sub-volume of the box centred on the studied galaxy while keeping the rest at the initial resolution (see *e.g.* [Semelin & Combes 2005, Naab *et al.* 2007]). The drawback of this technique is that all of the galaxies interacting with the studied one have to be encompassed

within the higher resolution sub-volume: this can lead to a very large high resolution sub-volume and significantly increase the computing resources needed for the zoom simulation.

[Martig *et al.* 2009] upgraded a recent technique for zoom simulations ([Kazantzidis *et al.* 2008, Read *et al.* 2008, Villalobos & Helmi 2008]): it consists of recording the full history of interactions of the studied galaxy (including mergers and gas accretion) with the low-resolution simulation and to re-simulate this history at higher resolution. The first low resolution simulation only includes dark matter (DM) particles: when a sub-halo of DM crosses a sphere of a given radius centred on the main halo (*i.e* the halo of the studied galaxy), information (such as the crossing time and mass, velocity, spin of the sub halo) are recorded. The re-simulation at high resolution is then launched using the information of the low resolution simulation, with the DM sub-halos being replaced by DM, star and gas particles. This technique enables to re-simulate a fixed sub-volume of the Universe as the incoming galaxies – which could be far from the studied galaxy at the beginning of the simulation – are created only when they should cross the sphere centred on the studied galaxy. It helps then to save computing resources and/or enables you to increase the resolution of the zoom.

4.4.2 Simulation and results

The re-simulation technique described above has been used to study a quenching process for star formation, called morphological quenching, in an early-type galaxy [Martig *et al.* 2009]. We here study the time evolution of the morphology and kinematics of the corresponding simulated galaxy.

The code used for the re-simulation is the particle mesh code with the sticky particles scheme described in Section 2.2 with a softening length of 130 pc. The DM halo has an initial mass of $2\times10^{11}M_{\odot}$ at $z = 2$, its final mass at $z = 0$ being $1.4\times10^{12}M_{\odot}$. The studied galaxy is chosen to be in a relatively low density environment and does not belong to a rich group or cluster of galaxies. The formation history of this galaxy can be decoupled in three phases: (1) between $z \sim 2$ and $z = 1$, an intense period of minor mergers (with four spiral progenitors having a mass ratio between 4:1 to 10:1); (2) between $z = 1$ and $z \sim 0.2$, a phase of smooth gas accretion from cosmic filaments without merger during which the morphological quenching occurs; (3) a major merger at $z = 0.2$ with a galaxy having a mass ratio of 1.5:1, shortly preceded by an intense peak of diffuse gas accretion. For more details, the reader should refer to [Martig *et al.* 2009].

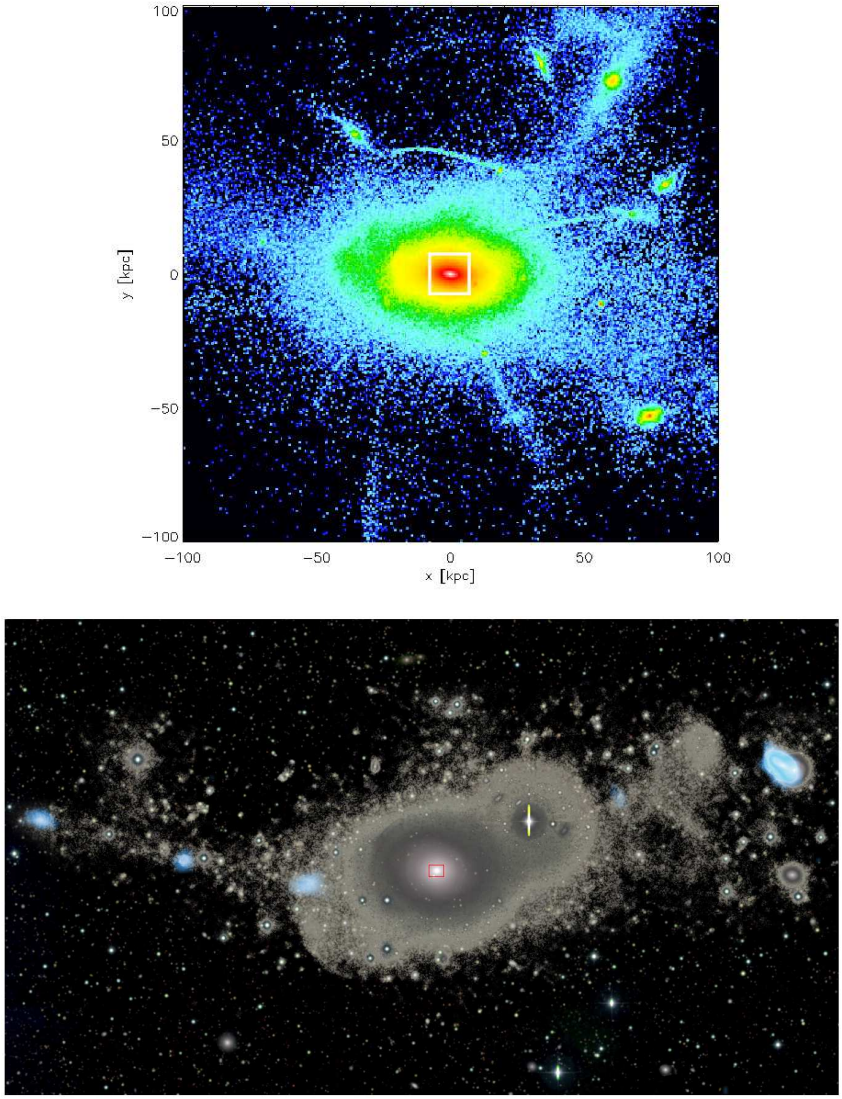

Figure 4.8: Top: Large field of view (200 × 200 kpc^2) of the intensity map of the cosmological re-simulation at t=5.6 Gyr (z ∼ 1). The analysis of the morphology and the kinematics is performed in the white square of 15 × 15 kpc^2. Bottom: (extracted from Duc et al. 2011, ATLAS^{3D} paper *in prep*) CFHT/MegaCam g-band surface brightness map of NGC 5557. A true colour (composite of the g, r and i bands) image is superimposed in regions of high-surface brightness. The distribution of the HI gas mapped by the WSRT is overlaid in blue. The red rectangle corresponds to the SAURON field of view.

For this galaxy, we have here studied the previously mentioned morphological and kinematical parameters (the ellipticity ϵ, the λ_R value, the effective radius R_e, see Section 3.2.2) on 2D projected maps as a function of time. We have only projected the stellar particles within a sphere of 40 kpc centred on the studied galaxy to avoid the contamination of particles of spiral progenitors at large radii. However if a progenitor is very close to the main galaxy, the 2D intensity, velocity and velocity dispersion maps are "contaminated": the values of ϵ, λ_R, R_e are then meaningless. The analysis is conducted up to 7.5 kpc which corresponds to $6R_e$ at $z = 2$ and $3R_e$ at $z = 0$, Fig. 4.8 shows a large field of view (200×200 kpc^2) of the intensity map of the cosmological re-simulation at t=5.6 Gyr ($z \sim 1$) and the white square corresponds to the field of view in which the analysis is performed. Each snapshot are separated by 100 Myr and we therefore probe all the different phases of formation of the main galaxy.

Fig. 4.9 shows the time evolution of the parameters described above (ϵ, λ_R and R_e) as well as the time evolution of the stellar and gaseous mass and the Star Formation Rate (SFR) integrated in a sphere of 25 kpc around the main galaxy. The intensity and velocity fields of the edge-on projection of the points labelled from 1 to 10 are shown in Fig. 4.10. Projection P1 corresponds to the initial spiral at $z = 2$, P2 and P3 are during the minor mergers period, P4 to P7 show the phase of morphological quenching (without merger), P8 and P9 represent the galaxy after the major merger event and P10 corresponds to the final galaxy at $z = 0$.

The initial galaxy is a spiral galaxy with a stellar mass of 3×10^{10}M$_\odot$. During the first period of minor mergers (from P1 to P4), its stellar mass grows by a factor of 3.7 and the galaxy resembles more an ETG: its intrinsic ellipticity monotonically decreases from 0.83 at P1 to 0.5 at P4. The transformation of a spiral into an ETG via multiple minor mergers was previously shown in [Bournaud *et al.* 2007] with "idealized" simulations. We show here that this scenario is confirmed, at least in this specific case, in the context of cosmological simulations. The λ_R value also drops from 0.44 at P1 to 0.05 at P3 after several minor and intermediate mergers, but it starts to increase again between P3 and P4 to reach a value of $\lambda_R = 0.18$ with other minor mergers. This confirms the results of [Qu *et al.* 2010]: they show that the internal angular momentum of the primary galaxy, and then its λ_R value, can increase or decrease via minor mergers depending on the relative orientation of the orbital spin vectors. From P4 to P7, *i.e.* during the quiet phase of smooth accretion of gas, the values of ϵ and λ_R slightly increase: as seen in Fig. 4.10, this

is due to the formation of a disc of newly formed stars created via the accretion of gas. This disc of new stars dominates the velocity map of the galaxy but not much the mass profile and then have a very small influence on the morphological and kinematical properties of the galaxy. After P7, it is hard to distinguish the role of the major merger and the intense peak of gas accretion: the ellipticity of the galaxy does not change and the λ_R value drops at P8 but increases after until P10. At P8 and P9, the velocity maps of the galaxy show both rotation along and perpendicular to the photometric position angle (PA_{phot}), while at P10 the rotation is only along PA_{phot}. However, one can see a small sub-structure perpendicular to PA_{phot}: this may be interpreted as a KDC. However, such a structure is not observed in the ATLAS^{3D} galaxies and may be only transitional.

The final galaxy is flat, which is consistent with the ellipticity observed for field galaxies. It is classified as a slow rotator, but it is closed to the limit defining the fast and slow classes. Moreover, the λ_R profile as a function of time is still rising at the end of the simulation and the galaxy may cross the limit to become a fast rotator after the transitional structure vanishes.

The analysis of this simulation is not yet complete. The next step will be to relate the orbits of merging of the companion galaxies to the evolution of the λ_R parameter of the main galaxy. Accordingly to the results showed in the previous Sections (but see also *e.g.* [Bournaud *et al.* 2007, Qu *et al.* 2010]), galaxy mergers – both minor and major – can obviously decrease the internal angular momentum of the main galaxy but can also increase it. If such variations are also found to be related to the orbits of merging in this cosmological simulation, it would confirm the need for understanding how exactly the total (internal+orbital) angular momentum of interacting systems is redistributed during a merger.

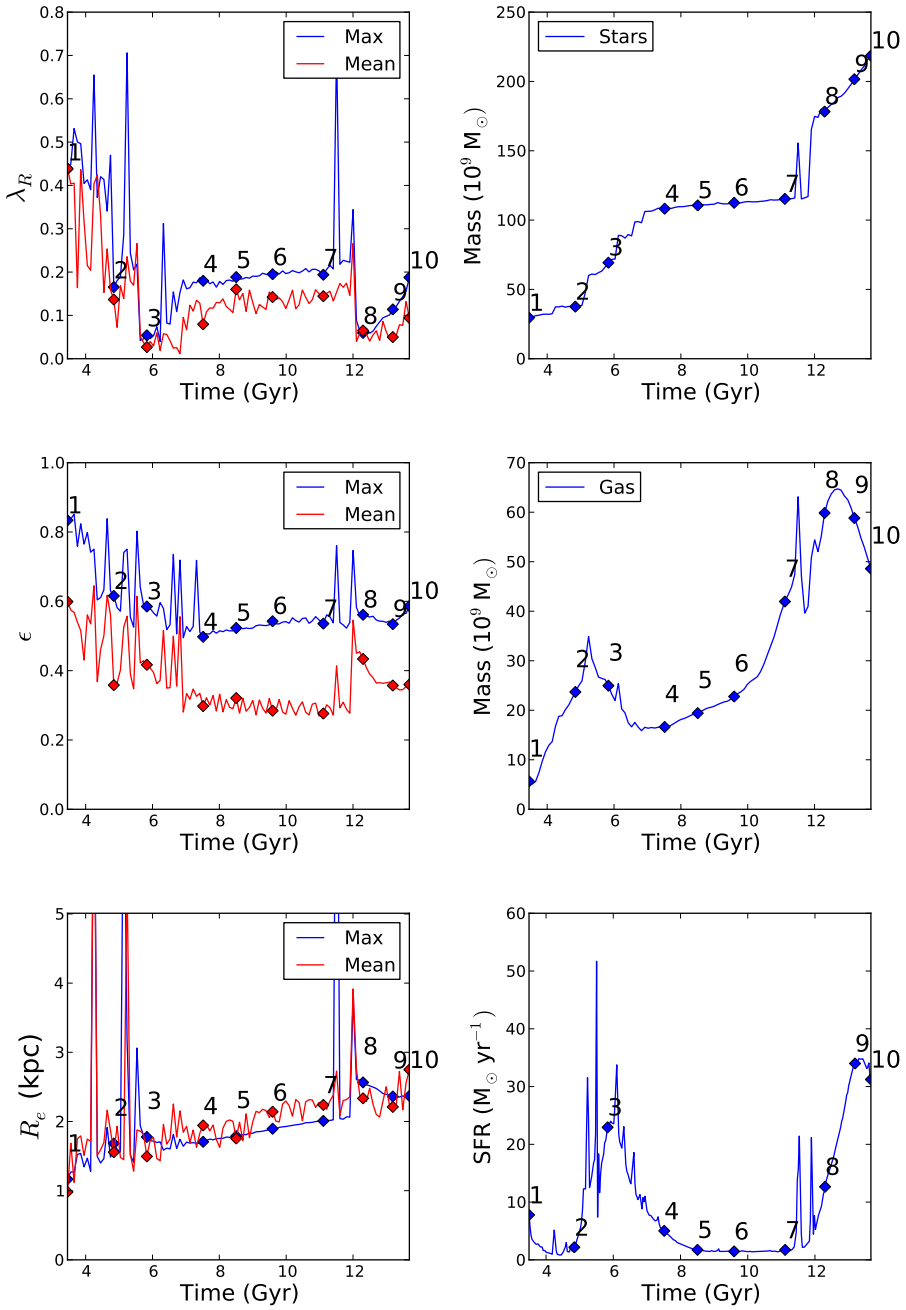

Figure 4.9: Time evolution of the λ_R parameter (top left), the ellipticity ϵ (middle left), the effective radius R_e (bottom left), stellar mass (top right), gaseous mass (middle right), Star Formation Rate (bottom right). The left panels show the time evolution of the parameters for a projection which maximizes the ellipticity (*i.e.* the edge-on projection, in blue) and for a mean projection (in red). The intensity and velocity fields of the edge-on projection of the points labelled from 1 to 10 are shown in Fig. 4.10. The time evolution of the stellar and gaseous mass and the SFR are integrated in a sphere of 25 kpc around the main galaxy.

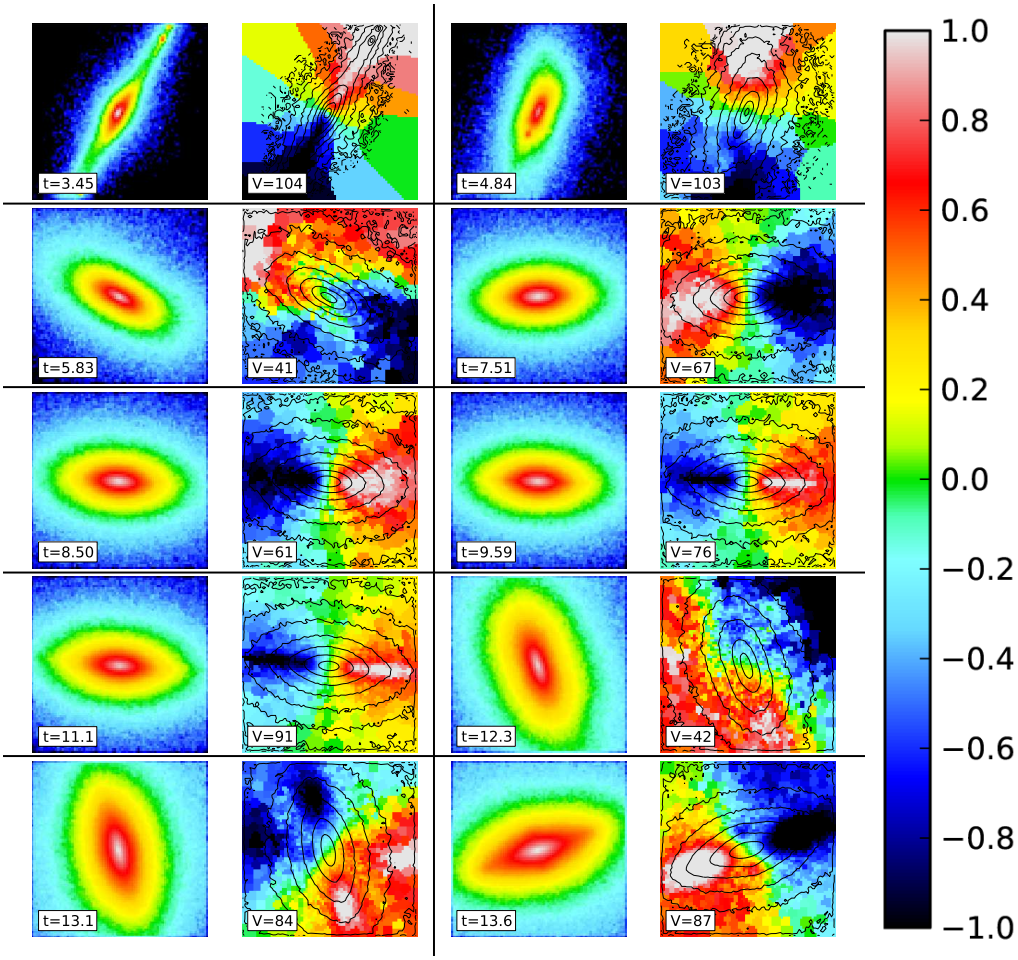

Figure 4.10: Intensity and velocity fields at the 10 different epochs of the cosmological re-simulation spotted in Fig. 4.9. The first snapshot (top left) corresponds to the start of the simulation at t = 3.45 Gyr ($z \simeq 2$), the last snapshot (bottom right) corresponds to the end of the simulation at t = 13.6 Gyr (z = 0). The time of a snapshot is written in the intensity field. The cuts in the intensity are the same for the different maps, the iso-magnitude contours are equally spaced in magnitude and are similar for all maps. The maximum velocity V_{max} is written in the velocity maps: the colorbar goes from -V_{max} to +V_{max}. The field of view is 15×15 kpc^2.

Chapter 5

Properties of ETGs & Comparison with observations

Contents

In the previous chapters, I have analysed the intrinsic properties of our simulated sample of merger remnants. These idealised simulations are useful to understand the formation processes of the fast and slow rotators and the associated sub-structures like the KDCs. Despite the fact that we do not simulate the cosmological context of their formation (but see previous Section), it could be interesting to test the relevance of our sample with respect to real galaxies. In this Chapter, I therefore make a direct comparison between our simulated (re)merger remnants and the 260 ATLAS^{3D} galaxies. These observed galaxies are in the local Universe, all within 42 Mpc: with the integral field spectograph `SAURON` it is therefore possible to build 2D-maps of these galaxies, to probe their morphology and kinematics up to 1 R_e.

In the first section of this chapter, I describe the sample of the 260 ATLAS^{3D} galaxies. In the second section, I compare the two simulated and observed samples of galaxies using the $\lambda_R - \epsilon$ diagram and the distribution of alignments between the photometric and kinematic axes.

In a last section, I show an attempt of implementing stellar populations in our sample of simulated remnants. I present the motivation for this study and I show the first results together with a comparison with the observed properties of the 48 SAURON galaxies.

5.1 ATLAS^{3D} sample of ETGs

The ATLAS^{3D} survey is a volume-limited sample of 260 ETGs. It consists of nearby (D $<$ 42 Mpc) morphologically-selected ETGs extracted from a parent sample of 871 galaxies (from all Hubble type) with stellar mass M $> 6 \times 10^9 M_\odot$. The sample is complete and statistically representative of nearby galaxies. The ETGs of the ATLAS^{3D} sample belong to the "red sequence" with only few objects from the "blue cloud". The sample is described in [Cappellari *et al.* 2010].

[Krajnović *et al.* 2011] and [Emsellem *et al.* 2011] have studied the morphology and the kinematics of the ATLAS^{3D} galaxies. As seen in Section 3.2.2.2, [Emsellem *et al.* 2011] have refined the criterion defining the fast and slow rotator families. In [Krajnović *et al.* 2011], new sub-classes within the slow rotator class have been introduced to separate the different observed features:

Non rotators: they do not show any apparent sign of rotation. These galaxies are the most massive ETGs of the sample.

Galaxies with a KDC: they present an abrupt change in their radial profile of the kinematical position angle ($> 30°$).

NRV : galaxies with Non Regular Velocity pattern but with no noticeable kinematic feature.

2-σ galaxies: they are characterised by two off-centred symmetric dispersion peaks along the major-axis. These galaxies are generally interpreted to have two stellar counter-rotating components (*i.e.* a KDC at 180° away from the outer body).

There is no sub-division within the fast rotators. They span a large range in ellipticities (from 0.05 to 0.9) but they all show a regular apparent rotation and with (or without) small minor-axis kinematic twists ([Krajnović *et al.* 2011, Emsellem *et al.* 2011]).

Using the integral field spectrograph SAURON, it is possible to derive the stellar kinematics together with the stellar absorption line indices (Hβ, Fe5015,

Mgb): it allows to build 2D-maps of these quantities. The analysis of the stellar populations of the ATLAS^{3D} sample of galaxies is on-going and will be published elsewhere (McDermid et al. 2011, Kuntschner et al. 2011). However, with the previous survey SAURON, the stellar populations of 48 local ETGs – which are included in the ATLAS^{3D} sample – have been derived [McDermid *et al.* 2006, Kuntschner *et al.* 2010]. I briefly describe their results in Section 5.3.1.

5.2 Photometric & Kinematic measurements

We here compare directly our sample of merger remnants (binary mergers and ETG remergers) with the sample of the 260 galaxies observed in the context of the ATLAS^{3D} project [Cappellari *et al.* 2010]. For that purpose, we first use the $\lambda_R - \epsilon$ diagram, and also compare the distribution of alignments between the photometric and kinematic axes.

5.2.1 The $\lambda_R - \epsilon$ diagram

Fig. 5.1 shows the $\lambda_R - \epsilon$ diagram for the 260 galaxies of the ATLAS^{3D} sample (extracted from [Emsellem *et al.* 2011]) and presents the distribution of projections for the simulated spiral progenitors, major remerger remnants, and merger remnants of binary disc galaxies. It also presents the distribution of projections for our merger remnants of binary disc galaxies weighted by the probability of the galaxy-galaxy merger rate as a function of the mass ratio in ΛCDM. From [Hopkins *et al.* 2010] for a galaxy of mass 10^{11} $M_\odot$ (*i.e.* with the mass of our main progenitor), if P is the probability of having a 1:1 merger, the probability to have a 2:1 merger (*resp.* 3:1 and 6:1) is $4P$ (*resp.* $6P$ and $9P$). The lower mass ratios are favoured, so does the formation/assembly of fast rotators via a binary galaxy merger.

By looking at where the observed ATLAS^{3D} galaxies and our sample of galaxy mergers lie in such a $\lambda_R - \epsilon$ diagram, we can make a first rough assessment of the relevance of binary disc mergers and remergers for nearby ETGs:

- For high values of λ_R ($\sim$ 0.5 – 0.8), the distribution of ATLAS^{3D} galaxies coincides in fact with the distribution of our progenitors, this has been also pointed out in [Jesseit *et al.* 2009]. These local galaxies often contain a bar and are consistent with disc galaxies. These could be disc galaxies which have evolved via various internal processes –

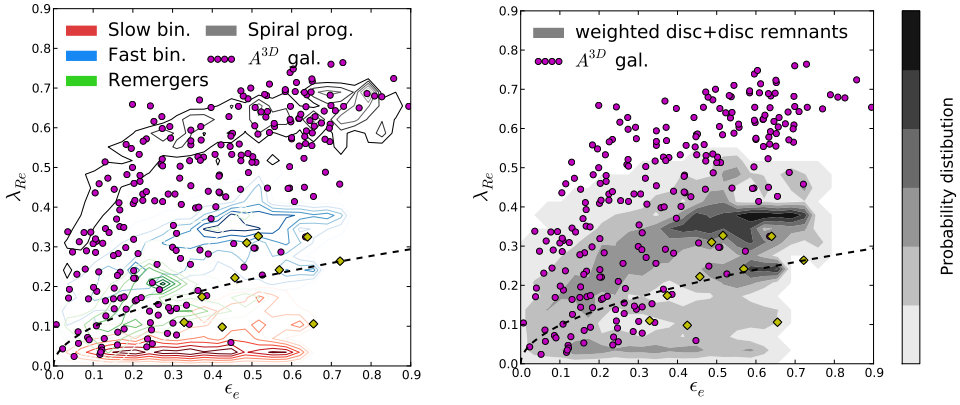

Figure 5.1: $\lambda_R - \epsilon$ diagram for the 260 galaxies of the ATLAS^{3D} sample compared to our simulation sample. The observed galaxies are represented with a magenta dot, the observed 2-σ galaxies with a yellow square. The dashed line corresponds to the limit defining the slow and fast rotators. Left: The contours represent the distribution of projections of the simulated fast rotator disc remnants in blue, slow rotators disc remnants in red, major remerger remnants in green and spiral progenitors in black. Right: The contours represent the distribution of projected remnants (slow+fast) of disc mergers statistically weighted depending on the likelihood of its mass ratio (see text for details).

at high redshift (*e.g.* [Elmegreen *et al.* 2008, Dekel *et al.* 2009]) and/or at low redshift [Athanassoula & Bureau 1999] – and through accretion of gas or very small companions [Toth & Ostriker 1992, Martig & Bournaud 2010, Moster *et al.* 2010].

- For intermediate values of λ_R ($\sim 0.25 - 0.5$), the ATLAS^{3D} galaxies are closer to the fast rotator merger remnants. These observed ETGs could thus be the remnants of a merger between a spiral galaxy and a companion with a mass ratio from 10:1 to 1:1, see *e.g.* [Bendo & Barnes 2000, Cretton *et al.* 2001, Naab & Burkert 2003, Bournaud *et al.* 2005, Naab & Trujillo 2006].

- In the ATLAS^{3D} sample, we find $\sim$ 30 galaxies with $\lambda_R < 0.25$ classified as fast rotators. These galaxies have rather small ellipticities: some of these therefore may be consistent with the remnants of a binary merger of disc galaxies viewed face-on, but this cannot hold for the full set of low λ_R fast rotators. As seen in Fig. 5.1, the result of a major remerger can form a galaxy with a relatively low intrinsic ellipticity and a low λ_R value and can better account for these galaxies. A remnant of a major binary merger of spirals followed by mergers of smaller companions, or the fast evolution of galaxies in groups, see *e.g.* [Konstantopoulos *et al.* 2010] may also lead to a similar output.

- The comparison with the observed slow rotators is less evidential. In the context of the sub-classes of slow rotators defined in [Krajnović *et al.* 2011], we can emphasise the following items. Observed non rotators are among the most massive objects in the ATLAS^{3D} sample ([Cappellari *et al.* 2010, Emsellem *et al.* 2011]) and very probably have a complex merger history [Nieto *et al.* 1991, Tremblay & Merritt 1996], clearly beyond the simple picture provided by the binary mergers described here. Galaxies observed to exhibit KDCs all have apparent $\epsilon < 0.4$: as already emphasised, the slow rotator remnants obtained in our sample of simulations are much too flat comparatively. This implies that only a few of the observed slow rotators could have been simply formed via binary mergers of disc galaxies, and these would in addition need to be viewed at relatively high inclination. Slow rotators could therefore be the result of a single major merger but then with significantly more violent initial conditions (*e.g.* with a very small impact parameter, Duc et al. 2011, *in prep*) or must have experienced further interactions: a sequence of small satellite mergers may produce

rounder remnants and at the same time preserve the KDCs. Such accretion of low-mass objects should be much more frequent than major mergers and are therefore expected, see *e.g.* [Khochfar & Silk 2006, Naab *et al.* 2007, Bournaud *et al.* 2007, Genel *et al.* 2008, Naab *et al.* 2009, Genel *et al.* 2010, Hopkins *et al.* 2010, Oser *et al.* 2010, Qu *et al.* 2010, Abadi *et al.* 2010] and ΛCDM models.

- With our sample of binary mergers of spiral galaxies, we can probably account for the 2-σ galaxies (see next Section).

5.2.2 The 2-σ galaxies

From the galaxies of the ATLAS^{3D} sample, [Krajnović *et al.* 2011] defined the 2-σ galaxies as follow: "*Double σ (2-σ) are found by visually inspecting the velocity dispersion maps. This feature is characterised by two off-centred but symmetric peaks in the velocity dispersion which lie on the major axis of the galaxy*". The velocity and velocity dispersion maps of these observed galaxies are shown in Fig. 5.2 and their positions in the $\lambda_R - \epsilon$ diagram of Fig. 5.1 are indicated with a yellow square. Three 2-σ galaxies are classified as fast rotators, three are clear slow rotators and four lie just at the limit defining the slow and fast classes. They have ellipticities larger than 0.3 and are overall flat. The 2-σ galaxies are interpreted to have two large-scale stellar disc-like counter-rotating components ([Emsellem *et al.* 2011]). Using CO data and numerical simulations of binary mergers, [Crocker *et al.* 2009] have shown that NGC 4550, one of the prototype 2-σ galaxy, may be the result from the co-planar merger of two counter-rotating disc galaxies. Other numerical simulations have studied the formation of counter-rotating components via binary mergers but none have mentioned a correlation with the presence of a double peak in the velocity dispersion profiles [Balcells & Quinn 1990, Hernquist & Barnes 1991, Balcells & González 1998, Barnes 2002, Jesseit *et al.* 2007].

As seen in Section 3.3.2, most of the KDCs in our sample of binary mergers of disc galaxies are only apparent KDC, *i.e.* formed with two counter-rotating discs. We have thus visually inspected the velocity dispersion maps of our slow rotators merger remnants. We have also inspected the remnants of 3:1 mergers formed via two spirals which end-up with two different orientations (i.e **rd** and **rr** orbits as the spin of the smaller progenitor acquires the spin of the orbital angular momentum): these remnants do not have an apparent KDC but may resemble the observed fast rotating 2-σ galaxies.

We show in Fig. 5.3 three merger remnants at mass ratio 1:1, 2:1, 3:1 which

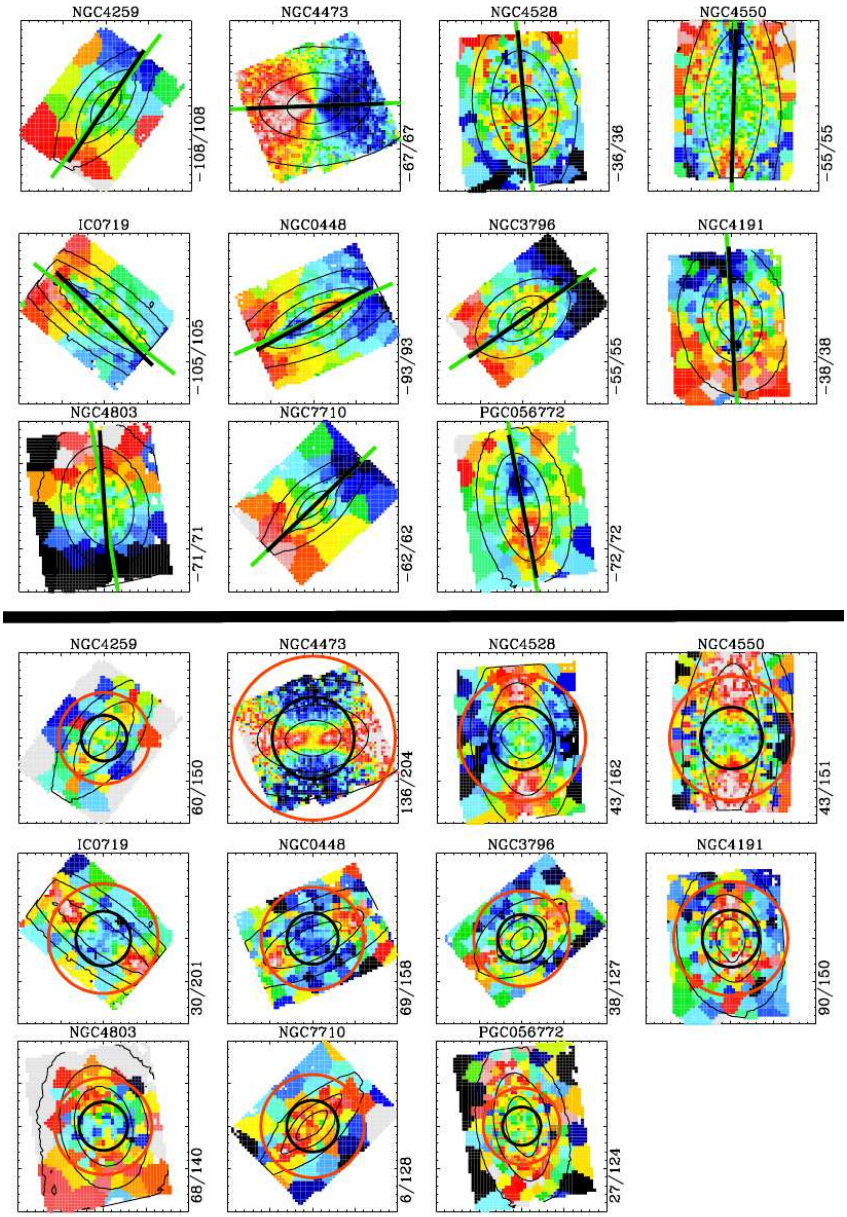

Figure 5.2: Top: Velocity maps of the observed 2-σ galaxies. Contours are isophotes of the surface brightness. North is up and east to the left on each map. Black line is the orientation of the PA_{kin} while the green line (extending beyond the map) is the orientation of the PA_{phot} (see next Section). The numbers on the right side of the each map show the range of the plotted velocities in km s^{-1}. Bottom: Velocity dispersion maps of the observed 2-σ galaxies. Over-plotted circles show one and half the effective radii. Numbers on the right show the range of the plotted velocity dispersions in km s^{-1}.

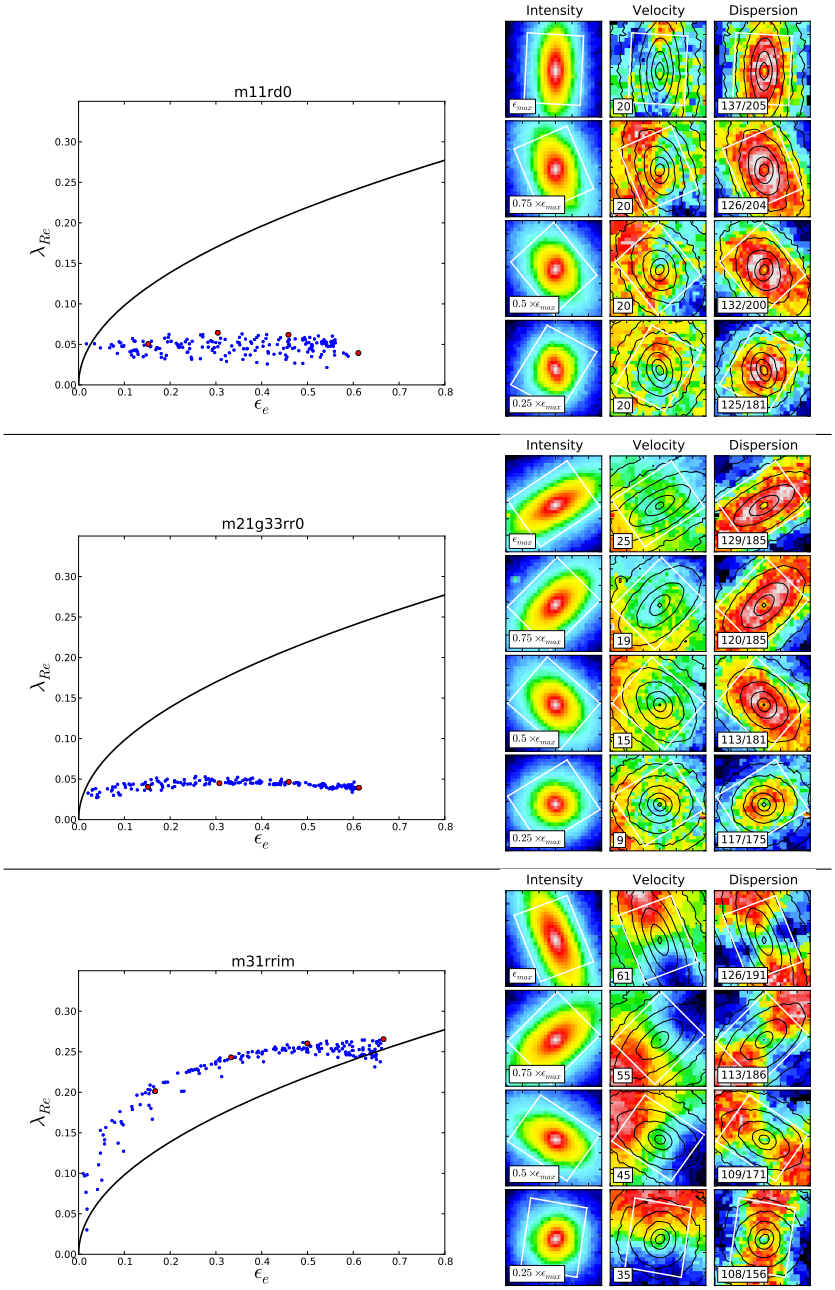

Figure 5.3: Three simulated 2-σ-like galaxies: a 1:1 slow rotator (top), a 2:1 slow rotator (middle) and a 3:1 fast rotator (bottom). The left panels represent the $\lambda_R - \epsilon$ diagram for the 200 projections plotted as blue dots, the red points correspond to the projection with the maximum ellipticity ϵ_{max} and the projections corresponding to $0.75 \times \epsilon_{max}$, $0.5 \times \epsilon_{max}$ and $0.25 \times \epsilon_{max}$. The right panels show the intensity, velocity and velocity dispersion maps of the red point projections. The field of view is 6×6 kpc^2 (6 kpc $\simeq 2.5 R_e$). The white rectangle indicates a typical field covered by the instrument SAURON, its orientation follows the photometric position angle taken at $3R_e$.

could be classified as 2-σ galaxies. The double peak in the velocity dispersion of the 1:1 remnant is aligned with the major axis of the galaxy only for the nearly edge-on projections. The double peak is aligned with the minor axis for more inclined viewing angles. This remnant would therefore be classified as a 2-σ galaxy only if it would be observed relatively edge-on. We thus may miss observed round 2-σ galaxies as the double peak of dispersion would not be aligned with the major axis of the galaxy. In the 2:1 remnant, the double peak in the velocity dispersion is aligned with the major axis of the galaxy for all projections. The 3:1 remnant is a fast rotator but also presents a clear evidence for a double σ peak for all its projections. The velocity and dispersion maps of the 3:1 remnant resemble the ones of NGC 4473: the cuts in V and σ are slightly different but we did not aim to specifically reproduce this observed galaxy.

Our sample of binary mergers is able to reproduce the features observed in the ETGs called 2-σ galaxies. We thus confirm that these galaxies may have been formed through a merger of two counter-rotating spiral galaxies. A more detailed comparison, including *e.g.* $h_{3,4} - V/\sigma$ diagrams, or gas distribution and kinematics, would be required to strengthen this result.

5.2.3 Photometric and kinematic alignments

Based on the [Franx *et al.* 1991] definition, we calculate the kinematic misalignment angle Ψ as the difference between the measured photometric and kinematic position angles taken at three effective radii (see also [Krajnović *et al.* 2011]) as:

$\sin \Psi = |\sin (\mathrm{PA}_{phot} - \mathrm{PA}_{kin})|$.

The measurement of this quantity at large radii minimises the impact of central decoupled structures such as *e.g.* a KDC or a bar. Ψ is defined between two observationally related quantities and it approximates the true kinematic misalignment angle which should be measured between the intrinsic minor axis and the intrinsic angular momentum vector. Ψ can range from 0 to 90° (the use of sin removes additional differences of 180° between PA_{phot} and PA_{kin}).

This analysis has been made for the sample of the 260 ATLAS^{3D} galaxies in [Krajnović *et al.* 2011]. The regular velocity pattern galaxies (*i.e* fast rotators) are mostly found at small Ψ values, and the galaxies with complex kinematic structures (non rotators, NRV, 2-σ and KDC galaxies) often exhibit strong misalignments between the photometry and kinematics.

Our simulations are in good agreements with these observational results. The left panel of Fig. 5.4 shows the histogram of the kinematic misalignment angles

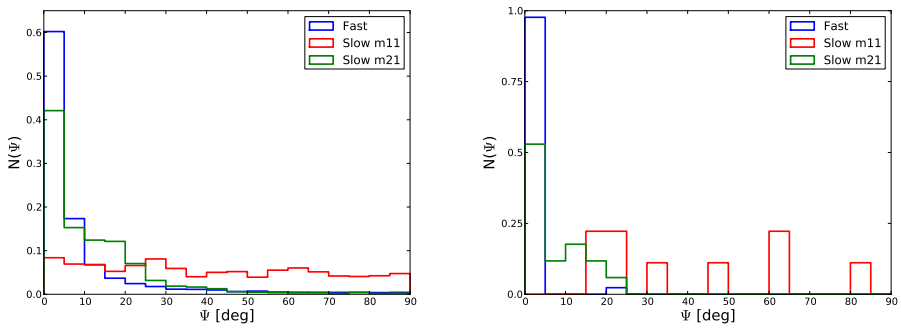

Figure 5.4: Left: Histogram of the kinematic misalignment angle (in degree) for all projections of the merger remnants. The y-axis is normalised to the total number of projections per category: the fast rotators (for mass ratios 1:1 to 6:1) are in blue, the slow rotators of mass ratio 1:1 in red, the slow rotators of mass ratio 2:1 (both 10 and 33 per cent of gas) in green. The errors on Ψ are within a bin size. Right: Same histogram but only for the projections which maximize the ellipticity (edge-on view) of the merger remnants.

for all projections of all binary disc merger remnants. The fast rotators have 60 per cent of their projections in the first bin with $\Psi < 5°$, with another 17 per cent with $5 < \Psi < 10°$, and 88 per cent of the projections have $\Psi < 20°$. The slow rotators for the 2:1 mergers have respectively 42, 15, 82 per cent of their projections in these domains, respectively. The slow rotators associated with 1:1 mergers are distributed homogeneously from 0 to 90°. Our fast rotator remnants should thus be considered as perfectly aligned: the spin axis of the stellar component is the photometric short-axis. The slow rotators associated with 2:1 mergers are also relatively well aligned: the most massive progenitor (the Sb spiral in this study) dominates the velocity rotation, and the galaxy remnant remains flat with a disc-like behaviour. The slow rotators formed in 1:1 mergers show significant misalignments: the two progenitors are contributing to the counter-rotating stellar component which almost cancel any central rotation around the photometric minor-axis. The rotation is then dominated by the kpc-size KDC and by rotation along the photometric minor-axis at larger radii [Hoffman *et al.* 2010]. These results are confirmed when selecting the projections which maximize the ellipticity (*i.e* the edge-on projections) of the merger remnants (see also Fig. 3.15 to 3.19 in Appendix of Chapter 3 for the corresponding velocity maps): the edge-on projections of the fast rotators are always aligned with $\Psi < 5°$ (except for the merger

remnant *m11rrip*), while some 2:1 slow rotators show significant misalignments and all 1:1 slow rotators do.

The same results are found by [Jesseit *et al.* 2009]: they have analysed misalignment angles for the oblate, prolate and triaxial simulated merger remnants described in [Thomas *et al.* 2007]. Their disc-like oblate system is a fast rotator and has most of its projections with $\Psi < 5^\circ$ while the more disturbed prolate and triaxial remnants show misalignments.

5.2.4 Summary

The properties of the fast rotators formed in our simulations are consistent with some observed fast rotators of the ATLAS^{3D} sample. Some of the simulated slow rotators may also be associated with a few observed 2-σ galaxies which present clear evidence of an apparent counter-rotating stellar component. Our simulations cannot, however, account for the other classes of slow rotators which are intrinsically rounder than any of our major merger remnants: these galaxies are generally massive and have certainly a more complex history of formation. To simulate these galaxies, the full cosmological context of their formation history has to be considered, including major merger(s), repeated minor mergers, stellar mass loss and also smooth accretion of gas from the cosmic filaments.

5.3 Stellar populations & the Mgb – V_{esc} relation

5.3.1 Stellar populations of observed ETGs

The morphology and the dynamics of a galaxy are not the only tracers of its formation and evolution, and we can also study its metallicity gradients, abundance ratios, and mean stellar ages. The vast majority of ETGs do not show sign of ongoing star formation: these are thus good indicators of when they could have built their mass. Due to the limitations and the large uncertainties of the first models of stellar populations, early spectroscopic studies did not really achieved detailed dating of the stellar component (see *e.g.* [O'Connell 1980, Rose 1985]). Using the series of hydrogen Balmer lines, [Worthey 1994] has been able to determine with precision the age of stellar populations of ETGs, introducing the Lick/IDS indices (see also [Worthey & Ottaviani 1997]).

Mostly using the Lick/IDS indices, many studies have analysed the stellar populations of local ETGs. The majority of these studies have treated the ETGs as unresolved sources (see *e.g.* [Bernardi *et al.* 2006, Thomas *et al.* 2010] and the

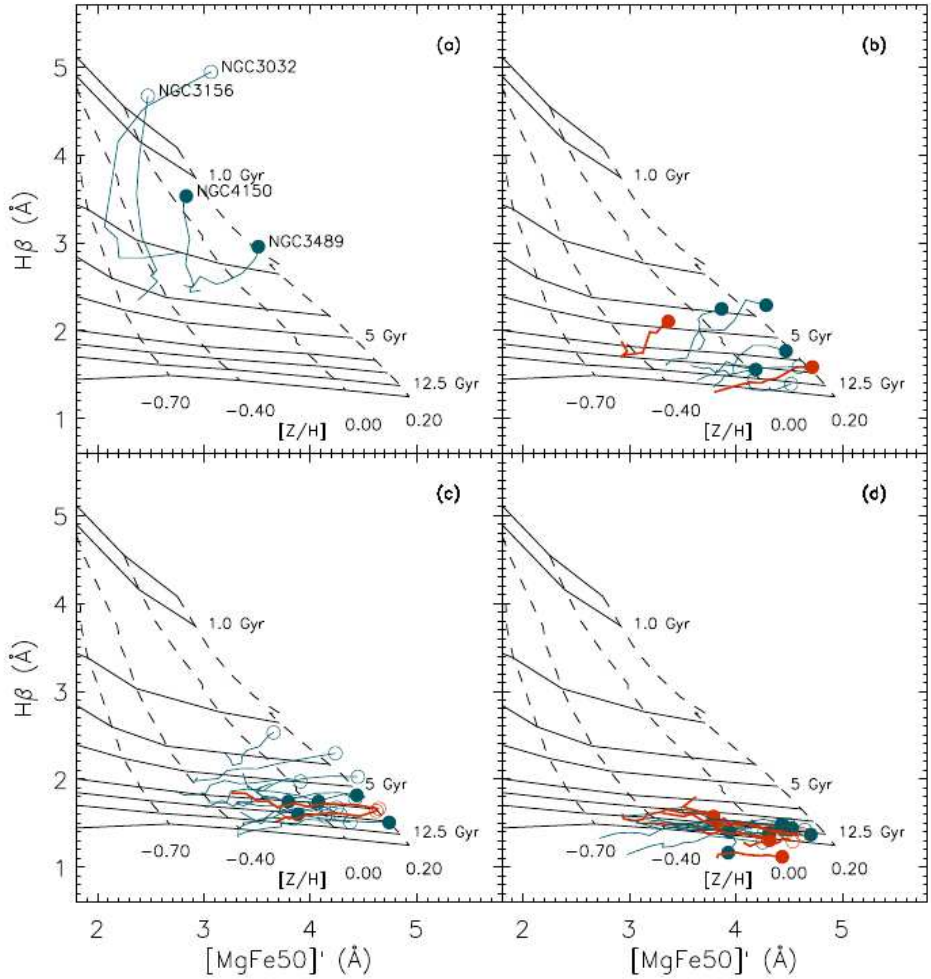

Figure 5.5: (Extracted from [Kuntschner *et al.* 2010]) Age/metallicity diagnostic diagrams for the sample of the early-type galaxies in the SAURON survey. For each galaxy a radial gradient averaged along isophotes is shown. The centre of each galaxy is indicated by a filled circle and open circle for cluster and field galaxies, respectively. The colour indicates whether a galaxy belongs to the fast rotators (blue) or slow rotators (red). Overplotted are stellar population models by [Schiavon 2007]. (a) Galaxies with an extended, recent star-formation episode; (b) galaxies with signs of a central, spatially constrained, region of younger stellar populations; (c) galaxies with milder but spatially extended signs of a younger stellar population; and (d) galaxies consistent with overall old stellar populations.

Sloan Digital Sky Survey [York *et al.* 2000]), while very few have investigated line strength gradients (see *e.g.* [Davies *et al.* 1993, Sánchez-Blázquez *et al.* 2007]). With the recent development of integral field spectrographs, it is now possible to build spatially resolved stellar population 2D maps of local ETGs ([McDermid *et al.* 2006, Chilingarian *et al.* 2009, Pracy *et al.* 2009]). Within the SAURON survey, [Kuntschner *et al.* 2010] have analysed the ages, metallicity and abundance ratio of 48 local ETGs (see Fig. 5.5). With these results in hand, they addressed a possible scenario of formation for the slow and fast rotator classes. The fast rotators can have young (age $<$ 3 Gyr) or intermediate (3 $<$ age $<$ 9 Gyr) stellar populations and thus have experienced periods of secondary star-formation. The slow rotators (often with KDCs) have, in stark contrast, a homogeneously old ($>$ 10 Gyr) stellar population: they did not have much interacted with large gas reservoirs (spiral galaxies, infalling gas from cosmic filaments) although they may have interacted with other collisionless systems (*i.e.* gas poor galaxies).

A study of [Franx & Illingworth 1990] showed that the colour of a galaxy (*i.e.* its metallicity and stellar age) can be related to its local escape velocity V_{esc}. This relation was confirmed by [Davies *et al.* 1993] and [Carollo & Danziger 1994] with the Mg_2 – V_{esc} relation. The interesting point is that this relation is preserved locally (within a galaxy) but also globally (within a sample of galaxies). This suggests that the gravitational potential Φ (which is related to V_{esc}) could be closely linked with the metal enrichment history of galaxies. [Scott *et al.* 2009] have explored the Mgb – V_{esc}, Fe5015 – V_{esc} and Hβ – V_{esc} relations for the 48 galaxies of the SAURON sample. They confirm that the lines indices – V_{esc} relations show a remarkably tight correlation, with the smallest scatter for the Mgb – V_{esc} relation. They did not find any difference between lenticular and elliptical galaxies and no difference between fast and slow rotators. Each galaxy has a different history of formation and thus how the Mgb – V_{esc} relation is preserved through interactions need to be understood.

5.3.2 Implementation in the simulations

Our large sample of galaxy mergers made at high resolution is a robust tool to test the observations, we have therefore decided to implement stellar populations in our galaxies via optical spectra. Our goal is twofold: (1) how spiral galaxies – for which we do not know if they follow the Mgb – V_{esc} relation – produce a merger remnant which lie on that relation; and (2) how mergers of ETGs can preserve the Mgb – V_{esc} relation.

5.3.2.1 Technical part

In the simulations, it is not possible to model a single star with a particle: a particle represents a group of stars and thus a group of different populations of stars. The particle needs to describe the stars with low masses as well as stars with high masses. For that purpose, we assign an Initial Mass Function (IMF) to particles using the Kroupa IMF [Kroupa 2001]: the IMF corresponds to the initial distribution of stars as a function of mass. This Kroupa IMF is similar to the Salpeter IMF [Salpeter 1955] for stars of masses above 0.5 $M_\odot$, but with a decreasing contribution at lower masses.

To implement the stellar populations in the simulations, we have made use of the MILES stellar library for which the spectra of $\sim$ 1000 stars has been obtained [Sánchez-Blázquez *et al.* 2006]. Associated Single Stellar Population (SSP) models have been computed by [Vazdekis *et al.* 2010] covering a large domain of stellar ages and metallicity. The spectra cover a large range of wave-length but we will focus our study only in the range of 4800 – 5380 Å, *i.e.* the range covered by the `SAURON` instrument. To create the 2D maps of the different line indices, we have used the pipeline routine `XSAURON` [Bacon *et al.* 2001].

5.3.2.2 First test

As a first test of the implementation of stellar populations for our sample of simulations, we decided to look at a remerger of ETGs: the simulation called rem2x11 on a **rr** orbit (see Section 4.1). The initial progenitors are themselves remnants of two 1:1 spiral-spiral mergers, one is a slow rotator with KDC and the other is a fast rotator. They should be both classified as ETG-like and thus should follow the Mgb – V_{esc} relation as pointed out by [Scott *et al.* 2009]. The two ETG progenitors still have $\sim$ 2 per cent of gas in their baryonic mass (while the fraction of gas was 10 per cent in the initial spiral): during the remerger very few "new new" stars will be formed. However, we decided to ignore this second episode of star formation with the goal to study the role of a collisionless merger on the Mgb – V_{esc} relation. The term "young stars" will then refer to the stars formed during the initial spiral-spiral merger.

In the ETG progenitors, we have manually set-up a metallicity gradient consistent with the Mgb – V_{esc} relation for the old stars: a metallicity $[Z/H] = 2\ [Z/H]_\odot$ (*i.e.* metal rich) in the centre (maximum V_{esc}) and $[Z/H] = 0.25\ [Z/H]_\odot$ (*i.e.* metal poor) at large radii (minimum V_{esc}). The old stars have a constant age of 12 Gyr. For the young stars, we chose a constant age of 10 Gyr and a metallicity

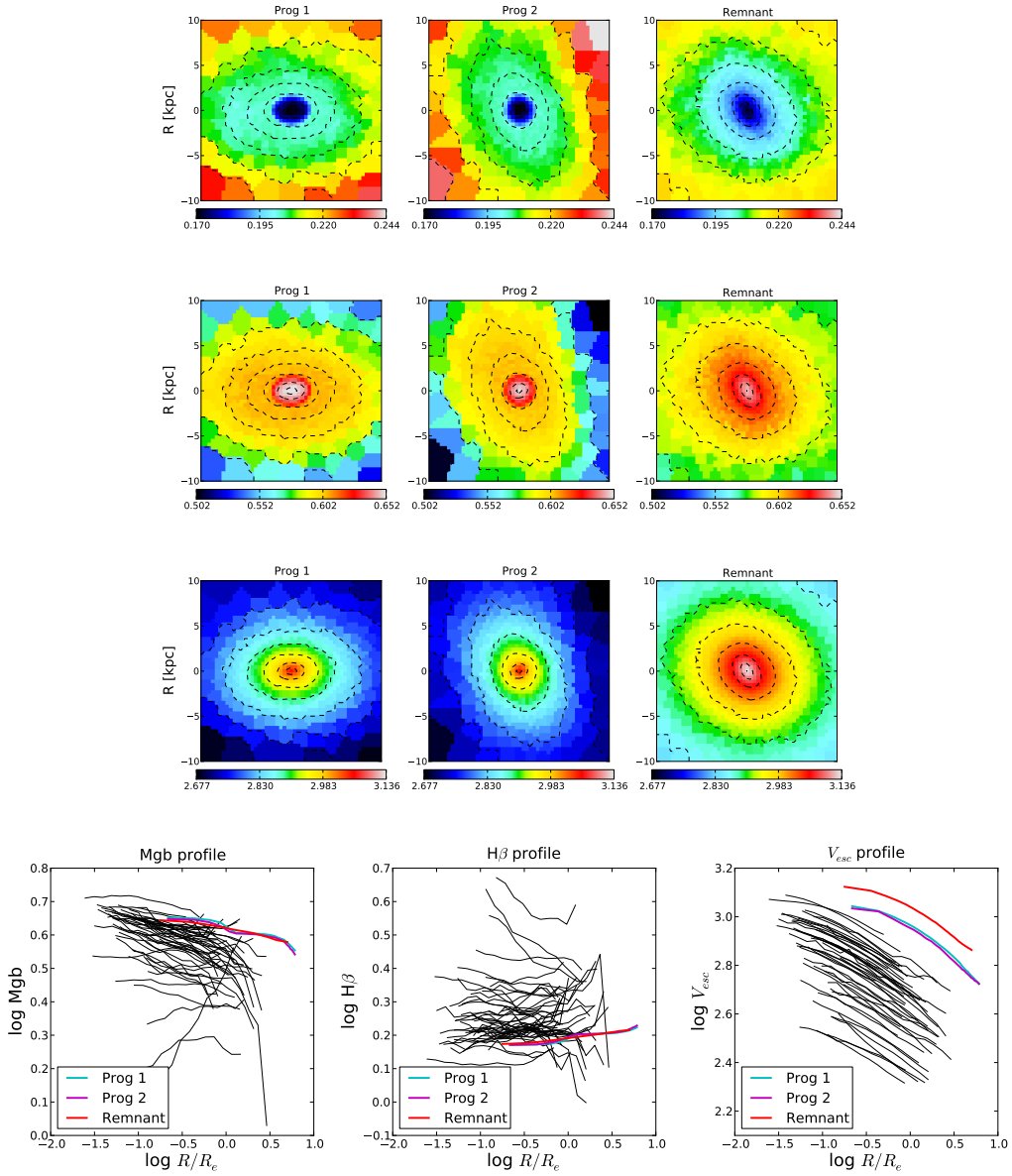

Figure 5.6: 2D maps of Hβ (top), Mgb (middle top) indices and the escape velocity V_{esc} (middle bottom) for the two progenitors (left and middle panels) and the remnant (right panels). The bottom line shows the radial profiles (as a function of the radius divided by the effective radius) of Mgb (left), Hβ (middle) and the escape velocity V_{esc} (right) for the merger remnant (in red) and the two progenitors (in cyan and magenta) as well as the radial profiles of the 48 SAURON galaxies (in black).

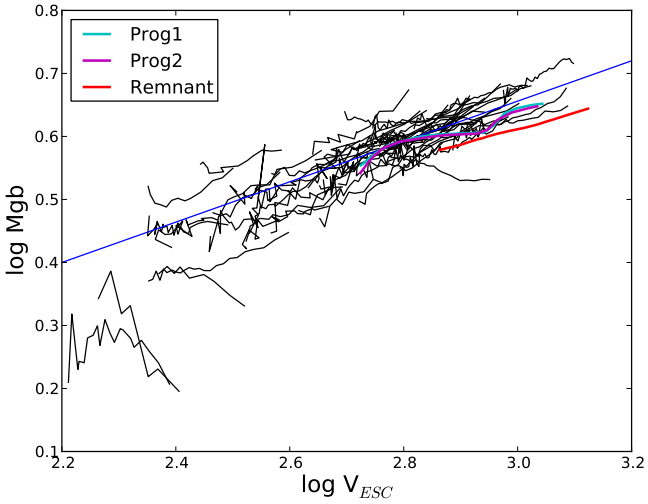

Figure 5.7: The Mgb – V_{esc} relation (both in log) for the 48 galaxies of the SAURON sample, for the two progenitors (in cyan and magenta) and for the remnant (red). The blue line shows the correlation found by [Scott *et al.* 2009].

of $[Z/H] = 3\ [Z/H]_{\odot}$. Fig. 5.6 shows the 2D maps and radial profiles of the Hβ and Mgb line indices and the 2D maps and radial profiles of V_{esc} for the two progenitors and Fig. 5.7 shows their behaviours on the Mgb – V_{esc} diagram. We then easily check that the progenitors are consistent with the 48 observed ETGs of the SAURON sample.

For the analysis of the remnant, we use the same technique applied for the SAURON galaxies. We search for the photometric position angle (PA) and the ellipticity (ϵ) of the isophote at the largest radius, and we compute the luminosity weighted line indices and V_{esc} within shell-ellipses with the given PA and ϵ at all radii. Fig. 5.6 and 5.7 show the 2D maps of the remerger remnant, the radial profiles of Hβ, Mgb, V_{esc} and the Mgb – V_{esc} relation. The radial profiles of Hβ and Mgb are strictly similar to the progenitors, and its V_{esc} profile is also similar but obviously shifted to higher V_{esc} values. We note here that the V_{esc} of the remerger remnant is high compared to the SAURON galaxies. The total baryonic mass of the remnant is four times the mass of the initial spiral progenitor, i.e. a mass of $5.2 \times 10^{11} M_{\odot}$. This mass is slightly above the one of the most massive galaxy within the SAURON sample. The similar behaviour of the remnant is also reported on the Mgb – V_{esc} diagram: the remnant keeps the same Mgb gradient but does not follow the relation anymore as it has acquired a deeper potential

well (and correspondingly higher V_{esc} values).

5.3.2.3 Conclusion

From this first test, we can conclude that a collisionless merger preserve the local Mgb – V_{esc} relation but not the global one. However, the remerger remnant remains close to the scatter of the relation. This result could have been predicted: the Mgb values are most strongly influenced by the metallicity which is only slightly affected by the merger itself (besides a potential dilution due to the radial redistribution of stars), while V_{esc} is more significantly increased (although not dramatically), which thus explains the slight shift to the right of the V_{esc} diagram for the remnant. To preserve the global Mgb – V_{esc} relation, the remnant would require some gas to form new enriched stars and correspondingly increase its metallicity.

Our study of only one case is evidently limited and has to be complemented with other simulations of ETG remergers. We would also need to take into account the role of the gas and the resulting star formation.

Chapter 6

Summary and Perspectives

Contents

In this thesis, I investigated the morphology and the kinematics of binary merger remnants of spiral galaxies and ETGs. I first probed the role of the resolution on the intrinsic properties of the remnants. I then linked the initial conditions of the mergers to the formation of fast and slow rotators, and the formation or destruction of the KDCs.

6.1 The need for resolution

In Chapter 2, I studied the effects of the numerical resolution on the morphology and the kinematics of the merger remnants. In a simulation, the resolution depends on the number of particles and the size of the grid in which the particles are placed. In order to understand how the resolution affect the mergers, we have simulated four simulations of binary mergers of spiral galaxies at three different resolutions. Two remnants are classified as fast rotators at the highest resolution and two are classified as slow rotators and hold a Kinematically Distinct Core. The three resolutions correspond to the present-day standard resolution for the lowest one, to the resolution used for our large sample of binary mergers for the middle one, and to a very high resolution as in [Bournaud *et al.* 2008].

The two fast rotators (one with and one without gas) are overall correctly reproduced at the three probed resolutions: we do not observed major discrepancies in the morphology and the kinematics of the remnants. The systems that are slow rotators at high resolution rotate more rapidly when the resolution is lowered, and can be observed as true fast rotators at standard-day resolution (includ-

ing the formation of a bar). When present in the simulation, gas at present-day standard-resolution largely lies in smooth structures, and the formation of new stars during the merger proceeds in a relatively smooth way. When an increased resolution is used, thinner gas structures are resolved during the merger, which can result in structured and clustered star formation. These local density peaks are accompanied by rapid variations of the gravitational potential, which help to scatter stellar orbits, evacuate the angular momentum, and form – for specific orbital configurations – slow rotating ETGs.

6.2 Formation of ETGs via binary mergers of disc galaxies

In Chapter 3, I presented simulations of binary mergers of disc galaxies (which include stars, gas, dark matter, star formation and energy feedback from supernovae) made at a high enough resolution. These binary mergers are either called major mergers (with mass ratio between progenitors of 1:1 or 2:1) or intermediate mass mergers (mass ratio 3:1 or 6:1). For each mass ratio, we simulated 15 mergers with different initial conditions changing the orientation, inclination, impact parameter or incoming velocity of the progenitors. The two progenitors are spiral galaxies with bulge to disc ratios typical of a Sb and a Sc galaxy: these have, as expected, high central baryonic angular momentum, measured by the λ_R parameter, similar to the fastest rotators observed in the ATLAS^{3D} sample of early-type galaxies. I find both fast rotators and slow rotators in our sample of relaxed remnants of binary disc mergers.

Confirming previous studies (see *e.g.* [Jesseit *et al.* 2009]), intermediate mass mergers produce only fast rotators while major mergers can produce both fast and slow rotators. An intrinsic difference between fast and slow rotators is that none of the fast rotators harbour a KDC, while the majority of slow rotators do harbour a clear KDC: these behaviours are observed in the 260 ATLAS^{3D} galaxies ([Emsellem *et al.* 2011]). I also note that fast rotators all have aligned kinematic and photometric axes, slow rotators frequently appear with kinematic misalignments, in agreement with the results of [Krajnović *et al.* 2011] on the ATLAS^{3D} sample. The definition of slow and fast rotators seems to robustly disentangle two distinct families of ETGs with different intrinsic properties: the mass ratio of the progenitors and their initial orientations are clearly important parameters for the formation of these two classes.

In Chapter 5, the comparison between the ATLAS^{3D} galaxies and the sample

of binary merger remnants reveals how the fast and slow rotating ETGs could (or could not) have been formed. The observed fast rotators are consistent with the sample of simulated spiral progenitors and simulated fast rotators. In turn, the observed slow rotators are intrinsically rounder than the simulated ones and should have a more complex history of formation. However, the sample of simulated slow rotators can reproduce the *so-called* 2-σ galaxies. These 2-σ galaxies are often (but not always) classified as slow rotators and present a clear signature in their velocity and velocity dispersion maps of two counter-rotating embedded discs: they may have experienced a major merger between two disc-like galaxies.

6.3 Galaxy remergers: a way for round slow rotators ?

In Chapter 4, I analysed numerical simulations of galaxy remergers, *i.e.* mergers between a merger remnant of disc galaxies and an other galaxy. We have previously seen that the slow rotators formed in binary mergers of disc galaxies are too flat compared to the observed ones. Additional mergers could make the simulated slow rotators rounder: this effect is seen in major remergers (i.e. ETG remergers). However, in ETG remergers, the initial KDCs in the galaxies are destroyed: the final remnants are then rounder but classified as fast rotators (or close to the limit defining the two classes) and present clear rotation patterns. These remnants are comparable to some observed ATLAS^{3D} fast rotators with an intrinsic low ellipticity.

To study the survival of the KDCs in remergers, we have then simulated remergers between a slow rotator with a KDC formed in a binary merger of disc galaxies and a smaller spiral companion. Its survival/destruction is directly linked with the initial orientation of the galaxies, similarly to its formation process. However, it does not seem to be strongly influenced by the mass of the companion. Minor remergers can thus preserve the KDC in a galaxy, but do not really make the central part of the galaxy rounder: the gain in ellipticity is less than 0.1. A succession of minor mergers seems suitable for that purpose but it would constrain the range of allowed orbital configurations. To confirm these results, a new series of simulations – including gas and different initial conditions – would be clearly an asset to improve on our understanding of the formation of the massive and round slow rotators with a KDC.

In Chapter 4, I have also studied the time evolution of a galaxy simulated with a new technique of zoom simulations (see [Martig *et al.* 2009]) to take into

account the cosmological context of galaxy formation. The initial spiral galaxy has suffered several minor mergers during its early history which have destroyed its disc-like shape and transformed it into a slow rotator. A quiet phase of smooth gas accretion has followed, and this has not significantly altered its morphology and only slightly its kinematics. The last interaction was a major merger which severely impacted the kinematics of the galaxy. But after the final relaxation, the galaxy recovered a clear rotation pattern.

The analysis of this simulation is only a first step towards the study of a larger sample of cosmological simulations. These will enable us to link the final state of a galaxy with its history of formation.

6.4 Perspectives

In this Section, I briefly describe some studies I wish to perform both in a near future and on a longer term.

Expending the sample of galaxy mergers: At the moment, the sample of simulations consists of 70 simulations of binary mergers of disc galaxies which encompass various mass ratios, orientations, inclinations, impact parameters, incoming velocities and gas fractions. These simulations enabled us to examine the importance of the mass ratios of the progenitors and their initial orientations. However, the other parameters appear to have no strong effect on the morphology and kinematics of the merger remnants. Either they really have no impact on the remnants, or our choice of values for these parameters were to restrictive. This question could be easily solved with a larger sample of simulations, varying:

The gas fraction: In [Hoffman *et al.* 2010], the gas plays a major role in the formation of the KDCs and the fast rotators. In our sample of simulations, having 10 or 33 per cent of gas does not seem to affect much the remnants. Is this only a numerical problem of resolution and treatment of the gas ? With new simulations of spiral mergers with different gas fractions, from gas-poor to gas-rich, we would be able to put strong constraints on how the gas can change (or not) the remnants.

The impact parameter: In the present sample, we have simulated mergers with a lower impact parameter: decreasing it from 60 to 35 kpc. No difference has been observed in the remnants. In [Jesseit *et al.* 2009], using a very small impact parameter (around 7 kpc), their remnants were found to be rounder

than ours. This could be a way to form the round slow rotators with a KDC found in the ATLAS^{3D} sample.

Spiral Hubble type: I have shown in this thesis that the Hubble type of the spiral progenitors certainly influences the outputs of the simulations: our Sb spiral remains dynamically stable during the merger while the Sc companion is disrupted and adopts the sign of the orbital angular momentum. I would like then to simulate galaxy mergers with different pairs of spiral Hubble type, *e.g.* Sb – Sb or Sc – Sc, to clearly understand how the galaxies behave during the merger and how this could modify the formation process of the KDC. This was already achieved in the extensive simulation database GalMer [Chilingarian *et al.* 2010] but unfortunately at a relatively low spatial and mass resolution.

The initial mass and shape of the progenitors: The spiral progenitors used in this thesis are among the most massive spirals observed in the local Universe (see *e.g.* Fig. 1.2). Their mass profiles are also built to match those of the local spirals. A study of the age of the slow rotators, observed within the SAURON survey, tells us that these are old. If these slow rotators are formed via a merger of disc galaxies, we should thus use masses and shapes of early spiral galaxies (see *e.g.* [Bournaud *et al.* 2009]).

Expending the sample of galaxy remergers: I presented also in the thesis a sample of 16 major and 12 minor remergers. These simulations show that major remergers always destroy the initial KDCs but form rounder ETGs while minor remergers can preserve the KDCs but do not affect much the morphology. This further motivates the need to extend our sample of simulations with both major and minor remergers.

In the current sample, one of the progenitor of the major remergers is always a slow rotator. During the merger, this progenitor acquires angular momentum from the orbit and starts to rotate: the remnant is a fast rotator. In one case, we merge a fast rotating ETG and a spiral both with a retrograde spin: the remnant is the slowest rotating ETG among the sample and presents different components in its velocity field (but no KDC). This could be a possible formation scenario for the round slow rotators and other simulations with similar initial conditions are needed to solve that question. But first, the sample of minor remergers has

to be completed with other simulations: introducing gas in the spiral encounters and varying the initial conditions. Expending the sample of remnants of binary merger of spiral galaxies with other initial conditions (low or very high gas fraction, small impact parameter, mass of the spirals) will also enable us to use different type of slow rotators with a KDC as progenitors for our simulations. It will be possible to see if a trend exists between the survival of the KDC and the initial gas fraction, shape or mass of the progenitor.

Analysing a larger sample of cosmological zoom simulations will also give us a broader view of the processes of galaxy formation (gas accretion, minor and major mergers).

Implementing the stellar populations: I have recently implemented stellar population models in one galaxy remerger. This study will be conducted for all remerger remnants with the goal to understand how the ETGs can follow the Mgb – V_{esc} relation while they undergo mergers. I will also implement stellar populations in binary mergers of disc galaxies with the goal to investigate how spiral galaxies – for which we do not know if they follow the Mgb – V_{esc} relation – can produce ETGs with a Mgb gradient similar to observed galaxies. Having a larger sample of simulations with very different initial conditions will also for this study helps us to constrain the formation of observed ETGs.

In a second stage, I want to implement the stellar population models in cosmological zoom simulations in order to follow the time evolution of the metallicity gradients and ages of the studied galaxies.

Observation of distant galaxies: The ATLAS^{3D} project aims to characterize local ($z = 0$) red sequence galaxies. At redshift around one, current instruments have difficulties to spatially resolve the stellar kinematics of distant galaxies due to their low surface brightness. This will be possible with the next generation of instruments of the VLT.

The MUSE (Multi Unit Spectroscopic Explorer) deep and medium deep fields will, for instance, provide a sample of field galaxies in the $z \sim 0.5 - 1$ redshift regime that will allow the investigation of the internal galactic properties. Studies of galaxy clusters will also be developed, the number density of galaxies in these clusters is high and will allow the analysis of large samples of resolved early-type galaxies at $z \sim 0.8$. At these intermediate epochs, major galactic transformations in clusters driven by environmental processes such as harassment and tidal stripping are predicted. It will be a great challenge to follow the time evolution of the

fast and slow rotators, uncovering the fossil record of their formation.

Using the extended sample of simulations, with spiral progenitor typical for high redshift ones and the cosmological simulations, it will be possible to link these different periods and better understand the processes involved in the formation and assembly of the most massive early-type galaxies as observed today.

Appendix A

List of publications

A.1 Refereed Publications

- Khochfar S., Emsellem E., Serra P., **Bois M.**, et al. *The ATLAS^{3D} project - VIII. Modelling the Formation and Evolution of Fast and Slow Rotator Early-Type Galaxies within ΛCDM.* 2010, submitted to MNRAS
- Cappellari M., Emsellem E., ..., **Bois M.**, et al. *The ATLAS^{3D} project - VII. Revisiting the morphology of nearby galaxies: the kinematic morphology-density relation.* 2010, submitted to MNRAS
- **Bois M.**, Emsellem E., Bournaud F., et al. *The ATLAS^{3D} project - VI. Simulations of binary galaxy mergers and its link with Fast Rotators, Slow Rotators, and Kinematically Distinct Cores.* 2010, submitted to MNRAS
- Davis T.A., Bureau M., ..., **Bois M.**, et al. *The ATLAS^{3D} project - V. The CO Tully-Fisher relation of early-type galaxies.* 2010, submitted to MNRAS
- Young L.M., Bureau M., ..., **Bois M.**, et al. *The ATLAS^{3D} project - IV. The molecular gas content of early-type galaxies.* 2010, submitted to MNRAS
- Emsellem E., ..., **Bois M.**, et al. *The ATLAS^{3D} project - III. A census of the stellar angular momentum within the effective radius of early-type galaxies: unveiling the distribution of Fast and Slow Rotators.* 2010, submitted to MNRAS
- Krajnović D., Emsellem E., ..., **Bois M.**, et al. *The ATLAS^{3D} project - II. Morphologies, kinemetric features and alignment between photometric and kinematic axes of early-type galaxies.* 2010, submitted to MNRAS
- Cappellari M., Emsellem E., ..., **Bois M.**, et al. *The ATLAS^{3D} project - I. A volume-limited sample of 260 nearby early-type galaxies: science goals and selection criteria.* 2010, accepted by MNRAS
- **Bois M.**, Bournaud F., Emsellem E., et al. *Formation of slowly rotating early-type galaxies via major mergers: a Resolution Study.* 2010, MNRAS, 406, 240

A.2 Non-refereed Publications

- Serra P., Morganti R., Oosterloo T., Alatalo K., Blitz L., **Bois M.**, et al. *Early-type Galaxies in Isolation: an HI Perspective with ATLAS^{3D}*. 2010, ASPC, 421, 49

- Cappellari M., Scott N., Alatalo K., Blitz L., **Bois M.**, Bournaud F., et al. *Scaling relations in early-type galaxies from integral-field stellar kinematics*. 2010, HiA, 15, 81

- **Bois M.**, Bournaud F., Emsellem E., et al. *Formation of Slowly Rotating Elliptical Galaxies in Major Mergers. A Resolution Study*. 2010, AIPC, 1240, 405

- Emsellem E., Alatalo K., Blitz L., **Bois M.**, Bournaud F., et al. *The ATLAS^{3D} Project: A Paradigm Shift for Early-Type Galaxies*. 2010, AIPC, 1240, 335

- Serra P., McDermid R. M., Alatalo K., Blitz L., **Bois M.**, Bournaud F., et al. *Stellar populations of early-type galaxies in the ATLAS^{3D} sample*. 2009, AIPC, 1111, 111

- Serra P., Morganti R., Oosterloo T., Alatalo K., Blitz L., **Bois M.**, et al. *An HI view of the on-going assembly of early-type galaxies: present and future observations*. 2009, pra confE, 56

- Bournaud F., **Bois M.**, Emsellem E., Duc P.-A. *Galaxy mergers at high resolution : From elliptical galaxies to tidal dwarfs and globular clusters*. 2008, AN, 329, 1025

Bibliography

[Aarseth & Fall 1980] S. J. Aarseth and S. M. Fall. *Cosmological N-body simulations of galaxy merging*. ApJ, vol. 236, pages 43–57, February 1980. 23

[Aarseth & Saslaw 1972] S. J. Aarseth and W. C. Saslaw. *Virial Mass Determinations of Bound and Unstable Groups of Galaxies.* ApJ, vol. 172, pages 17–+, February 1972. 18

[Aarseth 1963] S. J. Aarseth. *Dynamical evolution of clusters of galaxies, I.* MNRAS, vol. 126, pages 223–+, 1963. 18

[Abadi *et al.* 2010] M. G. Abadi, J. F. Navarro, M. Fardal, A. Babul and M. Steinmetz. *Galaxy-induced transformation of dark matter haloes*. MNRAS, vol. 407, pages 435–446, September 2010. 88, 106

[Archibald *et al.* 2010] J. David Archibald, W. A. Clemens, Kevin Padian, Timothy Rowe, Norman Macleod, Paul M. Barrett, Andrew Gale, Pat Holroyd, Hans-Dieter Sues, Nan Crystal Arens, John R. Horner, Gregory P. Wilson, Mark B. Goodwin, Christopher A. Brochu, Donald L. Lofgren, Stuart H. Hurlbert, Joseph H. Hartman, David A. Eberth, Paul B. Wignall, Philip J. Currie, Anne Weil, Guntupalli V. R. Prasad, Lowell Dingus, Vincent Courtillot, Angela Milner, Andrew Milner, Sunil Bajpai, David J. Ward and Ashok Sahni. *Cretaceous Extinctions: Multiple Causes*. Science, vol. 328, no. 5981, page 973, 2010. 17

[Athanassoula & Bureau 1999] E. Athanassoula and M. Bureau. *Bar Diagnostics in Edge-on Spiral Galaxies. II. Hydrodynamical Simulations*. ApJ, vol. 522, pages 699–717, September 1999. 105

[Bacon *et al.* 2001] R. Bacon, Y. Copin, G. Monnet, B. W. Miller, J. R. Allington-Smith, M. Bureau, C. M. Carollo, R. L. Davies, E. Emsellem, H. Kuntschner, R. F. Peletier, E. K. Verolme and P. T. de Zeeuw. *The SAURON project - I. The panoramic integral-field spectrograph*. MNRAS, vol. 326, pages 23–35, September 2001. 16, 114

[Balcells & González 1998] M. Balcells and A. C. González. *Formation of Kinematic Subsystems in Stellar Spiral-Spiral Mergers*. ApJ, vol. 505, pages L109–L112, October 1998. 106

[Balcells & Quinn 1990] M. Balcells and P. J. Quinn. *The formation of counterrotating cores in elliptical galaxies*. ApJ, vol. 361, pages 381–393, October 1990. 22, 66, 106

[Baldry *et al.* 2004] I. K. Baldry, K. Glazebrook, J. Brinkmann, Ž. Ivezić, R. H. Lupton, R. C. Nichol and A. S. Szalay. *Quantifying the Bimodal Color-Magnitude Distribution of Galaxies*. ApJ, vol. 600, pages 681–694, January 2004. 15

[Baldry *et al.* 2006] I. K. Baldry, M. L. Balogh, R. G. Bower, K. Glazebrook, R. C. Nichol, S. P. Bamford and T. Budavari. *Galaxy bimodality versus stellar mass and environment*. MNRAS, vol. 373, pages 469–483, December 2006. 11, 15

[Barnes & Hernquist 1996] J. E. Barnes and L. Hernquist. *Transformations of Galaxies. II. Gas dynamics in Merging Disk Galaxies*. ApJ, vol. 471, pages 115–+, November 1996. 18

[Barnes 1988] J. E. Barnes. *Encounters of disk/halo galaxies*. ApJ, vol. 331, pages 699–717, August 1988. 19

[Barnes 1992] J. E. Barnes. *Transformations of galaxies. I - Mergers of equal-mass stellar disks*. ApJ, vol. 393, pages 484–507, July 1992. 44

[Barnes 1998] J. E. Barnes. *Dynamics of Galaxy Interactions*. In R. C. Kennicutt Jr., F. Schweizer, J. E. Barnes, D. Friedli, L. Martinet, & D. Pfenniger, editeur, Saas-Fee Advanced Course 26: Galaxies: Interactions and Induced Star Formation, pages 275–+, 1998. 19

[Barnes 2002] J. E. Barnes. *Formation of gas discs in merging galaxies*. MNRAS, vol. 333, pages 481–494, July 2002. 106

[Bekki & Shioya 1997] K. Bekki and Y. Shioya. *Formation of Boxy and Disky Elliptical Galaxies in Early Dissipative Mergers*. ApJ, vol. 478, pages L17+, March 1997. 20

[Bender 1988] R. Bender. *Rotating and counter-rotating cores in elliptical galaxies*. A&A, vol. 202, pages L5–L8, August 1988. 16

[Bendo & Barnes 2000] G. J. Bendo and J. E. Barnes. *The line-of-sight velocity distributions of simulated merger remnants*. MNRAS, vol. 316, pages 315–325, August 2000. 105

[Bernardi *et al.* 2006] M. Bernardi, R. C. Nichol, R. K. Sheth, C. J. Miller and J. Brinkmann. *Evolution and Environment of Early-Type Galaxies*. AJ, vol. 131, pages 1288–1317, March 2006. 111

[Bigiel *et al.* 2008] F. Bigiel, A. Leroy, F. Walter, E. Brinks, W. J. G. de Blok, B. Madore and M. D. Thornley. *The Star Formation Law in Nearby Galaxies on Sub-Kpc Scales*. AJ, vol. 136, pages 2846–2871, December 2008. 15

[Bois *et al.* 2010] M. Bois, F. Bournaud, E. Emsellem, K. Alatalo, L. Blitz, M. Bureau, M. Cappellari, R. L. Davies, T. A. Davis, P. T. de Zeeuw, P.-A. Duc, S. Khochfar, D. Krajnović, H. Kuntschner, P.-Y. Lablanche, R. M. McDermid, R. Morganti, T. Naab, T. Oosterloo, M. Sarzi, N. Scott, P. Serra, A. Weijmans and L. M. Young. *Formation of slowly rotating early-type galaxies via major mergers: a resolution study*. MNRAS, vol. 406, pages 2405–2420, August 2010. 25

[Bournaud *et al.* 2004] F. Bournaud, F. Combes and C. J. Jog. *Unequal-mass galaxy merger remnants: Spiral-like morphology but elliptical-like kinematics*. A&A, vol. 418, pages L27–L30, April 2004. 20, 22, 56, 58

[Bournaud *et al.* 2005] F. Bournaud, C. J. Jog and F. Combes. *Galaxy mergers with various mass ratios: Properties of remnants*. A&A, vol. 437, pages 69–85, July 2005. 20, 22, 44, 105

[Bournaud *et al.* 2007] F. Bournaud, C. J. Jog and F. Combes. *Multiple minor mergers: formation of elliptical galaxies and constraints for the growth of spiral disks*. A&A, vol. 476, pages 1179–1190, December 2007. 20, 44, 85, 88, 96, 97, 106

[Bournaud *et al.* 2008] F. Bournaud, P.-A. Duc and E. Emsellem. *High-resolution simulations of galaxy mergers: resolving globular cluster formation*. MNRAS, vol. 389, pages L8–L12, September 2008. 21, 119

[Bournaud *et al.* 2009] F. Bournaud, B. G. Elmegreen and M. Martig. *The Thick Disks of Spiral Galaxies as Relics from Gas-rich, Turbulent, Clumpy Disks at High Redshift*. ApJ, vol. 707, pages L1–L5, December 2009. 123

[Bournaud *et al.* 2010a] F. Bournaud, D. Chapon, L. Delaye, L. C. Powell, B. G. Elmegreen, D. M. Elmegreen, P.-A. Duc, R. Teyssier, T. Contini, B. Epinat and K. L. Shapiro. *Hydrodynamics of high-redshift galaxy collisions: From gas-rich disks to dispersion-dominated mergers and compact spheroids*. ArXiv e-prints, June 2010. 20, 58, 70

[Bournaud *et al.* 2010b] F. Bournaud, B. G. Elmegreen, R. Teyssier, D. L. Block and I. Puerari. *ISM properties in hydrodynamic galaxy simulations: turbulence cascades, cloud formation, role of gravity and feedback*. MNRAS, vol. 409, pages 1088–1099, December 2010. 21

[Burkert 1995] A. Burkert. *The Structure of Dark Matter Halos in Dwarf Galaxies*. ApJ, vol. 447, pages L25+, July 1995. 47

[Cappellari & Copin 2003] M. Cappellari and Y. Copin. *Adaptive spatial binning of integral-field spectroscopic data using Voronoi tessellations*. MNRAS, vol. 342, pages 345–354, June 2003. 50

[Cappellari *et al.* 2007] M. Cappellari, E. Emsellem, R. Bacon, M. Bureau, R. L. Davies, P. T. de Zeeuw, J. Falcón-Barroso, D. Krajnović, H. Kuntschner, R. M. McDermid, R. F. Peletier, M. Sarzi, R. C. E. van den Bosch and G. van de Ven. *The SAURON project - X. The orbital anisotropy of elliptical and lenticular galaxies: revisiting the (V/σ, ϵ) diagram with integral-field stellar kinematics*. MNRAS, vol. 379, pages 418–444, August 2007. 17, 44, 51

[Cappellari *et al.* 2010] M. Cappellari, E. Emsellem, D. Krajnović, R. M. McDermid, N. Scott, G. A. Verdoes Kleijn, L. M. Young, K. Alatalo, R. Bacon, L. Blitz, M. Bois, F. Bournaud, M. Bureau, R. L. Davies, T. A. Davis, P. T. de Zeeuw, P.-A. Duc, S. Khochfar, H. Kuntschner, P.-Y. Lablanche, R. Morganti, T. Naab, T. Oosterloo, M. Sarzi, P. Serra and A.-M. Weijmans. *The Atlas3D project – I. A volume-limited sample of 260 nearby early-type galaxies: science goals and selection criteria*. ArXiv e-prints, December 2010. 44, 51, 102, 103, 105

[Carollo & Danziger 1994] C. M. Carollo and I. J. Danziger. *Dynamics and Stellar Populations in Early Type Galaxies*. MNRAS, vol. 270, pages 523–+, October 1994. 113

[Chilingarian *et al.* 2009] I. V. Chilingarian, S. De Rijcke and P. Buyle. *Internal Kinematics and Stellar Populations of the Poststarburst Galaxy SDSS J230743.41+152558.4*. ApJ, vol. 697, pages L111–L115, June 2009. 113

[Chilingarian *et al.* 2010] I. V. Chilingarian, P. Di Matteo, F. Combes, A.-L. Melchior and B. Semelin. *The GalMer database: galaxy mergers in the virtual observatory*. A&A, vol. 518, pages A61+, July 2010. 71, 123

[Cox *et al.* 2006a] T. J. Cox, S. N. Dutta, T. Di Matteo, L. Hernquist, P. F. Hopkins, B. Robertson and V. Springel. *The Kinematic Structure of Merger Remnants*. ApJ, vol. 650, pages 791–811, October 2006. 20

[Cox *et al.* 2006b] T. J. Cox, P. Jonsson, J. R. Primack and R. S. Somerville. *Feedback in simulations of disc-galaxy major mergers*. MNRAS, vol. 373, pages 1013–1038, December 2006. 19, 25

[Cretton *et al.* 2001] N. Cretton, T. Naab, H.-W. Rix and A. Burkert. *The Kinematics of 3:1 Merger Remnants and the Formation of Low-Luminosity Elliptical Galaxies*. ApJ, vol. 554, pages 291–297, June 2001. 105

[Crocker *et al.* 2009] A. F. Crocker, H. Jeong, S. Komugi, F. Combes, M. Bureau, L. M. Young and S. Yi. *Molecular gas and star formation in the red-sequence counter-rotating disc galaxy NGC 4550*. MNRAS, vol. 393, pages 1255–1264, March 2009. 23, 106

[Daddi *et al.* 2010a] E. Daddi, F. Bournaud, F. Walter, H. Dannerbauer, C. L. Carilli, M. Dickinson, D. Elbaz, G. E. Morrison, D. Riechers, M. Onodera, F. Salmi, M. Krips and D. Stern. *Very High Gas Fractions and Extended Gas Reservoirs in z = 1.5 Disk Galaxies*. ApJ, vol. 713, pages 686–707, April 2010. 20, 58

[Daddi *et al.* 2010b] E. Daddi, D. Elbaz, F. Walter, F. Bournaud, F. Salmi, C. Carilli, H. Dannerbauer, M. Dickinson, P. Monaco and D. Riechers. *Different Star Formation Laws for Disks Versus Starbursts at Low and High Redshifts*. ApJ, vol. 714, pages L118–L122, May 2010. 15

[Davies *et al.* 1993] R. L. Davies, E. M. Sadler and R. F. Peletier. *Line-strength gradients in elliptical galaxies*. MNRAS, vol. 262, pages 650–680, June 1993. 113

[de Vaucouleurs 1948] G. de Vaucouleurs. *Recherches sur les Nebuleuses Extragalactiques*. Annales d'Astrophysique, vol. 11, pages 247–+, January 1948. 15

[de Zeeuw & Franx 1991] T. de Zeeuw and M. Franx. *Structure and dynamics of elliptical galaxies*. ARA&A, vol. 29, pages 239–274, 1991. 16

[de Zeeuw *et al.* 2002] P. T. de Zeeuw, M. Bureau, E. Emsellem, R. Bacon, C. M. Carollo, Y. Copin, R. L. Davies, H. Kuntschner, B. W. Miller, G. Monnet, R. F. Peletier and E. K. Verolme. *The SAURON project - II. Sample and early results*. MNRAS, vol. 329, pages 513–530, January 2002. 17, 44

[Dekel *et al.* 2009] A. Dekel, R. Sari and D. Ceverino. *Formation of Massive Galaxies at High Redshift: Cold Streams, Clumpy Disks, and Compact Spheroids*. ApJ, vol. 703, pages 785–801, September 2009. 105

[Di Matteo *et al.* 2007] P. Di Matteo, F. Combes, A.-L. Melchior and B. Semelin. *Star formation efficiency in galaxy interactions and mergers: a statistical study*. A&A, vol. 468, pages 61–81, June 2007. 71

[Di Matteo *et al.* 2008a] P. Di Matteo, F. Bournaud, M. Martig, F. Combes, A.-L. Melchior and B. Semelin. *On the frequency, intensity, and duration of starburst episodes triggered by galaxy interactions and mergers*. A&A, vol. 492, pages 31–49, December 2008. 19, 25

[Di Matteo *et al.* 2008b] P. Di Matteo, F. Combes, A.-L. Melchior and B. Semelin. *Old stellar counter-rotating components in early-type galaxies from elliptical-spiral mergers*. A&A, vol. 477, pages 437–442, January 2008. 22

[Di Matteo *et al.* 2009] P. Di Matteo, C. J. Jog, M. D. Lehnert, F. Combes and B. Semelin. *Generation of rotationally dominated galaxies by mergers of pressure-supported progenitors*. A&A, vol. 501, pages L9–L13, July 2009. 22, 85

[Dubinski *et al.* 1996] J. Dubinski, J. C. Mihos and L. Hernquist. *Using Tidal Tails to Probe Dark Matter Halos*. ApJ, vol. 462, pages 576–+, May 1996. 21

[Elmegreen *et al.* 2008] B. G. Elmegreen, F. Bournaud and D. M. Elmegreen. *Bulge Formation by the Coalescence of Giant Clumps in Primordial Disk Galaxies*. ApJ, vol. 688, pages 67–77, November 2008. 105

[Emsellem *et al.* 2007] E. Emsellem, M. Cappellari, D. Krajnović, G. van de Ven, R. Bacon, M. Bureau, R. L. Davies, P. T. de Zeeuw, J. Falcón-Barroso, H. Kuntschner, R. McDermid, R. F. Peletier and M. Sarzi. *The SAURON project - IX. A kinematic classification for early-type galaxies*. MNRAS, vol. 379, pages 401–417, August 2007. 17, 44, 51

[Emsellem *et al.* 2011] E. Emsellem, M. Cappellari, D. Krajnović, K. Alatalo, L. Blitz, M. Bois, F. Bournaud, M. Bureau, R. L. Davies, T. A. Davis, P. T. de Zeeuw, S. Khochfar, H. Kuntschner, P.-Y. Lablanche, R. M. McDermid, R. Morganti, T. Naab, T. Oosterloo, M. Sarzi, N. Scott, P. Serra, G. van de Ven, A.-M. Weijmans and L. M. Young. *The Atlas3D project – III. A census of the stellar angular momentum within the effective radius of early-type galaxies:*

unveiling the distribution of Fast and Slow Rotators. Submitted to MNRAS, 2011. 51, 52, 55, 85, 88, 102, 103, 105, 106, 120

[Eskridge *et al.* 2000] P. B. Eskridge, J. A. Frogel, R. W. Pogge, A. C. Quillen, R. L. Davies, D. L. DePoy, M. L. Houdashelt, L. E. Kuchinski, S. V. Ramírez, K. Sellgren, D. M. Terndrup and G. P. Tiede. *The Frequency of Barred Spiral Galaxies in the Near-Infrared*. AJ, vol. 119, pages 536–544, February 2000. 14

[Fall & Efstathiou 1980] S. M. Fall and G. Efstathiou. *Formation and rotation of disc galaxies with haloes*. MNRAS, vol. 193, pages 189–206, October 1980. 17

[Farouki & Shapiro 1982] R. T. Farouki and S. L. Shapiro. *Simulations of merging disk galaxies*. ApJ, vol. 259, pages 103–115, August 1982. 18

[Fathi *et al.* 2009] K. Fathi, J. E. Beckman, N. Piñol-Ferrer, O. Hernandez, I. Martínez-Valpuesta and C. Carignan. *Pattern Speeds of Bars and Spiral Arms from Hα Velocity Fields*. ApJ, vol. 704, pages 1657–1675, October 2009. 45

[Feldmann *et al.* 2008] R. Feldmann, L. Mayer and C. M. Carollo. *Tidal Debris in Elliptical Galaxies as Tracers of Mergers with Disks*. ApJ, vol. 684, pages 1062–1074, September 2008. 21

[Feldmann *et al.* 2010] R. Feldmann, C. M. Carollo, L. Mayer, A. Renzini, G. Lake, T. Quinn, G. S. Stinson and G. Yepes. *The Evolution of Central Group Galaxies in Hydrodynamical Simulations*. ApJ, vol. 709, pages 218–240, January 2010. 24

[Ferrarese *et al.* 2006] L. Ferrarese, P. Côté, A. Jordán, E. W. Peng, J. P. Blakeslee, S. Piatek, S. Mei, D. Merritt, M. Milosavljević, J. L. Tonry and M. J. West. *The ACS Virgo Cluster Survey. VI. Isophotal Analysis and the Structure of Early-Type Galaxies*. ApJS, vol. 164, pages 334–434, June 2006. 16

[Ferreras *et al.* 2009] I. Ferreras, T. Lisker, A. Pasquali, S. Khochfar and S. Kaviraj. *On the formation of massive galaxies: a simultaneous study of number density, size and intrinsic colour evolution in GOODS*. MNRAS, vol. 396, pages 1573–1578, July 2009. 17

[Ferrière 2001] K. M. Ferrière. *The interstellar environment of our galaxy*. Reviews of Modern Physics, vol. 73, pages 1031–1066, October 2001. 21

[Franx & Illingworth 1988] M. Franx and G. D. Illingworth. *A counterrotating core in IC 1459*. ApJ, vol. 327, pages L55–L59, April 1988. 16

[Franx & Illingworth 1990] M. Franx and G. Illingworth. *Color gradients in elliptical galaxies*. ApJ, vol. 359, pages L41–L45, August 1990. 113

[Franx *et al.* 1991] M. Franx, G. Illingworth and T. de Zeeuw. *The ordered nature of elliptical galaxies - Implications for their intrinsic angular momenta and shapes*. ApJ, vol. 383, pages 112–134, December 1991. 109

[Freeman 1970] K. C. Freeman. *On the Disks of Spiral and so Galaxies*. ApJ, vol. 160, pages 811–+, June 1970. 14

[Genel *et al.* 2008] S. Genel, R. Genzel, N. Bouché, A. Sternberg, T. Naab, N. M. F. Schreiber, K. L. Shapiro, L. J. Tacconi, D. Lutz, G. Cresci, P. Buschkamp, R. I. Davies and E. K. S. Hicks. *Mergers and Mass Accretion Rates in Galaxy Assembly: The Millennium Simulation Compared to Observations of z ˜ 2 Galaxies*. ApJ, vol. 688, pages 789–793, December 2008. 88, 106

[Genel *et al.* 2010] S. Genel, N. Bouché, T. Naab, A. Sternberg and R. Genzel. *The Growth of Dark Matter Halos: Evidence for Significant Smooth Accretion*. ApJ, vol. 719, pages 229–239, August 2010. 88, 106

[Gerhard 1981] O. E. Gerhard. *N-body simulations of disc-halo galaxies - Isolated systems, tidal interactions and merging*. MNRAS, vol. 197, pages 179–208, October 1981. 18

[Gingold & Monaghan 1977] R. A. Gingold and J. J. Monaghan. *Smoothed particle hydrodynamics - Theory and application to non-spherical stars*. MNRAS, vol. 181, pages 375–389, November 1977. 19

[Governato *et al.* 2009] F. Governato, C. B. Brook, A. M. Brooks, L. Mayer, B. Willman, P. Jonsson, A. M. Stilp, L. Pope, C. Christensen, J. Wadsley and T. Quinn. *Forming a large disc galaxy from a $z > 1$ major merger*. MNRAS, vol. 398, pages 312–320, September 2009. 71

[Hernquist & Barnes 1991] L. Hernquist and J. E. Barnes. *Origin of kinematic subsystems in elliptical galaxies*. Nature, vol. 354, pages 210–212, November 1991. 22, 44, 106

[Hernquist 1990] L. Hernquist. *An analytical model for spherical galaxies and bulges*. ApJ, vol. 356, pages 359–364, June 1990. 45

[Hoffman *et al.* 2010] L. Hoffman, T. J. Cox, S. Dutta and L. Hernquist. *Orbital Structure of Merger Remnants. I. Effect of Gas Fraction in Pure Disk Mergers*. ApJ, vol. 723, pages 818–844, November 2010. 11, 21, 22, 67, 68, 69, 70, 110, 122

[Holmberg 1941] E. Holmberg. *On the Clustering Tendencies among the Nebulae. II. a Study of Encounters Between Laboratory Models of Stellar Systems by a New Integration Procedure.* ApJ, vol. 94, pages 385–+, November 1941. 18

[Hopkins *et al.* 2007] P. F. Hopkins, K. Bundy, L. Hernquist and R. S. Ellis. *Observational Evidence for the Coevolution of Galaxy Mergers, Quasars, and the Blue/Red Galaxy Transition*. ApJ, vol. 659, pages 976–996, April 2007. 82

[Hopkins *et al.* 2008] P. F. Hopkins, L. Hernquist, T. J. Cox, S. N. Dutta and B. Rothberg. *Dissipation and Extra Light in Galactic Nuclei. I. Gas-Rich Merger Remnants*. ApJ, vol. 679, pages 156–181, May 2008. 19, 21, 25

[Hopkins *et al.* 2009a] P. F. Hopkins, T. J. Cox, S. N. Dutta, L. Hernquist, J. Kormendy and T. R. Lauer. *Dissipation and Extra Light in Galactic Nuclei. II. "Cusp" Ellipticals*. ApJS, vol. 181, pages 135–182, March 2009. 21

[Hopkins *et al.* 2009b] P. F. Hopkins, T. J. Cox, J. D. Younger and L. Hernquist. *How do Disks Survive Mergers?* ApJ, vol. 691, pages 1168–1201, February 2009. 20, 58

[Hopkins *et al.* 2009c] P. F. Hopkins, T. R. Lauer, T. J. Cox, L. Hernquist and J. Kormendy. *Dissipation and Extra Light in Galactic Nuclei. III. "Core" Ellipticals and "Missing" Light*. ApJS, vol. 181, pages 486–532, April 2009. 21

[Hopkins *et al.* 2010] P. F. Hopkins, K. Bundy, D. Croton, L. Hernquist, D. Keres, S. Khochfar, K. Stewart, A. Wetzel and J. D. Younger. *Mergers and Bulge Formation in ΛCDM: Which Mergers Matter?* ApJ, vol. 715, pages 202–229, May 2010. 88, 103, 106

[Hubble 1926] E. P. Hubble. *Extragalactic nebulae.* ApJ, vol. 64, pages 321–369, December 1926. 13

[Hubble 1936] E. P. Hubble. Realm of the Nebulae. 1936. 13

[Jedrzejewski & Schechter 1988] R. Jedrzejewski and P. L. Schechter. *Evidence for dynamical subsystems in elliptical galaxies*. ApJ, vol. 330, pages L87–L91, July 1988. 16

[Jesseit *et al.* 2005] R. Jesseit, T. Naab and A. Burkert. *Orbital structure of collisionless merger remnants: on the origin of photometric and kinematic properties of elliptical and S0 galaxies*. MNRAS, vol. 360, pages 1185–1200, July 2005. 45

[Jesseit *et al.* 2007] R. Jesseit, T. Naab, R. F. Peletier and A. Burkert. *2D kinematics of simulated disc merger remnants*. MNRAS, vol. 376, pages 997–1020, April 2007. 22, 106

[Jesseit *et al.* 2009] R. Jesseit, M. Cappellari, T. Naab, E. Emsellem and A. Burkert. *Specific angular momentum of disc merger remnants and the λ_R/-parameter*. MNRAS, vol. 397, pages 1202–1214, August 2009. 11, 22, 50, 51, 55, 56, 67, 68, 69, 74, 103, 111, 120, 122

[Kazantzidis *et al.* 2008] S. Kazantzidis, J. S. Bullock, A. R. Zentner, A. V. Kravtsov and L. A. Moustakas. *Cold Dark Matter Substructure and Galactic Disks. I. Morphological Signatures of Hierarchical Satellite Accretion*. ApJ, vol. 688, pages 254–276, November 2008. 94

[Kennicutt 1998] R. C. Kennicutt Jr. *The Global Schmidt Law in Star-forming Galaxies*. ApJ, vol. 498, pages 541–+, May 1998. 15

[Khochfar & Burkert 2003] S. Khochfar and A. Burkert. *The Importance of Spheroidal and Mixed Mergers for Early-Type Galaxy Formation*. ApJ, vol. 597, pages L117–L120, November 2003. 82

[Khochfar & Burkert 2006] S. Khochfar and A. Burkert. *Orbital parameters of merging dark matter halos*. A&A, vol. 445, pages 403–412, January 2006. 48, 69

[Khochfar & Silk 2006] S. Khochfar and J. Silk. *On the origin of stars in bulges and elliptical galaxies*. MNRAS, vol. 370, pages 902–910, August 2006. 88, 106

[Khochfar & Silk 2009] S. Khochfar and J. Silk. *Dry mergers: a crucial test for galaxy formation*. MNRAS, vol. 397, pages 506–510, July 2009. 82

[Konstantopoulos *et al.* 2010] I. S. Konstantopoulos, S. C. Gallagher, K. Fedotov, P. R. Durrell, A. Heiderman, D. M. Elmegreen, J. C. Charlton, J. E. Hibbard, P. Tzanavaris, R. Chandar, K. E. Johnson, A. Maybhate, A. E. Zabludoff, C. Gronwall, D. Szathmary, A. E. Hornschemeier, J. English, B. Whitmore, C Mendes de Oliveira and J. Mulchaey. *Galaxy evolution in a complex environment: a multi-wavelength study of HCG 7*. ArXiv e-prints, July 2010. 105

[Kormendy & Bender 1996] J. Kormendy and R. Bender. *A Proposed Revision of the Hubble Sequence for Elliptical Galaxies*. ApJ, vol. 464, pages L119+, June 1996. 11, 16

[Krajnović *et al.* 2008] D. Krajnović, R. Bacon, M. Cappellari, R. L. Davies, P. T. de Zeeuw, E. Emsellem, J. Falcón-Barroso, H. Kuntschner, R. M. McDermid, R. F. Peletier, M. Sarzi, R. C. E. van den Bosch and G. van de Ven. *The SAURON project - XII. Kinematic substructures in early-type galaxies: evidence for discs in fast rotators*. MNRAS, vol. 390, pages 93–117, October 2008. 16

[Krajnović *et al.* 2011] D. Krajnović, E. Emsellem, M. Cappellari, K. Alatalo, L. Blitz, M. Bois, F. Bournaud, M. Bureau, R. L. Davies, T. A. Davis, P. T. de Zeeuw, S. Khochfar, H. Kuntschner, P.-Y. Lablanche, R. M. McDermid, R. Morganti, T. Naab, T. Oosterloo, M. Sarzi, N. Scott, P. Serra, G. van de Ven, A.-M. Weijmans and L. M. Young. *The Atlas3D project – II. Morphologies, kinemetric features and alignment between photometric and kinematic axes of early-type galaxies*. Submitted to MNRAS, 2011. 12, 55, 102, 105, 106, 109, 120

[Kroupa 2001] P. Kroupa. *On the variation of the initial mass function*. MNRAS, vol. 322, pages 231–246, April 2001. 114

[Kuntschner *et al.* 2010] H. Kuntschner, E. Emsellem, R. Bacon, M. Cappellari, R. L. Davies, P. T. de Zeeuw, J. Falcón-Barroso, D. Krajnović, R. M. McDermid, R. F. Peletier, M. Sarzi, K. L. Shapiro, R. C. E. van den Bosch and G. van de Ven. *The SAURON project - XVII. Stellar population analysis of the absorption line strength maps of 48 early-type galaxies*. MNRAS, vol. 408, pages 97–132, October 2010. 12, 103, 112, 113

[Lequeux 2005] J. Lequeux. The interstellar medium. 2005. 21

[Lucy 1977] L. B. Lucy. *A numerical approach to the testing of the fission hypothesis*. AJ, vol. 82, pages 1013–1024, December 1977. 19

[Marochnik & Suchkov 1996] L. S. Marochnik and A. A. Suchkov. The Milky Way Galaxy. Nauka, 1996. 14

[Martig & Bournaud 2008] M. Martig and F. Bournaud. *Triggering of merger-induced starbursts by the tidal field of galaxy groups and clusters*. MNRAS, vol. 385, pages L38–L42, March 2008. 47

[Martig & Bournaud 2010] M. Martig and F. Bournaud. *Formation of Late-type Spiral Galaxies: Gas Return from Stellar Populations Regulates Disk Destruction and Bulge Growth*. ApJ, vol. 714, pages L275–L279, May 2010. 105

[Martig *et al.* 2009] M. Martig, F. Bournaud, R. Teyssier and A. Dekel. *Morphological Quenching of Star Formation: Making Early-Type Galaxies Red*. ApJ, vol. 707, pages 250–267, December 2009. 24, 94, 121

[McDermid *et al.* 2006] R. M. McDermid, E. Emsellem, K. L. Shapiro, R. Bacon, M. Bureau, M. Cappellari, R. L. Davies, T. de Zeeuw, J. Falcón-Barroso, D. Krajnović, H. Kuntschner, R. F. Peletier and M. Sarzi. *The SAURON project - VIII. OASIS/CFHT integral-field spectroscopy of elliptical and lenticular galaxy centres*. MNRAS, vol. 373, pages 906–958, December 2006. 56, 103, 113

[Menéndez-Delmestre *et al.* 2007] K. Menéndez-Delmestre, K. Sheth, E. Schinnerer, T. H. Jarrett and N. Z. Scoville. *A Near-Infrared Study of 2MASS Bars in Local Galaxies: An Anchor for High-Redshift Studies*. ApJ, vol. 657, pages 790–804, March 2007. 14

[Meza *et al.* 2003] A. Meza, J. F. Navarro, M. Steinmetz and V. R. Eke. *Simulations of Galaxy Formation in a ΛCDM Universe. III. The Dissipative Formation of an Elliptical Galaxy*. ApJ, vol. 590, pages 619–635, June 2003. 23

[Michel-Dansac *et al.* 2010] L. Michel-Dansac, P.-A. Duc, F. Bournaud, J.-C. Cuillandre, E. Emsellem, T. Oosterloo, R. Morganti, P. Serra and R. Ibata. *A Collisional Origin for the Leo Ring*. ApJ, vol. 717, pages L143–L148, July 2010. 21

[Mihos *et al.* 1995] J. C. Mihos, I. R. Walker, L. Hernquist, C. Mendes de Oliveira and M. Bolte. *A Merger Origin for X Structures in S0 Galaxies*. ApJ, vol. 447, pages L87+, July 1995. 44

[Mihos *et al.* 1998] J. C. Mihos, J. Dubinski and L. Hernquist. *Tidal Tales Two: The Effect of Dark Matter Halos on Tidal Tail Morphology and Kinematics*. ApJ, vol. 494, pages 183–+, February 1998. 21

[Moster *et al.* 2010] B. P. Moster, A. V. Macciò, R. S. Somerville, P. H. Johansson and T. Naab. *Can gas prevent the destruction of thin stellar discs by minor mergers?* MNRAS, vol. 403, pages 1009–1019, April 2010. 20, 105

[Naab & Burkert 2003] T. Naab and A. Burkert. *Statistical Properties of Collisionless Equal- and Unequal-Mass Merger Remnants of Disk Galaxies*. ApJ, vol. 597, pages 893–906, November 2003. 20, 22, 44, 56, 58, 105

[Naab & Ostriker 2009] T. Naab and J. P. Ostriker. *Are Disk Galaxies the Progenitors of Giant Ellipticals?* ApJ, vol. 690, pages 1452–1462, January 2009. 82

[Naab & Trujillo 2006] T. Naab and I. Trujillo. *Surface density profiles of collisionless disc merger remnants*. MNRAS, vol. 369, pages 625–644, June 2006. 20, 105

[Naab *et al.* 1999] T. Naab, A. Burkert and L. Hernquist. *On the Formation of Boxy and Disky Elliptical Galaxies*. ApJ, vol. 523, pages L133–L136, October 1999. 20

[Naab *et al.* 2006a] T. Naab, R. Jesseit and A. Burkert. *The influence of gas on the structure of merger remnants*. MNRAS, vol. 372, pages 839–852, October 2006. 20, 21

[Naab *et al.* 2006b] T. Naab, S. Khochfar and A. Burkert. *Properties of Early-Type, Dry Galaxy Mergers and the Origin of Massive Elliptical Galaxies*. ApJ, vol. 636, pages L81–L84, January 2006. 82

[Naab *et al.* 2007] T. Naab, P. H. Johansson, J. P. Ostriker and G. Efstathiou. *Formation of Early-Type Galaxies from Cosmological Initial Conditions*. ApJ, vol. 658, pages 710–720, April 2007. 19, 24, 25, 88, 93, 106

[Naab *et al.* 2009] T. Naab, P. H. Johansson and J. P. Ostriker. *Minor Mergers and the Size Evolution of Elliptical Galaxies*. ApJ, vol. 699, pages L178–L182, July 2009. 24, 88, 106

[Navarro *et al.* 2010] J. F. Navarro, A. Ludlow, V. Springel, J. Wang, M. Vogelsberger, S. D. M. White, A. Jenkins, C. S. Frenk and A. Helmi. *The diversity and similarity of simulated cold dark matter haloes*. MNRAS, vol. 402, pages 21–34, February 2010. 19, 25

[Negroponte & White 1983] J. Negroponte and S. D. M. White. *Simulations of mergers between disc-halo galaxies*. MNRAS, vol. 205, pages 1009–1029, December 1983. 19

[Nieto *et al.* 1991] J.-L. Nieto, R. Bender and P. Surma. *Central brightness profiles and isophotal shapes in elliptical galaxies*. A&A, vol. 244, pages L37–L40, April 1991. 105

[O'Connell 1980] R. W. O'Connell. *Galaxy spectral synthesis. II - M32 and the ages of galaxies*. ApJ, vol. 236, pages 430–440, March 1980. 111

[Oh *et al.* 2008] S. H. Oh, W.-T. Kim, H. M. Lee and J. Kim. *Physical Properties of Tidal Features in Interacting Disk Galaxies*. ApJ, vol. 683, pages 94–113, August 2008. 18

[Oser *et al.* 2010] L. Oser, J. P. Ostriker, T. Naab, P. H. Johansson and A. Burkert. *The Two Phases of Galaxy Formation*. ArXiv e-prints, October 2010. 88, 106

[Powell *et al.* 2010] L. C. Powell, F. Bournaud, D. Chapon, J. Devriendt, A. Slyz and R. Teyssier. *Galactic star formation in parsec-scale resolution simulations*. ArXiv e-prints, September 2010. 21, 71

[Pracy *et al.* 2009] M. B. Pracy, H. Kuntschner, W. J. Couch, C. Blake, K. Bekki and F. Briggs. *The kinematics and spatial distribution of stellar populations in E+A galaxies*. MNRAS, vol. 396, pages 1349–1369, July 2009. 113

[Qu *et al.* 2010] Y. Qu, P. Di Matteo, M. Lehnert, W. van Driel and C. J. Jog. *The slowing down of galaxy disks in dissipationless minor mergers*. A&A, vol. 515, pages A11+, June 2010. 22, 85, 88, 96, 97, 106

[Read *et al.* 2008] J. I. Read, G. Lake, O. Agertz and V. P. Debattista. *Thin, thick and dark discs in ΛCDM*. MNRAS, vol. 389, pages 1041–1057, September 2008. 94

[Renaud *et al.* 2009] F. Renaud, C. M. Boily, T. Naab and C. Theis. *Fully Compressive Tides in Galaxy Mergers*. ApJ, vol. 706, pages 67–82, November 2009. 64

[Rix & White 1992] H.-W. Rix and S. D. M. White. *Optimal estimates of line-of-sight velocity distributions from absorption line spectra of galaxies - Nuclear discs in elliptical galaxies*. MNRAS, vol. 254, pages 389–403, February 1992. 16

[Roberts & Haynes 1994] M. S. Roberts and M. P. Haynes. *Physical Parameters along the Hubble Sequence*. ARA&A, vol. 32, pages 115–152, 1994. 15

[Robertson *et al.* 2006] B. Robertson, J. S. Bullock, T. J. Cox, T. Di Matteo, L. Hernquist, V. Springel and N. Yoshida. *A Merger-driven Scenario for Cosmological Disk Galaxy Formation*. ApJ, vol. 645, pages 986–1000, July 2006. 20, 58

[Rose 1985] J. A. Rose. *Constraints on stellar populations in elliptical galaxies*. AJ, vol. 90, pages 1927–1956, October 1985. 111

[Salpeter 1955] E. E. Salpeter. *The Luminosity Function and Stellar Evolution.* ApJ, vol. 121, pages 161–+, January 1955. 114

[Sánchez-Blázquez *et al.* 2006] P. Sánchez-Blázquez, R. F. Peletier, J. Jiménez-Vicente, N. Cardiel, A. J. Cenarro, J. Falcón-Barroso, J. Gorgas, S. Selam and A. Vazdekis. *Medium-resolution Isaac Newton Telescope library of empirical spectra*. MNRAS, vol. 371, pages 703–718, September 2006. 114

[Sánchez-Blázquez *et al.* 2007] P. Sánchez-Blázquez, D. A. Forbes, J. Strader, J. Brodie and R. Proctor. *Spatially resolved spectroscopy of early-type galaxies over a range in mass*. MNRAS, vol. 377, pages 759–786, May 2007. 113

[Schiavon 2007] R. P. Schiavon. *Population Synthesis in the Blue. IV. Accurate Model Predictions for Lick Indices and UBV Colors in Single Stellar Populations*. ApJS, vol. 171, pages 146–205, July 2007. 112

[Schulte *et al.* 2010] P. Schulte, L. Alegret, I. Arenillas, J. A. Arz, P. J. Barton, P. R. Bown, T. J. Bralower, G. L. Christeson, P. Claeys, C. S. Cockell, G. S. Collins, A. Deutsch, T. J. Goldin, K. Goto, J. M. Grajales-Nishimura, R. A. F. Grieve, S. P. S. Gulick, K. R. Johnson, W. Kiessling, C. Koeberl, D. A. Kring, K. G. MacLeod, T. Matsui, J. Melosh, A. Montanari, J. V. Morgan, C. R. Neal, D. J. Nichols, R. D. Norris, E. Pierazzo, G. Ravizza, M. Rebolledo-Vieyra, W. U. Reimold, E. Robin, T. Salge, R. P. Speijer, A. R. Sweet, J. Urrutia-Fucugauchi, V. Vajda, M. T. Whalen and P. S. Willumsen. *The Chicxulub Asteroid Impact and Mass Extinction at the Cretaceous-Paleogene Boundary*. Science, vol. 327, no. 5970, pages 1214–1218, March 2010. 17

[Schweizer 1982] F. Schweizer. *Colliding and merging galaxies. I - Evidence for the recent merging of two disk galaxies in NGC 7252*. ApJ, vol. 252, pages 455–460, January 1982. 17

[Scott *et al.* 2009] N. Scott, M. Cappellari, R. L. Davies, R. Bacon, P. T. de Zeeuw, E. Emsellem, J. Falcón-Barroso, D. Krajnović, H. Kuntschner, R. M. McDermid, R. F. Peletier, A. Pipino, M. Sarzi, R. C. E. van den Bosch, G. van de Ven and E. van Scherpenzeel. *The SAURON Project - XIV. No escape from V_{esc}: a global and local parameter in early-type galaxy evolution*. MNRAS, vol. 398, pages 1835–1857, October 2009. 113, 114, 116

[Searle & Zinn 1978] L. Searle and R. Zinn. *Compositions of halo clusters and the formation of the galactic halo*. ApJ, vol. 225, pages 357–379, October 1978. 17

[Semelin & Combes 2005] B. Semelin and F. Combes. *New multi-zoom method for N-body simulations: application to galaxy growth by accretion*. A&A, vol. 441, pages 55–67, October 2005. 93

[Sérsic 1968] J. L. Sérsic. Atlas de galaxias australes. 1968. 14

[Shapiro *et al.* 2010] K. L. Shapiro, J. Falcón-Barroso, G. van de Ven, P. T. de Zeeuw, M. Sarzi, R. Bacon, A. Bolatto, M. Cappellari, D. Croton, R. L. Davies, E. Emsellem, O. Fakhouri, D. Krajnović, H. Kuntschner, R. M. McDermid, R. F. Peletier, R. C. E. van den Bosch and G. van der Wolk. *The SAURON project - XV. Modes of star formation in early-type galaxies and the evolution of the red sequence*. MNRAS, vol. 402, pages 2140–2186, March 2010. 15

[Spergel *et al.* 2003] D. N. Spergel, L. Verde, H. V. Peiris, E. Komatsu, M. R. Nolta, C. L. Bennett, M. Halpern, G. Hinshaw, N. Jarosik, A. Kogut, M. Limon, S. S. Meyer, L. Page, G. S. Tucker, J. L. Weiland, E. Wollack and E. L. Wright. *First-Year Wilkinson Microwave Anisotropy Probe (WMAP) Observations: Determination of Cosmological Parameters*. ApJS, vol. 148, pages 175–194, September 2003. 17, 23

[Springel & Hernquist 2005] V. Springel and L. Hernquist. *Formation of a Spiral Galaxy in a Major Merger*. ApJ, vol. 622, pages L9–L12, March 2005. 20, 58

[Springel & White 1999] V. Springel and S. D. M. White. *Tidal tails in cold dark matter cosmologies*. MNRAS, vol. 307, pages 162–178, July 1999. 21

[Springel 2000] V. Springel. *Modelling star formation and feedback in simulations of interacting galaxies*. MNRAS, vol. 312, pages 859–879, March 2000. 44

[Springel 2005] V. Springel. *The cosmological simulation code GADGET-2*. MNRAS, vol. 364, pages 1105–1134, December 2005. 67

[Strateva *et al.* 2001] I. Strateva, Ž. Ivezić, G. R. Knapp, V. K. Narayanan, M. A. Strauss, J. E. Gunn, R. H. Lupton, D. Schlegel, N. A. Bahcall, J. Brinkmann, R. J. Brunner, T. Budavári, I. Csabai, F. J. Castander, M. Doi, M. Fukugita, Z. Győry, M. Hamabe, G. Hennessy, T. Ichikawa, P. Z. Kunszt, D. Q. Lamb, T. A. McKay, S. Okamura, J. Racusin, M. Sekiguchi, D. P. Schneider, K. Shimasaku and D. York. *Color Separation of Galaxy Types in the Sloan Digital Sky Survey Imaging Data*. AJ, vol. 122, pages 1861–1874, October 2001. 15

[Struve *et al.* 2010] C. Struve, T. Oosterloo, R. Sancisi, R. Morganti and B. H. C. Emonts. *Cold gas in massive early-type galaxies: the case of NGC 1167*. A&A, vol. 523, pages A75+, November 2010. 17

[Tacconi *et al.* 2010] L. J. Tacconi, R. Genzel, R. Neri, P. Cox, M. C. Cooper, K. Shapiro, A. Bolatto, N. Bouché, F. Bournaud, A. Burkert, F. Combes, J. Comerford, M. Davis, N. M. F. Schreiber, S. Garcia-Burillo, J. Gracia-Carpio, D. Lutz, T. Naab, A. Omont, A. Shapley, A. Sternberg and B. Weiner. *High molecular gas fractions in normal massive star-forming galaxies in the young Universe*. Nature, vol. 463, pages 781–784, February 2010. 20, 58

[Teyssier *et al.* 2010] R. Teyssier, D. Chapon and F. Bournaud. *The Driving Mechanism of Starbursts in Galaxy Mergers*. ApJ, vol. 720, pages L149–L154, September 2010. 15, 21, 71

[Thomas *et al.* 2007] J. Thomas, R. Jesseit, T. Naab, R. P. Saglia, A. Burkert and R. Bender. *Axisymmetric orbit models of N-body merger remnants: a dependency of reconstructed mass on viewing angle*. MNRAS, vol. 381, pages 1672–1696, November 2007. 111

[Thomas *et al.* 2010] D. Thomas, C. Maraston, K. Schawinski, M. Sarzi and J. Silk. *Environment and self-regulation in galaxy formation*. MNRAS, vol. 404, pages 1775–1789, June 2010. 111

[Toomre & Toomre 1972] A. Toomre and J. Toomre. *Galactic Bridges and Tails*. ApJ, vol. 178, pages 623–666, December 1972. 18, 44

[Toomre 1977] A. Toomre. *Theories of spiral structure*. ARA&A, vol. 15, pages 437–478, 1977. 14

[Toth & Ostriker 1992] G. Toth and J. P. Ostriker. *Galactic disks, infall, and the global value of Omega*. ApJ, vol. 389, pages 5–26, April 1992. 105

[Tremblay & Merritt 1996] B. Tremblay and D. Merritt. *Evidence From Intrinsic Shapes for Two Families of Elliptical Galaxies*. AJ, vol. 111, pages 2243–+, June 1996. 105

[Trujillo *et al.* 2007] I. Trujillo, C. J. Conselice, K. Bundy, M. C. Cooper, P. Eisenhardt and R. S. Ellis. *Strong size evolution of the most massive galaxies since z ~ 2*. MNRAS, vol. 382, pages 109–120, November 2007. 17

[van den Bosch *et al.* 2008] R. C. E. van den Bosch, G. van de Ven, E. K. Verolme, M. Cappellari and P. T. de Zeeuw. *Triaxial orbit based galaxy models with an application to the (apparent) decoupled core galaxy NGC 4365*. MNRAS, vol. 385, pages 647–666, April 2008. 66

[Vazdekis *et al.* 2010] A. Vazdekis, P. Sánchez-Blázquez, J. Falcón-Barroso, A. J. Cenarro, M. A. Beasley, N. Cardiel, J. Gorgas and R. F. Peletier. *Evolutionary stellar population synthesis with MILES - I. The base models and a new line index system*. MNRAS, vol. 404, pages 1639–1671, June 2010. 114

[Villalobos & Helmi 2008] Á. Villalobos and A. Helmi. *Simulations of minor mergers - I. General properties of thick discs*. MNRAS, vol. 391, pages 1806–1827, December 2008. 20, 94

[von Hoerner 1960] S. von Hoerner. *Die numerische Integration des n-Körper-Problemes für Sternhaufen. I*. ZAp, vol. 50, pages 184–214, 1960. 18

[von Hoerner 1963] S. von Hoerner. *Die numerische Integration des n-Körper-Problems für Sternhaufen, II*. ZAp, vol. 57, pages 47–82, 1963. 18

[Weil & Hernquist 1994] M. L. Weil and L. Hernquist. *Kinematic misalignments in remnants of multiple mergers*. ApJ, vol. 431, pages L79–L82, August 1994. 20, 44

[Weil & Hernquist 1996] M. L. Weil and L. Hernquist. *Global Properties of Multiple Merger Remnants*. ApJ, vol. 460, pages 101–+, March 1996. 20, 44

[Worthey & Ottaviani 1997] G. Worthey and D. L. Ottaviani. *$H\gamma$ and $H\delta$ Absorption Features in Stars and Stellar Populations*. ApJS, vol. 111, pages 377–+, August 1997. 111

[Worthey 1994] G. Worthey. *Comprehensive stellar population models and the disentanglement of age and metallicity effects*. ApJS, vol. 95, pages 107–149, November 1994. 111

[York *et al.* 2000] D. G York *et al. The Sloan Digital Sky Survey: Technical Summary*. AJ, vol. 120, pages 1579–1587, September 2000. 113

[Zwicky 1933] F. Zwicky. *Die Rotverschiebung von extragalaktischen Nebeln*. Helvetica Physica Acta, vol. 6, pages 110–127, 1933. 17